TRACE FINITE ELEMENT METHOD FOR MATERIAL SURFACE FLOWS

by
Alexander Zhiliakov

A dissertation submitted to the Department of Mathematics,
College of Natural Sciences and Mathematics
in partial fulfillment of the requirements for the degree of

Doctor of Philosophy

in Mathematics

Chair of Committee:	Maxim Olshanskii
Committee Member:	Alexander Mamonov
Committee Member:	Andreas Mang
Committee Member:	Alan Demlow

University of Houston
May 2022

In memory of Valentina Novak and Alan K. Womack

ABSTRACT

This dissertation studies a geometrically unfitted finite element method (FEM), known as trace FEM, for the numerical solution of the Navier–Stokes problem posed on a closed smooth material surface. The key result proved is an inf-sup stability of the discrete formulation based on standard Taylor–Hood bulk elements, with the stability constant uniformly bounded w.r.t. the mesh parameter and position of the surface in the bulk mesh. Optimal order convergence rates follow from this new stability result and interpolation properties of the trace FEM.

An augmented Lagrangian preconditioner which is robust w.r.t. variation of the Reynolds number is proposed, along with an efficient recycling strategy of the velocity matrix factorization. Eigenvalue bounds for the preconditioned Schur complement are derived.

Properties of the proposed method are illustrated with numerical examples which include simulation of Kelvin–Helmholtz instability at different Reynolds numbers on a sphere and torus, as well as tangential flow induced by inextensible radial deformations of a surface.

Contents

List of Figures

List of Tables

1 INTRODUCTION

Traditionally, 2D flows have been considered as a mathematical idealization of real-life 3D phenomena. However, recently we saw a growing interest in understanding and solving fluid systems posed on 2D surfaces (or, more generally, on Riemannian manifolds). See, e.g., (Nitschke, Voigt, and Wensch 2012; Jankuhn, Olshanskii, and Reusken 2018; Olshanskii, Quaini, Reusken, and Yushutin 2018; Fries 2018; Reuther and Voigt 2018; Nitschke, Reuther, and Voigt 2019; Olshanskii and Yushutin 2019; Gross, Trask, Kuberry, and Atzberger 2020; Bonito, Demlow, and Licht 2020; Jankuhn, Olshanskii, Reusken, and **Zhiliakov** 2020; Lederer, Lehrenfeld, and Schöberl 2020; Brandner and Reusken 2020; Olshanskii, Reusken, and **Zhiliakov** 2021; Jankuhn, Olshanskii, Reusken, and **Zhiliakov** 2020; Brandner, Reusken, and Schwering 2021; Olshanskii, Reusken, and **Zhiliakov** 2022).

Fluid partial differential equations (PDEs) posed on manifolds arise in continuum-based models of thin material layers exhibiting lateral viscosity, such as lipid bilayers and plasma membranes (Gurtin and Murdoch 1975; Arroyo and DeSimone 2009; Rangamani, Agrawal, Mandadapu, Oster, and Steigmann 2013; Torres-Sánchez, Millán, and Arroyo 2019; **Zhiliakov**, Wang, Quaini, Olshanskii, and Majd 2021; Wang, Palzhanov, Quaini, Olshanskii, and Majd 2022). Beyond biological sciences, fluid equations on surfaces appear in the literature on modeling of foams, emulsions, and liquid crystal (Scriven 1960; Slattery, Sagis, and Oh 2007; Fuller and Vermant 2012; Brenner 2013; Rahimi, DeSimone, and Arroyo 2013; Nitschke, Reuther, and Voigt 2019).

In this dissertation, we study a geometrically *unfitted* finite element method (FEM) for the simulation of incompressible flows on surfaces. Our approach builds on earlier work on an unfitted FEM for elliptic PDEs posed on surfaces (Olshanskii, Reusken, and Grande 2009a) called *trace FEM*. In this method, restrictions (or *traces*) of standard surface-independent finite element spaces defined in a 3D bulk domain are employed. Unlike some other geometrically unfitted methods for surface PDEs, the trace FEM allows for sharp surface representation. This method is suitable for approximating scalar quantities or vector fields on a surface, for which a parametrization or triangulation is not required, i.e., the surface can be defined implicitly.

Main advantages of the proposed method are that it

1. works well for PDEs posed on evolving surfaces (because no remeshing is required), including cases with strong deformations and topological changes (Lehrenfeld, Olshanskii, and Xu 2018), and

2. can be naturally extended to treat surface–bulk problems due to the presence of the background mesh in which the surface is embedded. See, e.g., (Olshanskii, Quaini, and Sun 2022).

Trace FEM has been extended to handle

1. the Stokes problem posed on a stationary surface for the trace $\mathbf{P}_1$–P_1 finite elements in (Olshanskii, Quaini, Reusken, and Yushutin 2018) and for the Taylor–Hood finite elements in (Olshanskii, Reusken, and **Zhiliakov** 2021; Jankuhn, Olshanskii, Reusken, and **Zhiliakov** 2020),

2. the Navier–Stokes problem posed on a stationary surface in (Olshanskii and Yushutin 2019; Olshanskii and **Zhiliakov** 2020), and recently to

3. the Navier–Stokes problem posed on an evolving surface with known geometrical evolution in (Olshanskii, Reusken, and **Zhiliakov** 2022).

In this dissertation, we mainly concentrate on the cases (1) and (2). To demonstrate flexibility of the proposed method, we include numerical simulations for the case (3).

The rest of the dissertation is organized as follows.

Chapter 2. We start by collecting necessary notations and results from differential geometry, tangential differential calculus, and present a continuum-based model that describes flows of inextensible material surfaces.

Chapter 3. Next we supplement the flow model with Boussinesq–Scriven constitutive law, giving rise to a set of PDEs governing the evolution of a viscous material layer: evolving surface Navier–Stokes equations. We discuss several simplifications of the model including the case of known radial motions, leading to the *tangential* Navier–Stokes equations. These equations are obtained employing tangential projection of the fluid system. We conclude the chapter

by showing the well-posedness of the (linearized) tangential Navier–Stokes problem posed on a stationary surface.

Chapter 4. We introduce the trace FEM to discretize the (linearized) tangential Navier–Stokes problem posed on a stationary surface. We (i) establish the inf-sup stability property for the case of Taylor–Hood trace finite element pair (which leads to well-posedness of the discrete method) and (ii) conclude the chapter by proving the error estimates for the trace FEM.

Chapter 5. We develop a fast and reliable solver for the discretized problem. We discuss properties of the resulting linear algebraic system, introduce a grad-div stabilization and an augmented Lagrangian preconditioner, and prove eigenvalue bounds for the preconditioned problem. We introduce a simple and efficient strategy to reuse factorizations of positive definite matrices that leads to a solver that is robust w.r.t. the mesh parameter and Reynolds number variations.

Chapter 6. We conclude by presenting a set of numerical experiments that confirm the theoretical results of the dissertation: simulations confirming the discrete inf-sup stability, tests for expected convergence rates for smooth solutions, Kelvin–Helmholtz instability simulations on a sphere and torus, robustness checks of the proposed algebraic solver w.r.t. the mesh parameter and Reynolds number variations, an energy dissipation study with a comparison to an $\mathbb{R}^2$-case, and tangential flow on a radially deforming inextensible sphere.

The author's contributions are listed in the beginning of the bibliography section. To cite this dissertation, please use the following BibTeX file:

```
@phdthesis{zhiliakov2022phd,
     author  = "Zhiliakov, Alexander",
     title   = "Trace finite element method for material surface flows",
     school  = "University of Houston",
     year    = "2022",
     month   = "May",
     url     = "https://u.pcloud.link/publink/show?code
                =XZ0wHFVZ1EUibC0Nw9jJPXS80JX7pJU3fVi7"
```

```
}
```

2 PRELIMINARIES

2.1 Embedded Surfaces in $\mathbb{R}^{d+1}$

We recall some basic background material of differential geometry following (Ciarlet 2013; Prüss and Simonett 2016). Let $d \in \mathbb{N}$. Latin indexes i, j, k etc. range over $\{1, 2, \dots, d+1\}$, Greek indexes α, β, μ etc. range over $\{1, 2, \dots, d\}$, and Einstein summation is assumed for repeated indexes, e.g.,

$$a_i b^i := \sum_{i=1}^{d+1} a_i b^i.$$

Intuitively, $\Gamma \subset \mathbb{R}^{d+1}$ is a d-dimensional hypersurface if locally it looks like $\mathbb{R}^d$. To elaborate on what "looks like" means, we first need to define neighborhoods (open subsets) of Γ: A subset $\gamma \subset \Gamma$ is a neighborhood of Γ if there exists a neighborhood $\mathcal{O}$ of $\mathbb{R}^{d+1}$ such that

$$\gamma = \Gamma \cap \mathcal{O}. \tag{2.1}$$

A map $f : \Gamma \to \mathbb{R}^d$ is called continuous if the preimage $f^{-1}(\mathcal{O}) := \{\mathbf{x} \in \Gamma : f(\mathbf{x}) \in \mathcal{O}\}$ of any neighborhood $\mathcal{O}$ is a neighborhood of Γ; we write $f \in C(\Gamma)$. Further, the map $f \in C(\Gamma)$ is called a **homeomorphism** if $f^{-1} \in C\left(\mathbb{R}^d\right)$, i.e., if both the map and its inverse are continuous. Two sets are called **homeomorphic** if there exists a homeomorphism between them.

We call a set $\Gamma \subset \mathbb{R}^{d+1}$ a d-dimensional **hypersurface** if for any $\mathbf{x} \in \Gamma$ there exists a neighborhood γ of Γ, see (2.1), containing $\mathbf{x}$, which is homeomorphic to $\mathbb{R}^d$. Such homeomorphism

$$\boldsymbol{\chi} : \mathbb{R}^d \leftrightarrow \gamma, \quad \boldsymbol{\chi}(\mathbf{0}) = \mathbf{x} \tag{2.2}$$

is called a local **parametrization** of Γ around $\mathbf{x}$, and its inverse $\boldsymbol{\chi}^{-1} : \gamma \leftrightarrow \mathbb{R}^d$ is called a local **chart**. Since any neighborhood Ξ of $\mathbb{R}^d$ is homeomorphic to $\mathbb{R}^d$, one may equivalently use Ξ as the parametrization domain in the definition (2.2). Euclidean coordinates $\boldsymbol{\xi} = (\xi_1, \cdots, \xi_d) \in \mathbb{R}^d$

of $\boldsymbol{\chi} = \boldsymbol{\chi}(\boldsymbol{\xi})$ are referred to as **convective coordinates**. Further we use the notation

$$\bullet_{,\alpha} \coloneqq \frac{\partial}{\partial \xi_\alpha} \bullet$$

for partial derivatives w.r.t. convective coordinates ξ_α of a function defined on $\mathbb{R}^d$.

If $\boldsymbol{\chi} \in C^k(\mathbb{R}^d, \gamma)$ for all $\mathbf{x} \in \Gamma$, we say that the hypersurface is of class C^k (or C^k-smooth for short), $\Gamma \in C^k$. Smoothness of a surface map $f : \Gamma \to \mathbb{R}$ is defined via superposition of f with the parametrization (2.2), i.e., we write $f \in C^k(\Gamma) \coloneqq C^k(\Gamma, \mathbb{R})$ if, for any $\mathbf{x} \in \Gamma$ and the corresponding parametrization $\boldsymbol{\chi}$, we have

$$f_{\boldsymbol{\chi}} \coloneqq f \circ \boldsymbol{\chi} \in C^k(\mathbb{R}^d).$$

Similar definitions hold for vector- and tensor-valued functions.

Let $\boldsymbol{\tau}_\alpha \coloneqq \boldsymbol{\chi}_{,\alpha}$ and define a **metric tensor** $\tau_{\alpha\beta} \coloneqq \boldsymbol{\tau}_\alpha \cdot \boldsymbol{\tau}_\beta$. If the latter is positive definite for all $\mathbf{x} \in \Gamma$ and the corresponding parametrizations $\boldsymbol{\chi}$,

$$(\tau_{\alpha\beta}) > 0, \tag{2.3}$$

the hypersurface is called **regular**. The regularity condition (2.3) guarantees that the Jacobian

$$(\boldsymbol{\tau}_1, \cdots, \boldsymbol{\tau}_d)$$

of $\boldsymbol{\chi}$ is injective, i.e., it has a full rank (equals to d), or, equivalently, that its columns $\boldsymbol{\tau}_\alpha$ are linearly independent. Let Γ be a regular hypersurface. A d-dimensional subspace

$$\begin{aligned} &T_{\boldsymbol{\chi}}\Gamma \coloneqq \operatorname{span}\{\boldsymbol{\tau}_1, \cdots, \boldsymbol{\tau}_d\} \subset \mathbb{R}^{d+1}, \\ &T_{\boldsymbol{\chi}}\Gamma \sim \mathbb{R}^d, \end{aligned} \tag{2.4}$$

is called a **tangent space** of Γ at $\boldsymbol{\chi}$. In particular, $T_{\mathbf{x}}\Gamma = T_{\boldsymbol{\chi}(\mathbf{0})}\Gamma$ is the tangent space of Γ at $\mathbf{x}$.

For two vectors $\boldsymbol{\sigma} = \sigma^\alpha \boldsymbol{\tau}_\alpha$ and $\boldsymbol{\omega} = \omega^\alpha \boldsymbol{\tau}_\alpha$ from $T_{\boldsymbol{\chi}}\Gamma$ we have

$$\boldsymbol{\sigma} \cdot \boldsymbol{\omega} = \sigma^\alpha \omega^\beta \tau_{\alpha\beta},$$

and hence $(\tau_{\alpha\beta})$ induces a metric on $T_{\boldsymbol{\chi}}\Gamma$ due to (2.3).

Let $\Gamma_{\text{sph}} \coloneqq \{\mathbf{x} \in \mathbb{R}^{d+1} : \|\mathbf{x}\| = 1\}$. A regular hypersurface Γ is called **orientable** if there exists a continuous vector field $\mathbf{n} \in C(\Gamma, \Gamma_{\text{sph}})$ such that

$$\mathbf{n}_{\boldsymbol{\chi}} \perp T_{\boldsymbol{\chi}}\Gamma, \quad T_{\boldsymbol{\chi}}\Gamma \oplus \{\mathbf{n}_{\boldsymbol{\chi}}\} = \mathbb{R}^{d+1}. \tag{2.5}$$

If the regular hypersurface Γ is compact, i.e.,

$$\sup_{\mathbf{x},\mathbf{y}\in\Gamma} \|\mathbf{x} - \mathbf{y}\| < \infty \quad \text{and} \quad \overline{\Gamma} = \Gamma$$

holds, then Γ is orientable. For brevity, we use the term **surface** for a regular, C^2-smooth, and compact hypersurface.

We set

$$\boldsymbol{\tau}_{d+1} \coloneqq \mathbf{n}_{\boldsymbol{\chi}}$$

so that $\operatorname{span}\{\boldsymbol{\tau}_1, \cdots, \boldsymbol{\tau}_{d+1}\} = \mathbb{R}^{d+1}$. We introduce a contravariant basis $\{\boldsymbol{\tau}^1, \cdots, \boldsymbol{\tau}^{d+1}\}$ through

$$\boldsymbol{\tau}_i \cdot \boldsymbol{\tau}^j = \delta_i^j.$$

Thus, we have $\boldsymbol{\tau}^{d+1} = \boldsymbol{\tau}_{d+1} = \mathbf{n}_{\boldsymbol{\chi}}$ and $(\tau^{ij}) = (\tau_{ij})^{-1}$. An **in-plane projector** $\mathbf{P}_{\boldsymbol{\chi}}$ of Γ at $\boldsymbol{\chi}$ is defined via

$$\begin{aligned} &\mathbf{P}_{\boldsymbol{\chi}} \coloneqq \boldsymbol{\tau}_\alpha \otimes \boldsymbol{\tau}^\alpha = \boldsymbol{\tau}_i \otimes \boldsymbol{\tau}^i - \boldsymbol{\tau}_3 \otimes \boldsymbol{\tau}^3 = \mathbf{I} - \mathbf{n}_{\boldsymbol{\chi}} \otimes \mathbf{n}_{\boldsymbol{\chi}}, \text{ so} \\ &\mathbf{P} = \mathbf{I} - \mathbf{n} \otimes \mathbf{n}, \quad \mathbf{P}^\perp = \mathbf{n} \otimes \mathbf{n}, \end{aligned} \tag{2.6}$$

where $(\mathbf{I}_{ij})$ is the identity tensor. Note that $\mathbf{P}^2 = \mathbf{P} = \mathbf{P}^T$, i.e., $\mathbf{P}$ is an orthogonal projector. Employing (2.6) we use the decomposition of a vector field $\mathbf{v} : \Gamma \to \mathbb{R}^{d+1}$ into tangential and normal

components:

$$\begin{aligned} \mathbf{v} &= \mathbf{v}_T + \mathbf{v}_N, \quad \text{with} \\ \mathbf{v}_T &\coloneqq \mathbf{P}\,\mathbf{v}, \quad \mathbf{v}_N \coloneqq \mathbf{P}^\perp \mathbf{v} = (\mathbf{v}\cdot\mathbf{n})\,\mathbf{n} = v_N\,\mathbf{n}, \end{aligned} \tag{2.7}$$

so that $\mathbf{v}_T \cdot \mathbf{n} = 0$ and $\mathbf{P}\,\mathbf{v}_N = \mathbf{0}$.

A **surface gradient** of $f \in C^1(\Gamma)$ and a **surface covariant derivative** of $\mathbf{v} \in C^1(\Gamma, \mathbb{R}^{d+1})$ are defined as

$$(\nabla_\Gamma f)_{\boldsymbol{\chi}} \coloneqq f_{\boldsymbol{\chi},\alpha}\boldsymbol{\tau}^\alpha, \tag{2.8}$$

$$(\nabla_\Gamma \mathbf{v})_{\boldsymbol{\chi}} \coloneqq (\boldsymbol{\tau}_\beta \cdot \mathbf{v}_{\boldsymbol{\chi},\alpha})\,\boldsymbol{\tau}^\beta \otimes \boldsymbol{\tau}^\alpha, \tag{2.9}$$

respectively. Note that $\nabla_\Gamma f(\mathbf{x}) \in T_{\mathbf{x}}\Gamma$ is an in-plane vector and $\nabla_\Gamma \mathbf{v}(\mathbf{x}) \in T_{\mathbf{x}}\Gamma \otimes T_{\mathbf{x}}\Gamma$ is an in-plane tensor.

Remark 2.1. ∇_Γ does not depend on the choice of parametrization $\boldsymbol{\chi}$.

A **shape operator H** (also known as the **Weingarten map**) is defined as

$$\mathbf{H}_{\boldsymbol{\chi}} \coloneqq \nabla_\Gamma \mathbf{n}_{\boldsymbol{\chi}} = \boldsymbol{\tau}_\beta \cdot \mathbf{n}_{\boldsymbol{\chi},\alpha}\boldsymbol{\tau}^\beta \otimes \boldsymbol{\tau}^\alpha = \underbrace{(\boldsymbol{\tau}_\beta \cdot \boldsymbol{\tau}_{3,\alpha})}_{\eta_{\beta\alpha}\coloneqq}\boldsymbol{\tau}^\beta \otimes \boldsymbol{\tau}^\alpha. \tag{2.10}$$

Differentiating $\boldsymbol{\tau}_\beta \cdot \boldsymbol{\tau}_3 = 0$ w.r.t. ξ_α we get

$$\eta_{\beta\alpha} = \boldsymbol{\tau}_\beta \cdot \boldsymbol{\tau}_{3,\alpha} = -\boldsymbol{\tau}_3 \cdot \boldsymbol{\tau}_{\beta,\alpha}, \tag{2.11}$$

and hence $\mathbf{H} = \mathbf{H}^T$ since $\boldsymbol{\tau}_{\beta,\alpha} = \boldsymbol{\chi}_{,\beta\alpha} = \boldsymbol{\chi}_{,\alpha\beta}$. Eigenvalues κ_α of $\mathbf{H}$ are called **principal curvatures**, and

$$\kappa \coloneqq \operatorname{tr}\mathbf{H} = -\boldsymbol{\tau}_3 \cdot (\boldsymbol{\tau}_{1,1} + \cdots + \boldsymbol{\tau}_{d,d}) = \kappa_1 + \cdots + \kappa_d$$

is a (doubled) **mean curvature**. Note that $\kappa_{d+1} = 0$ since $\operatorname{rank}\mathbf{H} \le d$. For $d = 2$, $K \coloneqq \kappa_1\kappa_2$ is a **Gauss curvature**.

Now we take a closer look at (2.9). Let $\boldsymbol{\nu} \coloneqq \mathbf{v}_{\boldsymbol{\chi}}$. Product rule yields

$$\boldsymbol{\nu}_{,\alpha} = \left(\nu_i \boldsymbol{\tau}^i\right)_{,\alpha} = \nu_{i,\alpha}\boldsymbol{\tau}^i + \nu_i \boldsymbol{\tau}^i_{,\alpha} = \nu_{i,\alpha}\boldsymbol{\tau}^i + \nu_\mu \boldsymbol{\tau}^\mu_{,\alpha} + \nu_3 \boldsymbol{\tau}^3_{,\alpha}. \tag{2.12}$$

We proceed by expressing $\boldsymbol{\tau}^i_{,\alpha}$ in terms of contravariant basis vectors $\{\boldsymbol{\tau}^1, \cdots, \boldsymbol{\tau}^{d+1}\}$. We start with $\boldsymbol{\tau}^3_{,\alpha} = \boldsymbol{\tau}_{3,\alpha} = (\boldsymbol{\tau}_{3,\alpha} \cdot \boldsymbol{\tau}_\lambda)\boldsymbol{\tau}^\lambda + (\boldsymbol{\tau}_{3,\alpha} \cdot \boldsymbol{\tau}_3)\boldsymbol{\tau}^3$. Since $\|\boldsymbol{\tau}_3(\boldsymbol{\xi})\| = 1$ for any $\boldsymbol{\xi} \in \mathbb{R}^d$ by construction, we have

$$0 = (\boldsymbol{\tau}_3 \cdot \boldsymbol{\tau}_3)_{,\alpha} = 2\boldsymbol{\tau}_{3,\alpha} \cdot \boldsymbol{\tau}_3,$$

and, hence, $\boldsymbol{\tau}_{3,\alpha}$ is an in-plane vector,

$$\boldsymbol{\tau}_{3,\alpha} = (\boldsymbol{\tau}_{3,\alpha} \cdot \boldsymbol{\tau}_\lambda)\boldsymbol{\tau}^\lambda \overset{(2.11)}{=} \eta_{\lambda\alpha}\boldsymbol{\tau}^\lambda. \tag{2.13}$$

Next we find contravariant coordinates of $\boldsymbol{\tau}^\mu_{,\alpha} = (\boldsymbol{\tau}^\mu_{,\alpha} \cdot \boldsymbol{\tau}_\lambda)\boldsymbol{\tau}^\lambda + (\boldsymbol{\tau}^\mu_{,\alpha} \cdot \boldsymbol{\tau}_3)\boldsymbol{\tau}^3$. Differentiating $\boldsymbol{\tau}^\mu \cdot \boldsymbol{\tau}_\lambda = \delta^\mu_\lambda$ and $\boldsymbol{\tau}^\mu \cdot \boldsymbol{\tau}_3 = 0$ w.r.t. ξ_α we get

$$\begin{aligned}
\boldsymbol{\tau}^\mu_{,\alpha} \cdot \boldsymbol{\tau}_\lambda &= -\boldsymbol{\tau}^\mu \cdot \boldsymbol{\tau}_{\lambda,\alpha} = -\boldsymbol{\tau}^\mu \cdot (\boldsymbol{\tau}_{\lambda,\alpha} \cdot \boldsymbol{\tau}^i)\boldsymbol{\tau}_i = -\boldsymbol{\tau}_{\lambda,\alpha} \cdot \boldsymbol{\tau}^\mu =: -\Gamma^\mu_{\lambda\alpha}, \\
\boldsymbol{\tau}^\mu_{,\alpha} \cdot \boldsymbol{\tau}_3 &= -\boldsymbol{\tau}^\mu \cdot \boldsymbol{\tau}_{3,\alpha} \overset{(2.13)}{=} -(\boldsymbol{\tau}^\mu \cdot \boldsymbol{\tau}^\lambda)\eta_{\lambda\alpha} = -\tau^{\mu\lambda}\eta_{\lambda\alpha} = -\eta^\mu_\alpha,
\end{aligned}$$

and thus

$$\boldsymbol{\tau}^\mu_{,\alpha} = -\Gamma^\mu_{\lambda\alpha}\boldsymbol{\tau}^\lambda - \eta^\mu_\alpha \boldsymbol{\tau}^3. \tag{2.14}$$

Substituting (2.13) and (2.14) into (2.12) and rearranging we get

$$\begin{aligned}
\boldsymbol{\nu}_{,\alpha} &= \left(\nu_{\lambda,\alpha} - \Gamma^\mu_{\lambda\alpha}\nu_\mu + \eta_{\lambda\alpha}\nu_3\right)\boldsymbol{\tau}^\lambda + \left(\nu_{3,\alpha} - \eta^\mu_\alpha \nu_\mu\right)\boldsymbol{\tau}^3 \\
&=: \left(\nu_{\lambda|\alpha} + \eta_{\lambda\alpha}\nu_3\right)\boldsymbol{\tau}^\lambda + \left(\nu_{3|\alpha} - \eta^\mu_\alpha \nu_\mu\right)\boldsymbol{\tau}^3.
\end{aligned} \tag{2.15}$$

Substituting this back in (2.8) yields

$$(\nabla_\Gamma \mathbf{v})_{\boldsymbol{\chi}} = \nu_{\beta|\alpha}\boldsymbol{\tau}^\beta \otimes \boldsymbol{\tau}^\alpha + \nu_3 \eta_{\beta\alpha}\boldsymbol{\tau}^\beta \otimes \boldsymbol{\tau}^\alpha,$$

and thus

$$\nabla_\Gamma \mathbf{v} = \nabla_\Gamma \mathbf{v}_T + v_N \, \mathbf{H} \tag{2.16}$$

provided that v_N is differentiable.

The symmetric part of the surface covariant derivative is given by

$$\mathbf{E}(\mathbf{v}) \coloneqq \frac{1}{2} \left(\nabla_\Gamma \mathbf{v} + \nabla_\Gamma^T \mathbf{v} \right). \tag{2.17}$$

If $\mathbf{v} = \mathbf{u}$ is a velocity field of a material surface, see Section 2.3, $\mathbf{E}(\mathbf{u})$ has the meaning of the **surface rate-of-strain** tensor (Gurtin and Murdoch 1975; Brandner, Reusken, and Schwering 2021). Similar to (2.16) we have

$$\mathbf{E}(\mathbf{v}) = \mathbf{E}(\mathbf{v}_T) + v_N \, \mathbf{H}$$

provided that v_N is differentiable.

A **surface divergence** of $\mathbf{v} \in C^1(\Gamma, \mathbb{R}^{d+1})$ is defined as

$$(\operatorname{div}_\Gamma \mathbf{v})_{\boldsymbol{\chi}} \coloneqq \operatorname{tr} (\nabla_\Gamma \mathbf{v})_{\boldsymbol{\chi}} = \operatorname{tr} \left((\boldsymbol{\tau}_\beta \cdot \mathbf{v}_{\boldsymbol{\chi},\alpha}) \, \boldsymbol{\tau}^\beta \otimes \boldsymbol{\tau}^\alpha \right) = \mathbf{v}_{\boldsymbol{\chi},\alpha} \cdot \boldsymbol{\tau}_\alpha .$$

For a tensor-valued map $\mathbf{T} \in C^1(\Gamma, \mathbb{R}^{(d+1)\times(d+1)})$ the surface divergence is

$$(\operatorname{div}_\Gamma \mathbf{T})_{\boldsymbol{\chi}} \coloneqq \mathbf{T}_{\boldsymbol{\chi},\alpha}^T \, \boldsymbol{\tau}^\alpha . \tag{2.18}$$

2.2 Tangential Differential Calculus on Surfaces

Concerning the implementation of numerical methods for PDEs posed on manifolds, there are two difficulties related to the evaluation of the surface differential operators introduced in the previous section:

1. the choice of parametrization $\boldsymbol{\chi}$ (which in practice may not be available, or its quality may depend on the computational mesh), and

2. the fact that the induced basis vectors $\boldsymbol{\tau}_i$ (or $\boldsymbol{\tau}^i$) of $T_{\boldsymbol{\chi}}\Gamma$ depend on the convective coor-

dinates $\boldsymbol{\xi}$. This implies that the computation of derivatives of a vector quantity $\boldsymbol{\nu} = \nu_i \boldsymbol{\tau}^i$ requires to differentiate not only its components, but also the basis vectors:

$$\mathbf{v}_{,\alpha} = \left(\nu_i \boldsymbol{\tau}^i\right)_{,\alpha} \neq \nu_{i,\alpha} \boldsymbol{\tau}^i,$$

see (2.15).

This motivates us to rewrite the differential operators employing tangential differential calculus (Delfour and Zolésio 2011). This approach uses the fixed standard basis vectors $\{\mathbf{e}_1, \cdots, \mathbf{e}_{d+1}\}$ of the embedding space $\mathbb{R}^{d+1} \supset \Gamma$ and avoids explicit surface parametrization by using the intrinsic tangential derivatives.

Let $\Omega \subset \mathbb{R}^{d+1}$ be a domain containing the surface, $\Gamma \subset \Omega$, and consider a map $f^e \in C^1(\Omega)$. We define $f \in C^1(\Gamma)$ to be the restriction of f^e to Γ, i.e.,

$$f \coloneqq f^e|_\Gamma. \tag{2.19}$$

Then the application of the chain rule in (2.8) yields

$$(\nabla_\Gamma f)_{\boldsymbol{\chi}} = (f^e \circ \boldsymbol{\chi})_{,\alpha} \boldsymbol{\tau}^\alpha = (\partial_i f^e)_{\boldsymbol{\chi}} (\boldsymbol{\tau}_\alpha \cdot \mathbf{e}_i) \boldsymbol{\tau}^\alpha = (\partial_i f^e)_{\boldsymbol{\chi}} \mathbf{P}_{\boldsymbol{\chi}} \mathbf{e}_i = \mathbf{P}_{\boldsymbol{\chi}} (\nabla f^e)_{\boldsymbol{\chi}},$$

or

$$\nabla_\Gamma f = \mathbf{P} \nabla f^e \tag{2.20}$$

on Γ. In particular, if $f^n = f^e$ extends f constantly along the surface normal, we have

$$\nabla f^n = \mathbf{P} \nabla f^n + \partial_n f^n \mathbf{n} = \mathbf{P} \nabla f^n = \nabla_\Gamma f \tag{2.21}$$

on Γ. Note that the in-plane projector $\mathbf{P}$ depends on the normal vector field $\mathbf{n}$, see (2.6), and if the surface is given implicitly, e.g., as a level contour of some function, then evaluation of (2.20) does not require parametrization.

Similarly, for the covariant derivative (2.9) we get

$$\nabla_\Gamma \mathbf{v} = \mathbf{P}\, \nabla \mathbf{v}^e\, \mathbf{P}$$

on Γ (Brandner, Reusken, and Schwering 2021). Note that

$$\begin{aligned} \nabla \mathbf{v}^n &= \mathbf{e}_i \otimes \nabla v_i^n \overset{(2.21)}{=} \mathbf{e}_i \otimes \nabla_\Gamma v_i = \left(\nabla_\Gamma v_1, \cdots, \nabla_\Gamma v_{d+1}\right)^T, \\ \nabla \mathbf{v}^n\, \mathbf{P} &= \left(\mathbf{P}\left(\nabla_\Gamma v_1, \cdots, \nabla_\Gamma v_{d+1}\right)\right)^T = \nabla \mathbf{v}^n, \end{aligned} \tag{2.22}$$

and thus

$$\nabla_\Gamma \mathbf{v} = \mathbf{P}\, \nabla \mathbf{v}^n$$

on Γ. For the surface divergence (2.18) we have

$$\operatorname{div}_\Gamma \mathbf{T} = \operatorname{div}_\Gamma \left(\mathbf{T}^T \mathbf{e}_i\right) \mathbf{e}_i,$$

i.e., the ith component $(\mathbf{e}_i \cdot \operatorname{div}_\Gamma \mathbf{T})$ of $\operatorname{div}_\Gamma \mathbf{T}$ is the surface divergence of the ith row $\left(\mathbf{T}^T \mathbf{e}_i\right)$ of $\mathbf{T}$.

Consider a **tubular neighborhood**

$$\mathcal{O}_\epsilon(\Gamma) \coloneqq \{\mathbf{x} + d\mathbf{n}(\mathbf{x}) : \mathbf{x} \in \Gamma,\ 2|d| < \epsilon\} \subset \mathbb{R}^{d+1}$$

of the surface Γ of width $\epsilon > 0$. We have the following result (Barrett, Garcke, and Nürnberg 2020): If the surface is compact and C^k-smooth, $k \geq 2$, then the closest point projection

$$\mathbf{p}(\mathbf{x}) \coloneqq \arg\min_{\mathbf{y} \in \Gamma} \|\mathbf{x} - \mathbf{y}\| = \mathbf{x} - \operatorname{dist}(\mathbf{x}) \nabla \operatorname{dist}(\mathbf{x}) \tag{2.23}$$

is well-defined for ϵ sufficiently small, and

$$\operatorname{dist} \in C^k\left(\mathcal{O}_\epsilon(\Gamma)\right), \quad \mathbf{p} \in C^{k-1}\left(\mathcal{O}_\epsilon(\Gamma), \Gamma\right).$$

Here dist is a signed-distance function on Γ, i.e.,

$$\begin{aligned}
&\operatorname{dist}\big|_{\Gamma} = 0, \\
&\operatorname{dist}(\mathbf{x}) = -\left\|\mathbf{x} - \mathbf{p}(\mathbf{x})\right\| < 0 \quad \text{inside the volume bounded by } \Gamma \text{ and} \\
&\operatorname{dist}(\mathbf{x}) = +\left\|\mathbf{x} - \mathbf{p}(\mathbf{x})\right\| > 0 \quad \text{outside.}
\end{aligned}$$

We have

$$\begin{aligned}
&\operatorname{dist}^2(\mathbf{x}) = \left\|\mathbf{x} - \mathbf{p}(\mathbf{x})\right\|^2 = \operatorname{dist}^2(\mathbf{x}) \left\|\nabla \operatorname{dist}(\mathbf{x})\right\|^2, \text{ or} \\
&\|\nabla \operatorname{dist}\| = 1
\end{aligned}$$

in $\mathcal{O}_\epsilon(\Gamma) \setminus \Gamma$. Continuity of dist yields $\|\nabla \operatorname{dist}\| = 1$ in $\mathcal{O}_\epsilon(\Gamma)$, so

$$\mathbf{n} \circ \mathbf{p} = (\nabla \operatorname{dist}) \circ \mathbf{p}$$

if one fixes the normal vector $\mathbf{n}$ to point outside the volume bounded by Γ. Moreover,

$$(\nabla \operatorname{dist}) \circ \mathbf{p} = \nabla \operatorname{dist}$$

in $\mathcal{O}_\epsilon(\Gamma)$ (Delfour and Zolésio 2011, Chapter 7, Theorem 8.4 (i)), and hence

$$\begin{aligned}
\mathbf{P} \circ \mathbf{p} &= \mathbf{I} - \nabla \operatorname{dist} \otimes \nabla \operatorname{dist}, \\
\nabla \mathbf{p} &= \mathbf{P} \circ \mathbf{p} - \operatorname{dist} \nabla^2 \operatorname{dist}, \\
\nabla^2 \operatorname{dist} = \nabla(\nabla \operatorname{dist}) &= \nabla\big((\nabla \operatorname{dist}) \circ \mathbf{p}\big) = \Big(\big(\nabla^2 \operatorname{dist}\big) \circ \mathbf{p}\Big) \nabla \mathbf{p} \\
&= \Big(\big(\nabla^2 \operatorname{dist}\big) \circ \mathbf{p}\Big) \Big(\mathbf{P} \circ \mathbf{p} - \operatorname{dist} \nabla^2 \operatorname{dist}\Big), \\
\Big(\nabla^2 \operatorname{dist}\Big) \circ \mathbf{p} &= \Big(\nabla^2 \operatorname{dist}\, \mathbf{P}\Big) \circ \mathbf{p}
\end{aligned}$$

in $\mathcal{O}_\epsilon(\Gamma)$. Since the Hessian matrix is symmetric,

$$\nabla^2 \operatorname{dist} = \mathbf{P}\,\nabla^2 \operatorname{dist}\,\mathbf{P}$$

on Γ, and

$$\mathbf{H}\circ\mathbf{p} = (\mathbf{P}\,\nabla\,(\mathbf{n}\circ\mathbf{p})\,\mathbf{P})\circ\mathbf{p} = \left(\mathbf{P}\,\nabla^2 \operatorname{dist}\,\mathbf{P}\right)\circ\mathbf{p} = \left(\nabla^2 \operatorname{dist}\right)\circ\mathbf{p}, \text{ or}$$
$$\mathbf{H} = \nabla^2 \operatorname{dist}$$

on Γ. Note that $\mathbf{n}\circ\mathbf{p} = \nabla \operatorname{dist}$ but $\mathbf{H}\circ\mathbf{p} \neq \nabla^2 \operatorname{dist}$.

Assume that $f \in C^1(\Gamma)$ is given. Akin to (2.19), the projection map (2.23) allows to get a bulk function $f\circ\mathbf{p} \in C^1(\mathcal{O}_\epsilon(\Gamma))$ that extends f off of the surface. We have

$$\begin{aligned}\nabla\,(f\circ\mathbf{p}) = \nabla\,(f\circ\mathbf{p}\circ\mathbf{p}) &= (\nabla\mathbf{p})^T\,\nabla\,(f\circ\mathbf{p})\circ\mathbf{p}\\ &= \left(\mathbf{P}\circ\mathbf{p} - \operatorname{dist}\,\nabla^2 \operatorname{dist}\right)\nabla\,(f\circ\mathbf{p})\circ\mathbf{p}, \qquad (2.24)\\ \nabla\,(f\circ\mathbf{p})\circ\mathbf{p} = (\,\mathbf{P}\,\nabla\,(f\circ\mathbf{p})\,)\circ\mathbf{p} &\overset{(2.20)}{=} \nabla_\Gamma f\circ\mathbf{p}, \qquad (2.25)\end{aligned}$$

in $\mathcal{O}_\epsilon(\Gamma)$. Note that

$$\partial_n\,(f\circ\mathbf{p})\circ\mathbf{p} = (\nabla\,(f\circ\mathbf{p})\cdot\mathbf{n})\circ\mathbf{p} = (\nabla_\Gamma f\cdot\mathbf{n})\circ\mathbf{p} = 0,$$

i.e., $\mathbf{p}$ extends f constantly along $\mathbf{n}$. In the literature such an extension is referred to as **canonical**. Akin to (2.21) and (2.22), further we will use the superscript $\bullet^n := \bullet\circ\mathbf{p}$ for the canonical extension.

Substituting (2.25) back into (2.24) yields

$$\nabla f^n(\mathbf{x}) = \left(\mathbf{I} - \operatorname{dist}(\mathbf{x})\nabla^2 \operatorname{dist}(\mathbf{x})\right)\nabla_\Gamma f(\mathbf{x} - \operatorname{dist}\nabla \operatorname{dist}(\mathbf{x}))$$

for $\mathbf{x} \in \mathcal{O}_\epsilon(\Gamma)$. It is interesting to note that one may recover the full gradient *evaluated off the surface* of the canonically extended surface function using the surface gradient and information about Γ, i.e., the distance function and its derivatives.

2.3 Modeling of Material Surface Flows

Intuitively, a surface is material if it evolves as a *material set* (Gurtin, Fried, and Anand 2010), i.e., it consists of the same set of material particles at any given time. The surface does not penetrate itself as it flows, adjacent particles stay adjacent, and there exists a velocity field associated with the surface flow (giving rise to a *material* derivative).

Let $I \coloneqq [0, T]$ be the time interval, $0 < T < \infty$, and consider a family of surfaces $\{\Gamma_t\}_{t\in I}$. We call $\Gamma : t \mapsto \Gamma_t$ a **material surface** if

1. there exists a (sufficiently smooth) map $\Psi : \Gamma_0 \times I \to \mathbb{R}^{d+1}$ such that $\Psi(\cdot, t) : \Gamma_0 \to \Gamma_t$ is a diffeomorphism between surfaces Γ_0 and Γ_t for $t \in I$, with $\Psi(\cdot, 0) = \text{identity}$, and
2. some initial density distribution $\rho_0 : \Gamma_0 \to \mathbb{R}$ is specified, $\rho_0 > 0$.

The physical interpretation of the definition above is the following. Consider a thin *material body* embedded in 3-dimensional space that consists of *material particles*, e.g., a *liposome* that consists of *lipid molecules*. We represent the body by the surface Γ_0: each $\mathbf{x}_P \in \Gamma_0$ corresponds to an initial location of one material particle. The map Ψ gives a *Lagrangian description* of the surface flow: a particle initially located at $\mathbf{x}_P$ moves along a trajectory $\Psi(\mathbf{x}_P, \cdot)$, i.e., its position at time t is given by $\Psi(\mathbf{x}_P, t) \in \Gamma_t$. The curve $\Psi(\mathbf{x}_P, \cdot) : I \to \mathbb{R}^{d+1}$ is called an **orbit** of $\mathbf{x}_P$, and $\Psi(\cdot, t) : \Gamma_0 \to \Gamma_t$ is a **flow map** of Γ_t.

Fix $t \in I$ and let $\Psi_t \coloneqq \Psi(\cdot, t)$. Note that $\Psi_t(\Gamma_0) = \Gamma_t$, and for another particle initially occupying $\mathbf{x}_{P'} \neq \mathbf{x}_P$ we have $\Psi_t(\mathbf{x}_{P'}) \neq \Psi_t(\mathbf{x}_P)$ since the flow map is diffeomorphic. In other words, there exists a unique inverse flow map $\Psi_t^{-1} : \Gamma_t \to \Gamma_0$:

$$\begin{aligned} \Psi_t^{-1}(\Psi_t(\mathbf{x}_P)) &= \mathbf{x}_P \in \Gamma_0, \\ \Psi_t(\Psi_t^{-1}(\mathbf{x})) &= \mathbf{x} \in \Gamma_t. \end{aligned} \tag{2.26}$$

Given a spatial coordinate $\mathbf{x} \in \Gamma_t$, the pullback map Ψ_t^{-1} recovers the initial location $\Psi_t^{-1}(\mathbf{x}) \in \Gamma_0$ of a material particle occupying $\mathbf{x}$ at t. See Figure 1 for an example.

Material velocity $\mathbf{U} : \Gamma_0 \times I \to \mathbb{R}^{d+1}$ describing particles motion is defined as

$$\mathbf{U}(\mathbf{x}_P, t) \coloneqq \partial_t \Psi_t(\mathbf{x}_P).$$

Using (2.26) we can define its spatial counterpart

$$\begin{aligned} \mathbf{u}(\mathbf{x}, t) &\coloneqq \mathbf{U}(\Psi_t^{-1}(\mathbf{x}), t) = \partial_t \Psi_t(\Psi_t^{-1}(\mathbf{x})), \\ \mathbf{U}(\mathbf{x}_P, t) &= \mathbf{u}(\Psi_t(\mathbf{x}_P), t) = \partial_t \Psi_t(\mathbf{x}_P). \end{aligned} \tag{2.27}$$

We emphasize that the domain Γ_t of $\mathbf{u}(\cdot, t)$ varies in time, while $\mathbf{U}(\cdot, t)$ is defined on the reference domain Γ_0. The spatial velocity $\mathbf{u}$ takes values on the **graph** $\boldsymbol{\Gamma}_I$ of Γ defined as

$$\boldsymbol{\Gamma}_I \coloneqq \bigcup_{t \in I} \Gamma_t \times \{t\} \subset \mathbb{R}^{d+2}. \tag{2.28}$$

The graph is a $(d+1)$-dimensional regular hypersurface embedded in $\mathbb{R}^{d+2}$, $\partial \boldsymbol{\Gamma}_I = \Gamma_0 \cup \Gamma_T$.

Akin to the notations introduced in Section 2.1, $\mathbf{n}(\cdot, t)$ denotes the unit normal vector field on Γ_t, $\mathbf{n} : \boldsymbol{\Gamma}_I \to \mathbb{R}^{d+1}$. In what follows we will use the same notation for the orthogonal projector $\mathbf{P}(\cdot, t)$, second fundamental form $\mathbf{H}(\cdot, t)$, principal curvatures $\kappa_\alpha(\cdot, t)$ etc. defined on Γ_t. We will use subscript $\bullet_I$ for the analogous quantities on $\boldsymbol{\Gamma}_I$.

The velocity field $\mathbf{u} = \mathbf{u}_T + u_N \mathbf{n}$, see decomposition (2.7), gives a *Eulerian description* of the flow, i.e., it gives the velocity of a material particle occupying $\mathbf{x} \in \Gamma_t$ at t. As is typical in hydrodynamics, equations governing fluid motion are formulated for the spatial fluid velocity $\mathbf{u}$ (see Chapter 3). This leads to an alternative way of the material surface description. Namely, given an initial surface Γ_0 and a spatial velocity field $\mathbf{u}$, one recovers the flow map Ψ via solving ODEs associated with every material point $\mathbf{x}_P \in \Gamma_0$:

$$\begin{aligned} \mathrm{d}_t \Psi_t(\mathbf{x}_P) &= \mathbf{u}(\Psi_t(\mathbf{x}_P), t), \quad t > 0, \\ \Psi_0(\mathbf{x}_P) &= \mathbf{x}_P. \end{aligned} \tag{2.29}$$

Let $F \in C^1(\Gamma_0 \times I)$ be a Lagrangian description of some material particles property, e.g., density,

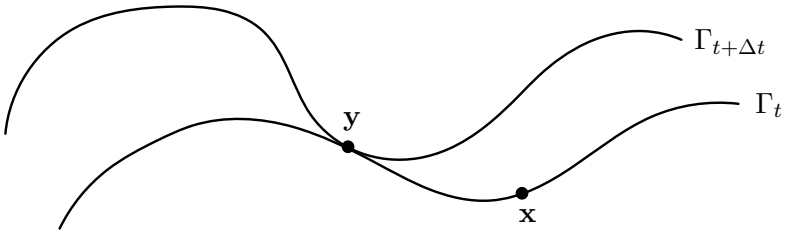

Figure 1: Illustration for the evolution of a material curve (1-dimensional surface) $t \mapsto \Gamma_t$.

- Since $\mathbf{x} \in \Gamma_t$, there exists a material particle associated with the position $\mathbf{x}_P = \Psi_t^{-1}(\mathbf{x}) \in \Gamma_0$. However, the pullback map $\Psi_{t+\Delta t}^{-1}(\mathbf{x})$ is undefined since $\mathbf{x} \notin \Gamma_{t+\Delta t}$, i.e., no particle occupies $\mathbf{x}$ at $t + \Delta t$ even for $h \ll 1$.
- We have $\mathbf{y} \in \Gamma_t \cap \Gamma_{t+\Delta t}$, and both pullbacks $\Psi_t^{-1}(\mathbf{y})$ and $\Psi_{t+\Delta t}^{-1}(\mathbf{y})$ are defined. They may or may not correspond to the same material particle.

temperature, pressure, etc. A **material** (time) **derivative** of the property F is its temporal rate-of-change $\partial_t F$.

We would like to get Eulerian description of the material derivative. Akin to (2.27), we can define a spatial map $f : \mathbf{\Gamma}_I \to \mathbb{R}$ corresponding to F via

$$f(\mathbf{x}, t) \coloneqq F(\Psi_t^{-1}(\mathbf{x}), t),$$
$$F(\mathbf{x}_P, t) = f(\Psi_t(\mathbf{x}_P), t),$$

and its **material derivative** $\dot{f} : \mathbf{\Gamma}_I \to \mathbb{R}$ as

$$\dot{f}(\mathbf{x}, t) \coloneqq \partial_t F(\Psi_t^{-1}(\mathbf{x}), t), \tag{2.30}$$
$$\partial_t F(\mathbf{x}_P, t) = \dot{f}(\Psi_t(\mathbf{x}), t).$$

Given location and time $(\mathbf{x}, t) \in \mathbf{\Gamma}_I$, $\dot{f}$ gives the temporal rate-of-change of F for the material particle that occupies $\mathbf{x} \in \Gamma_t$ at t.

Consider an arbitrary smooth extension f^e of f off of $\mathbf{\Gamma}_I$, i.e.,

$$f^e(\mathbf{x}, t) = f(\mathbf{x}, t) \text{ for } (\mathbf{x}, t) \in \mathbf{\Gamma}_I.$$

We have $F(\mathbf{x}_P, t) = f^e(\Psi_t(\mathbf{x}_P), t)$, and application of chain rule yields

$$\begin{aligned}
\partial_t F(\mathbf{x}_P, t) &= \partial_t f^e(\Psi_t(\mathbf{x}_P), t) + \nabla f^e(\Psi_t(\mathbf{x}_P), t) \cdot \partial_t \Psi_t(\mathbf{x}_P) \\
&= \partial_t f^e(\Psi_t(\mathbf{x}_P), t) + \nabla f^e(\Psi_t(\mathbf{x}_P), t) \cdot \mathbf{u}(\Psi_t(\mathbf{x}_P), t), \text{ or} \\
\dot{f} &= \partial_t f^e + \nabla f^e \cdot \mathbf{u} = \partial_t f^e + (\mathbf{u} \cdot \nabla) f^e. \qquad (2.31)
\end{aligned}$$

Similarly, for a vector-valued map $\mathbf{v} \in C^1(\mathbf{\Gamma}_I)$ we have

$$\dot{\mathbf{v}} = \partial_t \mathbf{v}^e + (\nabla \mathbf{v}^e)\, \mathbf{u} = \partial_t \mathbf{v}^e + (\mathbf{u} \cdot \nabla)\, \mathbf{v}^e.$$

In particular, Eulerian surface acceleration is given by

$$\dot{\mathbf{u}} = \partial_t \mathbf{u}^e + (\mathbf{u} \cdot \nabla)\, \mathbf{u}^e.$$

Remark 2.2 (Partial time derivative)**.** Note that we cannot replace $\partial_t f^e$ with $\partial_t f$: if $\mathbf{x} \in \Gamma_t$, there is no guarantee it stays in $\Gamma_{t+\Delta t}$ even for $h \ll 1$, see Figure 1. Thus $f(\mathbf{x}, t + \Delta t)$ in

$$\partial_t f(\mathbf{x}, t)\Delta t = f(\mathbf{x}, t + \Delta t) - f(\mathbf{x}, t) + o(\Delta t)$$

is undefined.

Corollary 2.1 (Spatial representation of material derivatives)**.** The following statements are true:

1. It is clear from the definition (2.30) that the material derivative is an *intrinsic* quantity, i.e., it does not depend on the off surface extension choice in (2.31).

2. Extending $f(\cdot, t)$ canonically, i.e., with constant values along normal vectors $\mathbf{n}(\cdot, t)$ of Γ_t, $f^e = f^n$, yields
$$\dot{f} = \partial_t f^n + \nabla_\Gamma f \cdot \mathbf{u}_T. \qquad (2.32)$$

3. If $\Gamma = \Gamma_t \equiv \Gamma_0$, then $\partial_t f(\mathbf{x}, t)$ is well-defined for any smooth f and $\mathbf{x} \in \Gamma$, and (2.32) simplifies

further to

$$\dot{f} = \partial_t f + \nabla_\Gamma f \cdot \mathbf{u}_T. \tag{2.33}$$

Let $\gamma_t \subset \Gamma_t$ be an arbitrary material subsurface and $f \in C^1(\mathbf{\Gamma}_I)$. The following transport relation (also known as a Leibniz rule for material surfaces) holds (Cermelli, Fried, and Gurtin 2005):

$$\mathrm{d}_t \int_{\gamma_t} f(\cdot,t)\,\mathrm{d}s = \int_{\gamma_t} \dot{f}(\cdot,t) + f(\cdot,t)\,\mathrm{div}_{\Gamma_t}\,\mathbf{u}(\cdot,t)\,\mathrm{d}s, \tag{2.34}$$

For the area and mass of $\gamma_t \subset \Gamma_t$,

$$\mathrm{area}_\gamma(t) \coloneqq \int_{\gamma_t} 1\,\mathrm{d}s, \quad \mathrm{mass}_\gamma(t) \coloneqq \int_{\gamma_t} \rho(\cdot,t)\,\mathrm{d}s,$$

we further impose two conditions:

1. **Inextensibility**, i.e., $\mathrm{d}_t\,\mathrm{area}_\gamma(t) \equiv 0$. The latter can be rewritten invoking the Leibniz rule (2.34) as

   $$\int_{\gamma_t} \mathrm{div}_{\Gamma_t}\,\mathbf{u}(\cdot,t)\,\mathrm{d}s = 0$$

   for $t \in I$. Since γ_t can be taken arbitrary, the above is equivalent to $\mathrm{div}_{\Gamma_t}\,\mathbf{u}(\mathbf{x},t) = 0$ for $(\mathbf{x},t) \in \mathbf{\Gamma}_I$. We write

   $$\mathrm{div}_\Gamma\,\mathbf{u} = 0 \quad \text{on } \Gamma_t. \tag{2.35}$$

2. **Mass conservation**, i.e., $\mathrm{d}_t\,\mathrm{mass}_\gamma(t) \equiv 0$. Similar arguments along with inextensibility condition (2.35) yield

   $$\dot{\rho} = 0 \quad \text{on } \Gamma_t. \tag{2.36}$$

In this dissertation we assume constant initial density distribution, $\rho_0 = \text{const}$. Mass conservation (2.36) implies $\rho(\cdot,t) = \rho_0$ for $t \in I$. For the case of non-constant density distribution treatment we refer to (Palzhanov, **Zhiliakov**, Quaini, and Olshanskii 2021; Olshanskii, Palzhanov, and Quaini 2021).

Next we make a couple of remarks about evolution of Γ.

Theorem 2.1 (Surface speed)**.** Assume that two different velocity fields $\mathbf{u} \neq \mathbf{u}'$ give rise to the same material surface Γ. Then $u_N = u'_N$.

Proof. Fix $(s, \mathbf{z}) \in \mathbf{\Gamma}_I$ and let Ψ and Ψ' be flows associated with $\mathbf{u}$ and $\mathbf{u}'$, respectively, see (2.29). We have

$$\Gamma_s = \Psi_s(\Gamma_0) = \Psi'_s(\Gamma_0),$$

and thus there exist $\mathbf{x}_P, \mathbf{x}_{P'} \in \Gamma_0$ such that

$$\mathbf{z} = \Psi_s(\mathbf{x}_P) = \Psi'_s(\mathbf{x}_{P'}). \tag{2.37}$$

Consider two $C^1(I, \mathbf{\Gamma}_I)$-curves

$$\mathbf{y}(t) \coloneqq (\Psi(\mathbf{x}_P, t), t), \qquad \mathbf{y}'(t) \coloneqq (\Psi'(\mathbf{x}_{P'}, t), t),$$
$$\mathbf{y}(s) = \mathbf{y}'(s) = (\mathbf{z}, s),$$

and let $\boldsymbol{\tau}_\alpha$ span the tangent space of Γ_s at $\mathbf{z}$,

$$T_{\mathbf{z}}\Gamma_s = \operatorname{span}\{\boldsymbol{\tau}_1, \boldsymbol{\tau}_2\}.$$

Then for the corresponding tangent space of $\mathbf{\Gamma}_I$ at $(\mathbf{z}, s)$ we have (Prüss and Simonett 2016, Section 5.2)

$$\begin{aligned} T_{(\mathbf{z},s)}\mathbf{\Gamma}_I &= \operatorname{span}\left\{(\boldsymbol{\tau}_1, 0), (\boldsymbol{\tau}_2, 0), \mathrm{d}_t\mathbf{y}(s)\right\} \\ &= \operatorname{span}\left\{(\boldsymbol{\tau}_1, 0), (\boldsymbol{\tau}_2, 0), (\partial_t\Psi_s(\mathbf{x}_P), 1)\right\} \qquad (2.38) \\ &= \operatorname{span}\left\{(\boldsymbol{\tau}_1, 0), (\boldsymbol{\tau}_2, 0), \mathrm{d}_t\mathbf{y}'(s)\right\} \\ &= \operatorname{span}\left\{(\boldsymbol{\tau}_1, 0), (\boldsymbol{\tau}_2, 0), (\partial_t\Psi'_s(\mathbf{x}_{P'}), 1)\right\}, \qquad (2.39) \end{aligned}$$

From (2.38) we have that $(\partial_t \Psi_s(\mathbf{x}_P), 1) \in T_{(\mathbf{z},s)}\mathbf{\Gamma}_I$, and expanding it in the basis (2.39) yields

$$\begin{aligned}(\partial_t \Psi_s(\mathbf{x}_P), 1) &= c_\alpha(\boldsymbol{\tau}_\alpha, 0) + c_3(\partial_t \Psi'_s(\mathbf{x}_{P'}), 1)\\ &= c_\alpha(\boldsymbol{\tau}_\alpha, 0) + (\partial_t \Psi'_s(\mathbf{x}_{P'}), 1),\\ \partial_t \Psi_s(\mathbf{x}_P) &= c_\alpha \boldsymbol{\tau}_\alpha + \partial_t \Psi'_s(\mathbf{x}_{P'}),\end{aligned} \tag{2.40}$$

where $c_\alpha \in \mathbb{R}$ are two basis coefficients. Using (2.29) and (2.37) we get

$$\partial_t \Psi_s(\mathbf{x}_P) = \mathbf{u}(\Psi_s(\mathbf{x}_P), s) = \mathbf{u}(\mathbf{z}, s), \tag{2.41}$$

$$\partial_t \Psi'_s(\mathbf{x}_{P'}) = \mathbf{u}'(\Psi'_s(\mathbf{x}_{P'}), s) = \mathbf{u}'(\mathbf{z}, s),$$

$$\mathbf{u}(\mathbf{z}, s) = c_\alpha \boldsymbol{\tau}_\alpha + \mathbf{u}'(\mathbf{z}, s). \tag{2.42}$$

Contracting (2.42) with $\mathbf{n}(\mathbf{z}, s) \perp \boldsymbol{\tau}_\alpha$ yields

$$u_N(\mathbf{z}, s) = u'_N(\mathbf{z}, s).$$

Noting that $(s, \mathbf{z}) \in \mathbf{\Gamma}_I$ is arbitrary completes the proof. □

Corollary 2.2 (Surface speed)**.** We have the following observations:

1. The surface speed u_N of the material surface Γ is *intrinsic*, i.e.,

$$u_N(\mathbf{x}, t) = \partial_t \Psi_t(\Psi_t^{-1}(\mathbf{x})) \cdot \mathbf{n}(\mathbf{x}, t) \tag{2.43}$$

   is independent of the flow map Ψ that realizes a given $\mathbf{\Gamma}_I$.

2. It is clear from (2.38) and (2.41) that

$$\mathbf{n}_I \coloneqq \frac{(\mathbf{n}, -u_N)}{\sqrt{1 + u_N^2}} \perp T\mathbf{\Gamma}_I,$$

   i.e., $\mathbf{n}_I$ is a unit normal vector field on $\mathbf{\Gamma}_I$. If $\mathbf{n}$ is continuous on $\mathbf{\Gamma}_I$, then the graph $\mathbf{\Gamma}_I$ is orientable.

3. If $u_N = 0$, then the graph normal vector $\mathbf{n}_I = (\mathbf{n}, 0)$ is perpendicular to t-axis, and $\mathbf{\Gamma}_I = \Gamma_0 \times I$ becomes a cylinder. In this case geometry of Γ stays unchanged, $\Gamma_t \equiv \Gamma_0$, and the flow is purely tangential. Conversely, $\Gamma_t \equiv \Gamma_0$ implies $u_N = 0$. If $u_N \neq 0$, material surface $\Gamma : t \mapsto \Gamma_t$ is called **evolving**. If $u_N = 0$, we call $\Gamma_t \equiv \Gamma_0$ **stationary** and use notation Γ for Γ_t, $t \in I$.

4. Note that $u_N = 0$ does not imply $\Psi_t =$ identity since $\mathbf{u} = \mathbf{u}_T$ does not necessarily vanish.

5. Any stationary surface is material. To see this, take $\Psi_t =$ identity.

Further we assume the existence of a global level set function $\phi \in C^2(\Omega \times I)$, $\Omega \subset \mathbb{R}^{d+1}$, such that

$$\Gamma_t = \phi^{-1}(\{0\}, t) \coloneqq \{\mathbf{x} \in \Omega : \phi(\mathbf{x}, t) = 0\}, \quad \|\nabla\phi(\cdot, t)\| > 0, \quad t \in I.$$

We assume that $\phi < 0$ inside the volume bounded by Γ and $\phi > 0$ outside, so $\mathbf{n} = \nabla\phi / \|\nabla\phi\|$ is an outward unit normal vector on Γ. The choice of the level set is not unique; one example is a signed-distance function $\phi = \text{dist}$, see Section 2.2.

Note that $\phi(\Psi_t(\mathbf{x}_p), t) \equiv 0$, and thus

$$0 = \dot{\phi} = \partial_t\phi + \nabla\phi \cdot \mathbf{u}$$

Given initial surface Γ_0, i.e., $\phi(\cdot, 0) = \phi_0$, and material velocity $\mathbf{u}$, one can recover $\Gamma_t = \phi^{-1}(\{0\}, t)$ via solving

$$\partial_t\phi + \nabla\phi \cdot \mathbf{u} = 0. \tag{2.44}$$

The second term in (2.44) can be rewritten as

$$\nabla\phi \cdot \mathbf{u} = \mathbf{u} \cdot \frac{\nabla\phi}{\|\nabla\phi\|} \|\nabla\phi\| = \mathbf{u} \cdot \mathbf{n} \|\nabla\phi\| = u_N \|\nabla\phi\|,$$

so the geometric evolution of Γ is independent of the tangential velocity $\mathbf{u}_T$: if ϕ satisfies (2.44), then it also satisfies

$$\partial_t\phi + u_N \|\nabla\phi\| = 0. \tag{2.45}$$

and vice-versa, i.e., $\mathbf{u}_T$ can be chosen arbitrary. This means that the flow map Ψ that solves (2.29)

and the flow map Ψ^n that solves

$$\begin{aligned} \mathrm{d}_t \Psi_t^n(\mathbf{x}_P) &= \mathbf{u}_N(\Psi_t^n(\mathbf{x}_P), t), \\ \Psi_0^n(\mathbf{x}_P) &= \mathbf{x}_P \end{aligned} \tag{2.46}$$

define the same material surface $\Gamma_t \equiv \Psi_t(\Gamma_0) \equiv \Psi_t^n(\Gamma_0)$.

Remark 2.3 (ALE)**.** One may employ equivalence of (2.29) and (2.46) to track the material interface Γ_t: by adding an appropriate tangential correction $\mathbf{u}_T$, one may expect to get a better discrete approximation of Γ_t w.r.t., e.g., quality of computational mesh. This is a basis for a so-called *arbitrary Lagrangian-Eulearian* approach (ALE), see, e.g., (Morigi 2010; Mikula, Remesíková, Sarkoci, and Sevcovic 2014; **Zhiliakov**, Svyatskiy, Olshanskii, Kikinzon, and Shashkov 2019) and references therein.

In this dissertation we use the Eulerian approach for the interface tracking based on the level set equation (2.45) first introduced in (Osher and Sethian 1988).

In agreement with Corollary 2.2, one readily sees from (2.45) that Γ is stationary if and only if $u_N = 0$, and $u_N = -\partial_t \phi \,/\, \|\nabla \phi\|$ is independent of a particular choice of the level set function.

3 MATHEMATICAL MODELS

3.1 Navier–Stokes Problem on Evolving Surfaces

Equipping material surface inextensibility condition (2.35) and mass conservation (2.36) (in the form $\rho = \text{const} > 0$) with conservation of linear momentum leads to the **evolving surface Navier–Stokes problem**, see (Jankuhn, Olshanskii, and Reusken 2018): Find the level set $\phi : \Omega \times I \to \mathbb{R}$, surface velocity $\mathbf{u} : \mathbf{\Gamma}_I \to \mathbb{R}^3$, and surface pressure $p : \mathbf{\Gamma}_I \to \mathbb{R}$ satisfying

$$\rho \dot{\mathbf{u}} - 2\mu \operatorname{div}_\Gamma \mathbf{E}(\mathbf{u}) + \nabla_\Gamma p - p\kappa \mathbf{n} = \mathbf{f}, \tag{3.1a}$$

$$\operatorname{div}_\Gamma \mathbf{u} = 0 \quad \text{on } \Gamma_{t>0} \coloneqq \phi^{-1}(\{0\}, t > 0), \tag{3.1b}$$

$$\partial_t \phi + u_N \|\nabla \phi\| = 0 \quad \text{in } \Omega, \tag{3.1c}$$

subject to given initial conditions ϕ_0 and $\mathbf{u}_0$:

$$\phi(\cdot, 0) = \phi_0 \quad \text{in } \Omega, \tag{3.2a}$$

$$\mathbf{u}(\cdot, 0) = \mathbf{u}_0 \quad \text{on } \Gamma_0 \coloneqq \phi_0^{-1}(\{0\}). \tag{3.2b}$$

Here $\mathbf{f} : \mathbf{\Gamma}_I \to \mathbb{R}^3$ is a given acting area external force term, constant $\mu > 0$ is a given dynamic viscosity coefficient arising from *Boussinesq–Scriven constitutive law* in the momentum equation (3.1a). We refer to (Brandner, Reusken, and Schwering 2021) for an overview and alternative forms of the system (3.1), (3.2).

We note that the geometric operators / quantities $\mathbf{n}$, $\mathbf{P}$, κ etc. above are computable in terms of ϕ, and (3.1) forms the system of five equations (three scalar equations in the vector momentum equation (3.1a), inextensibility condition (3.1b), and the level set equation (3.1c)) for five unknowns: $\mathbf{u} = (u_x, u_y, u_z)$, p, and ϕ.

3.1.1 Prescribed Geometric Evolution of the Surface

Further we assume that the geometrical evolution of the surface is known, i.e., ϕ is prescribed and hence u_N and all the geometric quantities are known. Applying $\mathbf{P}$ to the momentum equation (3.1a) leads to the following system for $\mathbf{u}_T$ and p:

$$\begin{aligned} \rho\,(\mathbf{P}\,\dot{\mathbf{u}}_T + u_N\,\mathbf{H}\,\mathbf{u}_T) - 2\mu\,\mathbf{P}\,\mathrm{div}_\Gamma\,\mathbf{E}(\mathbf{u}_T) + \nabla_\Gamma p &= \mathbf{b}_T, \\ \mathrm{div}_\Gamma\,\mathbf{u}_T &= g \quad \text{on } \Gamma_{t>0}, \end{aligned} \tag{3.3}$$

subject to the velocity initial condition

$$\mathbf{u}_T(\cdot,0) = \mathbf{P}\,(\cdot,0)\,\mathbf{u}_0 \quad \text{on } \Gamma_0. \tag{3.4}$$

The operator $\mathbf{P}\,\dot{\bullet}$ in the momentum equation can be interpreted as covariant material derivative.

The right-hand sides of (3.3) are known in terms of geometric quantities and u_N:

$$g \coloneqq -u_N\kappa, \qquad \mathbf{b}_T \coloneqq \mathbf{f}_T + 2\mu\,\mathbf{P}\,\mathrm{div}_\Gamma(u_N\,\mathbf{H}) + \frac{\rho}{2}\nabla_\Gamma u_N^2.$$

We call (3.3), (3.4) **evolving surface *tangential* Navier–Stokes problem**.

3.2 Navier–Stokes and Oseen Problems on Stationary Surfaces

Assuming that the surface is in geometric equilibrium,

$$\Gamma = \Gamma_t \equiv \Gamma_0 \quad \Leftrightarrow \quad u_N = 0,$$

we can rewrite the inertia term in the momentum equation of (3.3) as

$$\begin{aligned}
\mathbf{P}\,\dot{\mathbf{u}}_T + u_N\,\mathbf{H}\,\mathbf{u}_T &= \mathbf{P}\,\dot{\mathbf{u}}_T \\
\overset{(2.33)}{} \qquad &= \mathbf{P}\,(\partial_t \mathbf{u}_T + (\nabla_\Gamma \mathbf{u}_T)\,\mathbf{u}_T) \\
\partial_t\,\mathbf{P} = \mathbf{0} \qquad &= \partial_t\,(\mathbf{P}\,\mathbf{u}_T) + \mathbf{P}\,(\nabla_\Gamma \mathbf{u}_T)\,\mathbf{u}_T \\
\nabla_\Gamma \mathbf{u}_T \subset T\Gamma \otimes T\Gamma \qquad &= \partial_t \mathbf{u}_T + (\nabla_\Gamma \mathbf{u}_T)\,\mathbf{u}_T = \dot{\mathbf{u}}_T
\end{aligned}$$

on Γ. Thus the system (3.3) reduces to the **surface tangential Navier–Stokes problem**: Find $(\mathbf{u}_T, p)$ such that

$$\begin{aligned}
\rho\,(\partial_t \mathbf{u}_T + (\nabla_\Gamma \mathbf{u}_T)\,\mathbf{u}_T) - 2\mu\,\mathbf{P}\,\mathrm{div}_\Gamma\,\mathbf{E}(\mathbf{u}_T) + \nabla_\Gamma p &= \mathbf{f}_T, \\
\mathrm{div}_\Gamma\,\mathbf{u}_T &= 0 \quad \text{on } \Gamma,
\end{aligned} \tag{3.5}$$

subject to the velocity initial condition (3.4).

For the purpose of analysis, it is convenient to introduce one more supplementary model. Letting $\rho = 1$, applying a finite difference-based discretization to $\partial_t \mathbf{u}_T$, and linearizing inertia term $(\nabla_\Gamma \mathbf{u}_T)\,\mathbf{u}_T$ in (3.5) for each time step, one ends up with an Oseen-type problem: Find $(\mathbf{u}_T, p)$ such that

$$\begin{aligned}
\alpha\,\mathbf{u}_T + (\nabla_\Gamma \mathbf{u}_T)\,\mathbf{w} - 2\nu\,\mathbf{P}\,\mathrm{div}_\Gamma\,\mathbf{E}(\mathbf{u}_T) + \nabla_\Gamma p &= \mathbf{f}_T, \\
\mathrm{div}_\Gamma\,\mathbf{u}_T &= 0 \quad \text{on } \Gamma.
\end{aligned} \tag{3.6}$$

The constant $\alpha > 0$ is inversely proportional to a time step size, the r.h.s. $\mathbf{f}_T$ collects contributions from the area forces and from the previous step velocities of the discretized time derivative, and $\mathbf{w}$ is some known (e.g., extrapolated from divergence-free velocities from the previous time steps) flow field such that the inertia term is skew-symmetric:

$$\langle (\nabla_\Gamma \mathbf{u}_T)\,\mathbf{w}, \mathbf{v}_T \rangle_0 = -\langle (\nabla_\Gamma \mathbf{v}_T)\,\mathbf{w}, \mathbf{u}_T \rangle_0\,. \tag{3.7}$$

Here $\langle \cdot, \cdot \rangle_0 \coloneqq \int_\Gamma \langle \cdot, \cdot \rangle\,\mathrm{d}s$ is the L^2-scalar product on Γ, and $\|\cdot\|_0^2 \coloneqq \langle \cdot, \cdot \rangle_0$. We elaborate on the

discretization of the time derivative and linearization of the inertia term in Section 4.1.

If $\mathbf{w} \neq \mathbf{0}$, we call (3.6) **surface tangential *Oseen* problem**. As is typical in the analysis of Navier–Stokes equations, we presented (3.6) in dimensionless form with Reynolds number $\mathrm{Re} \propto \nu^{-1} > 0$ such that

$$\|\mathbf{w}\|_\infty \coloneqq \|\mathbf{w}\|_{L^\infty(\Gamma)} = 1. \tag{3.8}$$

Further we refer to ν as the viscosity coefficient.

If $\mathbf{w} = \mathbf{0}$, we call (3.6) **surface tangential *Stokes* problem**. The Stokes problem is an approximation of the Oseen problem for the case of slow (viscous) flows, $\nu \gg \|\mathbf{w}\|_\infty$.

3.2.1 Weak Formulation

Consider the surface Sobolev space $H^1(\Gamma)$ equipped with the scalar product and the induced norm

$$\langle u, v\rangle_1 \coloneqq \langle u, v\rangle_0 + \langle \nabla_\Gamma u, \nabla_\Gamma v\rangle_0 , \qquad \|\cdot\|_1^2 \coloneqq \langle \cdot, \cdot\rangle_1 .$$

We refer to (Aubin 1982, Chapter 2) for the detailed discussion of the concept of Sobolev spaces on manifolds. The vector space

$$\mathbf{H}^1(\Gamma) \coloneqq \left[H^1(\Gamma)\right]^{d+1} = \{ u_i \mathbf{e}_i : u_i \in H^1(\Gamma) \}$$

is defined componentwise.

Corollary 3.1. We have $\mathbf{u} \in \mathbf{H}^1(\Gamma)$ if and only if

$$\|\mathbf{u}\|_1^2 \coloneqq \|\mathbf{u}\|_0^2 + \|\nabla \mathbf{u}^n\|_0^2 = \int_\Gamma \|\mathbf{u}\|^2 + \|\nabla \mathbf{u}^n\|^2 \,\mathrm{d}s < \infty, \tag{3.9}$$

i.e., (3.9) defines a norm on $\mathbf{H}^1(\Gamma)$. Here

$$\|\mathbf{A}\| \coloneqq \sup_{\|\mathbf{x}\|=1} \|\mathbf{A}\,\mathbf{x}\|$$

is the spectral (i.e., induced by the Euclidean dot product) norm of $\mathbf{A} \in \mathbb{R}^{(d+1)\times(d+1)}$.

Proof. Note that

$$\nabla \mathbf{u}^n \overset{(2.22)}{=} (\nabla_\Gamma u_1, \cdots, \nabla_\Gamma u_{d+1})^T,$$
$$\|\nabla \mathbf{u}^n\|_0 = \|(\nabla_\Gamma u_1, \cdots, \nabla_\Gamma u_{d+1})\|_0,$$

and hence (3.9) includes only tangential gradients of each component. Thus we have

$$\|\nabla_\Gamma u_i\|_0 \leq \|(\nabla_\Gamma u_1, \cdots, \nabla_\Gamma u_{d+1})\|_0 \leq \|\nabla_\Gamma u_1\|_0 + \cdots + \|\nabla_\Gamma u_{d+1}\|_0$$

due to the estimate

$$\|\mathbf{A}\,\mathbf{e}_i\| \leq \|\mathbf{A}\| \leq \|\mathbf{A}\,\mathbf{e}_1\| + \cdots + \|\mathbf{A}\,\mathbf{e}_{d+1}\| \tag{3.10}$$

for any matrix $\mathbf{A} \in \mathbb{R}^{(d+1)\times(d+1)}$. □

Let $\mathbf{V}_T \coloneqq \{\mathbf{v} \in \mathbf{H}^1(\Gamma) : v_N = 0\}$ be a subspace of tangential vector fields. In the context of a discretization method developed in the next chapter, it is convenient to allow the velocity space to have a non-vanishing normal component. Hence we introduce

$$\mathbf{H}^1(\Gamma) \subset \mathbf{V} \coloneqq \{\mathbf{v}_T + v_N \mathbf{n} : \mathbf{v}_T \in \mathbf{V}_T,\ v_N \in L^2(\Gamma)\} \sim \mathbf{V}_T \oplus L^2(\Gamma), \text{ and} \tag{3.11}$$
$$\|\mathbf{v}\|_{\mathbf{V}}^2 \coloneqq \|\mathbf{v}_T\|_1^2 + \|v_N\|_0^2 = \|\nabla \mathbf{v}_T^n\|_0^2 + \|\mathbf{v}\|_0^2 \tag{3.12}$$

for $\mathbf{v} \in \mathbf{V}$.

The space (3.11) is a suitable test and trial space for velocity fields. Since the surface is closed (and thus no boundary conditions are prescribed), the pressure field is defined up to a hydrostatic mode. For the test and trial space of pressure fields we take

$$L_0^2(\Gamma) \coloneqq \left\{ q \in L^2(\Gamma) : \int_\Gamma q \,\mathrm{d}s = 0 \right\} \sim L^2(\Gamma) \setminus \mathbb{R}.$$

Consider the continuous bilinear forms

$$a(\mathbf{u},\mathbf{v}) \coloneqq \int_\Gamma \alpha\,\mathbf{u}_T\cdot\mathbf{v}_T + 2\nu\,\mathbf{E}(\mathbf{u}_T):\mathbf{E}(\mathbf{v}_T) + (\nabla_\Gamma \mathbf{u}_T)\,\mathbf{w}\cdot\mathbf{v} + \tau\,u_N v_N \,\mathrm{d}s, \tag{3.13a}$$

$$b_T(\mathbf{v},q) \coloneqq -\int_\Gamma q\,\mathrm{div}_\Gamma\,\mathbf{v}_T\,\mathrm{d}s \tag{3.13b}$$

for $\mathbf{u},\mathbf{v}\in\mathbf{V}$, $q\in L^2(\Gamma)$, with some penalty parameter $\tau>0$ for the normal component of the velocity field. The double-contraction in (3.13a) is defined via

$$\mathbf{A}:\mathbf{B} \coloneqq \langle \mathbf{A},\mathbf{B}\rangle \coloneqq \mathrm{tr}\left(\mathbf{A}\,\mathbf{B}^T\right)$$

for two square matrices $\mathbf{A}$ and $\mathbf{B}\in\mathbb{R}^{(d+1)\times(d+1)}$. For the induced spectral norm (3.10) we have

$$\|\mathbf{A}\|^2 = \mathbf{A}:\mathbf{A}\,.$$

Let $\lambda_i\in\mathrm{sp}\,(\mathbf{A})$ and $r=\mathrm{rank}\,(\mathbf{A})$. The Cauchy–Schwarz inequality

$$1\cdot\lambda_1+\cdots+1\cdot\lambda_r \le r^{\frac{1}{2}}\left(\lambda_1^2+\cdots+\lambda_r^2\right)^{\frac{1}{2}}$$

implies

$$\begin{aligned} |\,\mathrm{tr}\,\mathbf{A}\,|^2 = (\lambda_1+\cdots+\lambda_r)^2 &\le r\left(\lambda_1^2+\cdots+\lambda_r^2\right) = r\,\mathrm{tr}\,\mathbf{A}^2 = r\,\|\mathbf{A}\|^2\,,\\ \|\mathrm{div}_\Gamma\,\mathbf{v}_T\|_0 = \|\mathrm{tr}\,\nabla_\Gamma\mathbf{v}_T\|_0 &\le \sqrt{d}\,\|\nabla_\Gamma\mathbf{v}_T\|_0\,, \end{aligned} \tag{3.14}$$

and hence

$$\begin{aligned} b_T(\mathbf{v},q) &= -\int_\Gamma q\,\mathrm{tr}\,\nabla_\Gamma\mathbf{v}_T\,\mathrm{d}s\\ &\overset{\text{Cauchy–Schwarz}}{\le} \|q\|_0\,\|\mathrm{tr}\,\nabla_\Gamma\mathbf{v}_T\|_0\\ &\overset{(3.14)}{\le} \sqrt{d}\,\|q\|_0\,\|\nabla_\Gamma\mathbf{v}_T\|_0 \end{aligned} \tag{3.15}$$

for any $\mathbf{V}\times L^2(\Gamma)$. We further estimate

$$\begin{aligned} \|\nabla_\Gamma\mathbf{v}\|_0^2 = \int_\Gamma \|\mathbf{P}\,\nabla\mathbf{v}^n\|^2\,\mathrm{d}s &\le \int_\Gamma \|\mathbf{P}\|^2\,\|\nabla\mathbf{v}^n\|^2\,\mathrm{d}s = \|\nabla\mathbf{v}^n\|_0^2\,,\\ \|\nabla_\Gamma\mathbf{v}\|_0 &\le \|\nabla\mathbf{v}^n\|_0 \end{aligned} \tag{3.16}$$

for any $\mathbf{v} \in \mathbf{H}^1(\Gamma)$, since $\mathbf{P}$ is an orthogonal projector, $\|\mathbf{P}(\mathbf{x})\| = 1$ for any $\mathbf{x} \in \Gamma$. Hence the form b_T is continuous on $\mathbf{V} \times L^2(\Gamma)$:

$$\begin{aligned} b_T(\mathbf{v}, q) &\leq \sqrt{d}\, \|q\|_0 \, \|\nabla_\Gamma \mathbf{v}_T\|_0 \\ &\overset{(3.16)}{\leq} \sqrt{d}\, \|q\|_0 \, \|\nabla \mathbf{v}_T^n\|_0 \\ &\overset{(3.12)}{\leq} \sqrt{d}\, \|q\|_0 \, \|\mathbf{v}\|_{\mathbf{V}}\,. \end{aligned} \tag{3.17}$$

Due to linearity of the trace operator and $\operatorname{tr} \mathbf{A} = \operatorname{tr} \mathbf{A}^T$ we can alternatively write

$$b_T(\mathbf{v}, q) = -\int_\Gamma q \operatorname{tr} \mathbf{E}(\mathbf{v}_T)\, \mathrm{d}s.$$

Note that in the definition (3.13b) of $b_T(\mathbf{v}, \cdot)$ only *tangential* component of $\mathbf{v}$ is used, i.e.,

$$b_T(\mathbf{v}, \cdot) = b_T(\mathbf{v}_T, \cdot)$$

for any $\mathbf{v} \in \mathbf{V}$. This property motivates the notation b_T instead of b. If $q \in H^1(\Gamma)$, then integration by parts yields

$$b_T(\mathbf{v}, q) = \int_\Gamma \mathbf{v}_T \cdot \nabla_\Gamma q \, \mathrm{d}s = \int_\Gamma \mathbf{v} \cdot \nabla_\Gamma q \, \mathrm{d}s. \tag{3.18}$$

Using (3.8), estimating

$$\begin{aligned} \|\mathbf{E}(\mathbf{v})\|_0 &= \frac{1}{2} \left\| \nabla_\Gamma \mathbf{v} + \nabla_\Gamma^T \mathbf{v} \right\|_0 \\ &\leq \frac{1}{2} \left(\|\nabla_\Gamma \mathbf{v}\|_0 + \left\| \nabla_\Gamma^T \mathbf{v} \right\|_0 \right) \\ &= \|\nabla_\Gamma \mathbf{v}\|_0\,, \qquad \mathbf{v} \in \mathbf{H}^1(\Gamma)\,, \end{aligned} \tag{3.19}$$

and applying similar arguments as in (3.15), (3.17) yields

$$a(\mathbf{u}, \mathbf{v}) \leq C \, \|\mathbf{u}\|_{\mathbf{V}} \, \|\mathbf{v}\|_{\mathbf{V}}$$

for all $\mathbf{u}$, $\mathbf{v} \in \mathbf{V}$.

The weak formulation of the surface tangential Oseen problem (3.6) reads: Find $(\mathbf{u}, p) \in \mathbf{V} \times L_0^2(\Gamma)$

such that

$$\begin{aligned} a(\mathbf{u},\mathbf{v}) + b_T(\mathbf{v},p) &= \langle \mathbf{f}_T, \mathbf{v}\rangle_0\,, \\ b_T(\mathbf{u},q) &= 0 \end{aligned} \tag{3.20}$$

holds for all $(\mathbf{v},q) \in \mathbf{V}\times L^2(\Gamma)$. Equivalently, one may consider only test functions $q \in L^2_0(\Gamma)$ since

$$L^2(\Gamma) \setminus L^2_0(\Gamma) \sim \mathbb{R},$$

and

$$b_T(\mathbf{v}, \text{const}) = \int_\Gamma \mathbf{v}\cdot\nabla_\Gamma \,\text{const} = 0$$

holds due to (3.18) for any $\mathbf{v}\in\mathbf{V}$.

The following surface Korn inequality and Ladyzhenskaya–Babuška–Brezzi condition (also known as the inf-sup condition) were derived in (Jankuhn, Olshanskii, and Reusken 2018, Lemma 4.2 and equation (4.8)): Assuming Γ is C^2-smooth and compact, there exist $c_K > 0$ and $c_0 > 0$ such that

$$\|\mathbf{v}_T\|_0 + \|\mathbf{E}(\mathbf{v}_T)\|_0 \geq c_K \|\mathbf{v}_T\|_1 \tag{3.21}$$

for any $\mathbf{v}_T \in \mathbf{V}_T$, and

$$\sup_{\mathbf{v}_T\in\mathbf{V}_T} \frac{b_T(\mathbf{v}_T,q)}{\|\mathbf{v}_T\|_1} \geq c_0 \|q\|_0 \tag{3.22}$$

for any $q \in L^2_0(\Gamma)$.

Corollary 3.2. The norm (3.12) is equivalent to

$$\mathbf{V} \ni \mathbf{v} \mapsto \|\nabla_\Gamma \mathbf{v}_T\|_0^2 + \|\mathbf{v}\|_0^2\,.$$

The result follows from the estimates (3.16), (3.19), and the Korn inequality (3.21).

From the Korn inequality (3.21) we have

$$
\begin{aligned}
c_K^2 \left\|\mathbf{v}_T\right\|_1^2 &\leq \left(\left\|\mathbf{v}_T\right\|_0 + \left\|\mathbf{E}(\mathbf{v}_T)\right\|_0\right)^2 \\
&\leq 2\left(\left\|\mathbf{v}_T\right\|_0^2 + \left\|\mathbf{E}(\mathbf{v}_T)\right\|_0^2\right), \\
\min\{\nu, \frac{\alpha}{2}\} c_K^2 \left\|\mathbf{v}_T\right\|_1^2 &\leq \min\{2\nu, \alpha\} \left\|\mathbf{v}_T\right\|_0^2 + \min\{2\nu, \alpha\} \left\|\mathbf{E}(\mathbf{v}_T)\right\|_0^2 \\
&\leq \alpha \left\|\mathbf{v}_T\right\|_0^2 + 2\nu \left\|\mathbf{E}(\mathbf{v}_T)\right\|_0^2, \qquad (3.23) \\
\min\{\nu, \frac{\alpha}{2}\} c_K^2 \left\|\mathbf{v}_T\right\|_1^2 + \tau \left\|u_N\right\|_0^2 &\leq \alpha \left\|\mathbf{v}_T\right\|_0^2 + 2\nu \left\|\mathbf{E}(\mathbf{v}_T)\right\|_0^2 + \tau \left\|v_N\right\|_0^2 \\
&\overset{(3.7)}{=} a(\mathbf{v}, \mathbf{v}), \\
\min\left\{\tau, \min\left\{\nu, \frac{\alpha}{2}\right\} c_K^2\right\} \left\|\mathbf{v}\right\|_{\mathbf{V}}^2 &\leq a(\mathbf{v}, \mathbf{v})
\end{aligned}
$$

for any $\mathbf{v} \in \mathbf{V}$, i.e., the linear form a is coercive on $\mathbf{V}$. Since $\mathbf{V}_T \subset \mathbf{V}$ and $\left\|\mathbf{v}_T\right\|_1 = \left\|\mathbf{v}_T\right\|_{\mathbf{V}}$ for $\mathbf{v}_T \in \mathbf{V}_T$, (3.22) implies

$$
\sup_{\mathbf{v} \in \mathbf{V}} \frac{b_T(\mathbf{v}, q)}{\left\|\mathbf{v}\right\|_{\mathbf{V}}} \geq c_0 \left\|q\right\|_0 \qquad \text{(LBB)}
$$

for any $q \in L_0^2(\Gamma)$.

The inf-sup property (LBB) of the form b_T, the coercivity (3.23) of the form a, and the continuity of these forms imply well-posedness of the weak formulation (3.20), see, e.g., (Girault and Raviart 2012). The unique solution of (3.20) is denoted by $(\mathbf{u}^\star, p^\star)$.

Corollary 3.3. The solution $\mathbf{u}^\star$ is tangential, i.e., $\mathbf{u}^\star = \mathbf{u}_T^\star \in \mathbf{V}_T$.

To see this, consider the weak problem (3.20) with $\mathbf{V}$ replaced with $\mathbf{V}_T$ and note that its solution also solves (3.20).

4 PROBLEM DISTRETIZATION

4.1 Time Discretization and Linearization

We start with the time discretization of (3.5). We split the time interval I into $n_t \in \mathbb{N}$ subintervals,

$$0 = t^0 < t^1 < \cdots < t^{n_t} = T,$$

and assume a constant time step $\Delta t \coloneqq T \,/\, n_t$. We adopt the notation $\mathbf{u}^k$ for the approximation of the velocity solution $\mathbf{u}_T(\cdot, t^k)$ at time $t^k = k\Delta t$, and similar for p^k and $\mathbf{f}^k$. A semi-implicit time-stepping scheme for (3.5) reads: Given approximate solutions $\mathbf{u}^{k-1}$ and $\mathbf{u}^{k-2}$ from two previous steps, find $\mathbf{u}^k$ with $\mathbf{u}^k \cdot \mathbf{n} = 0$ and p^k such that

$$\begin{aligned} [\mathbf{u}]_t^k + \left(\nabla_\Gamma \mathbf{u}^k\right) \mathbf{w}^k - 2\nu\, \mathbf{P}\, \mathrm{div}_\Gamma\, \mathbf{E}(\mathbf{u}^k) + \nabla_\Gamma p^k &= \mathbf{f}^k, \\ \mathrm{div}_\Gamma\, \mathbf{u}^k &= 0 \quad \text{on } \Gamma \end{aligned} \tag{4.1}$$

for $k = 2, 3, \ldots, n_t$.

For the numerical experiments in Sections 6.2 and 6.3 we employ the second order method with

$$[\mathbf{u}]_t^k \coloneqq \frac{3\mathbf{u}^k - 4\mathbf{u}^{k-1} + \mathbf{u}^{k-2}}{2\Delta t}, \quad \mathbf{w}^k \coloneqq 2\mathbf{u}^{k-1} - \mathbf{u}^{k-2}, \tag{4.2}$$

but this particular choice has little effect on the properties of the resulting linear systems analyzed in Chapter 5. For $k = 1$ we utilize the initial condition (3.4), $\mathbf{u}^0 \coloneqq \mathbf{u}_T(\cdot, 0)$, and the backward Euler scheme

$$[\mathbf{u}]_t^1 \coloneqq \frac{\mathbf{u}^1 - \mathbf{u}^0}{\Delta t}, \quad \mathbf{w}^1 \coloneqq \mathbf{u}^0. \tag{4.3}$$

We see that on each time step the linearized semi-discrete problem (4.1) is the surface tangential Oseen problem (3.6) with $\mathbf{u}_T \coloneqq \mathbf{u}^k$, $\mathbf{w} \coloneqq \mathbf{w}^k$, $p \coloneqq p^k$, and

$$\alpha \coloneqq \frac{3}{2}\Delta t^{-1}, \quad \mathbf{f}_T \coloneqq \mathbf{f}^k + \frac{4\mathbf{u}^{k-1} - \mathbf{u}^{k-2}}{2\Delta t}$$

for (4.2). For (4.3) we have

$$\alpha \coloneqq \Delta t^{-1}, \quad \mathbf{f}_T \coloneqq \mathbf{f}^1 + \frac{\mathbf{u}^0}{\Delta t}.$$

Thus the weak formulation corresponding to (4.1) resembles (3.20) with the parameters specified above.

Remark 4.1 (Coercivity)**.** The wind field $\mathbf{w}$ above is only divergence free in a weak sense, i.e., it does not necessarily satisfy the condition (3.7) (and thus the form a is not necessarily coercive). In practice, one may eliminate this issue by skew-symmetrizing the form a in (3.13a), i.e., by replacing the term

$$\langle (\nabla_\Gamma \mathbf{u})\, \mathbf{w}, \mathbf{v} \rangle_0$$

with

$$\frac{1}{2} \left(\langle (\nabla_\Gamma \mathbf{u})\, \mathbf{w}, \mathbf{v} \rangle_0 - \langle (\nabla_\Gamma \mathbf{v})\, \mathbf{w}, \mathbf{u} \rangle_0 \right).$$

4.2 Trace Finite Element Method

We start by formulating the trace finite element method (Olshanskii, Reusken, and Grande 2009b) for discretization of the linearized surface Navier–Stokes problem (3.20). For a more detailed introduction of the trace FEM for elliptic and parabolic problems we refer to a review paper (Olshanskii and Reusken 2017). The method uses a surface-independent ambient (bulk) mesh to discretize a PDE posed on an immersed surface, and thus falls into a category of unfitted FEMs. In the context of interface PDEs posed in the bulk domain, the method is sometimes referred to as *cut FEM*; see, e.g., (Olshanskii, Quaini, and Sun 2021). Material in the current chapter extends the work in (Olshanskii, Reusken, and **Zhiliakov** 2021).

Further we assume $d = 2$, i.e., $\Gamma \subset \mathbb{R}^{d+1} = \mathbb{R}^3$. To formulate the method, consider a fixed polyhedral domain $\Omega \subset \mathbb{R}^3$ that strictly contains Γ and a family of tetrahedral triangulations $\{\Omega_h\}_{h>0}$ of Ω. The subset of tetrahedra that have a nonzero intersection with Γ is collected in the set denoted by $\mathcal{T}_h \subset \Omega_h$, see Figure 2. Tetrahedra from $\mathcal{T}_h$ form an active computational mesh.

Let $h_T := \operatorname{diam}(T)$. We assume $\{\mathcal{T}_h\}_{h>0}$ to be quasi-uniform, i.e.,

$$\frac{\max_{T\in\mathcal{T}_h} h_T}{\min_{T\in\mathcal{T}_h} h_T} \leq R_{\mathcal{T}}, \tag{4.4}$$

holds with a shape-regularity constant $R_{\mathcal{T}} > 0$ independent of h. We set $h := \max_{T\in\mathcal{T}_h} h_T$, and for numerical simulations in Chapter 6 we denote the typical mesh size of $\mathcal{T}_h$ by h.

The domain formed by all tetrahedra in $\mathcal{T}_h$ is denoted by

$$\mathcal{O}_h := \operatorname{int}\left(\cup_{T\in\mathcal{T}_h}\overline{T}\right) \subset \Omega. \tag{4.5}$$

On $\mathcal{T}_h$ we use standard finite element spaces of continuous functions, which are polynomials of degree k on each tetrahedron. These so-called *bulk finite element spaces* are denoted by V_h^k,

$$V_h^k := \{v \in C(\mathcal{O}_h) : v|_T \in P_k(T) \text{ for all } T \in \mathcal{T}_h\}. \tag{4.6}$$

Finite element spaces associated with velocity and pressure are chosen to be the Taylor–Hood spaces defined on the bulk mesh $\mathcal{T}_h$, i.e.,

$$\mathbf{V}_h := \left[V_h^{k+1}\right]^3, \quad Q_h := V_h^k \cap L_0^2(\Gamma), \tag{4.7}$$

with $k \geq 1$. In the *trace* FEM formulated below, *traces* of functions from $\mathbf{V}_h$ and Q_h on Γ are used to discretize (3.20).

Remark 4.2 (Surface approximation)**.** For the $\mathbf{P}_{k+1}$–P_k Taylor–Hood finite element pair the optimal rate of convergence for velocity (in the L^2-norm) is $O(h^{k+2})$. A piecewise planar surface approximation $\Gamma_h \simeq \Gamma$ leads to a geometric error of order $O(h^2)$ and a suboptimal discretization error. To overcome this, for the trace FEM a general higher order technique, based on a parametric mapping of the domain $\mathcal{O}_h$, has been developed (Grande, Lehrenfeld, and Reusken 2018). This approach can be directly applied to the Taylor–Hood spaces, see (Jankuhn, Olshanskii, Reusken, and **Zhiliakov** 2020). To avoid further technical issues related to the analysis of the parametric mapping, in this dissertation we do not study these isoparametric spaces. Instead we use assume

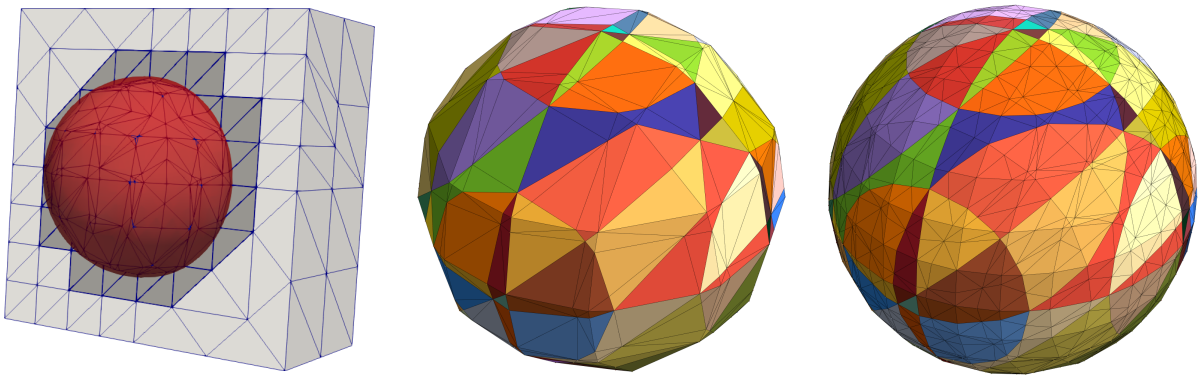

Figure 2: Left: Unit sphere Γ_{sph} (red) immersed into the bulk mesh Ω_h (light gray) and the active computational mesh $\mathcal{T}_h$ (dark gray). Middle and right: Induced surface triangulations of Γ_{sph}, see Remark 4.2.

that integrals over Γ can be computed exactly and analyze the spaces (4.7).

For numerical experiments in Chapter 6 we use the following approach. We use a Lagrange (nodal) P_1-interpolant of the level set ϕ defined on Ω_h, $I_h^1(\phi)$, to identify tetrahedrons cut by a discrete surface

$$\Gamma_h := \{\mathbf{x} \in \mathbb{R}^3 : \left(I_h^1 \circ \phi\right)(\mathbf{x}) = 0\},$$

and collect them to the set $\mathcal{T}_h$: Since $I_h^1(\phi)\big|_{T \in \Omega_h}$ is linear, we have

$$T \in \Omega_h \setminus \mathcal{T}_h \quad \Leftrightarrow \quad \text{values of } I_h^1(\phi) \text{ are of the same sign at vertices of } T. \tag{4.8}$$

To approximate integrals over Γ, we iterate over $T \in \mathcal{T}_h$ and refine each tetrahedron m times, $m \in \mathbb{N}$, getting a "virtual" mesh $T_{h\,2^{-m}}$. Then we build the nodal P_1-interpolant of ϕ on each subtetrahedron from $T_{h\,2^{-m}}$ and, using the same approach as in (4.8), get a piecewise planar approximation $\Gamma_{h\,2^{-m}}$ of Γ. We take m sufficiently large to ensure that the contribution of the surface approximation error is of lower order compared to the interpolation error. Note that with this approach one does not need to build $\Omega_{h\,2^{-m}}$, i.e., refine the whole bulk mesh. Figure 2 shows $\Gamma_{h/2}$ (left) and $\Gamma_{h/4}$ (right), where planar pieces of $\Gamma_{h/2}$ and $\Gamma_{h/4}$ have the same color if they belong to the same tetrahedron $T \in \mathcal{T}_h$.

There are two important issues specifically related to discretization of the surface *tangential*

problem (3.20):

1. Firstly, the numerical treatment of the tangentiality condition $\mathbf{u} \cdot \mathbf{n} = 0$ on Γ. Enforcing the tangentiality condition $\mathbf{u}_h \cdot \mathbf{n} = 0$ on Γ for polynomial functions $\mathbf{u}_h \in \mathbf{V}_h$ is inconvenient and may lead to locking, i.e., only $\mathbf{u}_h = \mathbf{0}$ satisfies it. Following (Hansbo and Larson 2016; Hansbo, Larson, and Larsson 2019; Jankuhn, Olshanskii, and Reusken 2018; Reuther and Voigt 2018; Olshanskii, Quaini, Reusken, and Yushutin 2018) we included a penalty term

$$\tau \langle u_N, v_N \rangle_0 \tag{4.9}$$

   in the weak formulation, see (3.13a), to enforce the tangential constraint weakly.

2. The second issue is related to possible small cuts of tetrahedra from $\mathcal{T}_h$ by the surface, see Figure 2. For the standard choice of finite element basis functions this may lead to poorly conditioned algebraic systems. The algebraic stability is recovered by adding certain volumetric terms to the finite element formulation.

Hence, the bilinear forms that we use in the discretization method contain a penalty term (4.9) and two terms related to algebraic stability. We introduce the following bilinear forms:

$$A(\mathbf{u}, \mathbf{v}) \coloneqq a(\mathbf{u}, \mathbf{v}) + \rho_u \int_{\mathcal{O}_h} \partial_n \mathbf{u} \cdot \partial_n \mathbf{v} \, \mathrm{d}\mathbf{x}, \tag{4.10a}$$

$$s_n(p, q) \coloneqq \rho_p \int_{\mathcal{O}_h} \partial_n p \, \partial_n q \, \mathrm{d}\mathbf{x}, \tag{4.10b}$$

with two stabilization parameters $\rho_p > 0$ and $\rho_u > 0$. The normal derivatives in the introduced volumetric terms require $\mathbf{n}$ to be defined in the strip $\mathcal{O}_h$. Such an extension may be naturally obtained from the level set ϕ, i.e., one may take

$$\mathbf{n}_\phi \coloneqq \frac{\nabla \phi}{\|\nabla \phi\|}, \quad \mathbf{n}_\phi\big|_\Gamma = \mathbf{n}. \tag{4.11}$$

If $\phi = \mathrm{dist}$, then one obtains the canonical extension of the normal vector, see Section 2.2; otherwise, (4.11) defines quasi-normal directions in $\mathcal{O}_h \setminus \Gamma$ (which is also admissible). In practice, the exact

level set ϕ may be replaced with a sufficiently accurate approximation, e.g., with the kth order nodal interpolant $\phi_h := I_h^k(\phi)$, $k \in \mathbb{N}$.

The trace FEM for the surface tangential Oseen problem (3.20) reads as follows: Find $(\mathbf{u}_h, p_h) \in \mathbf{V}_h \times Q_h$ such that

$$\begin{aligned} A(\mathbf{u}_h, \mathbf{v}_h) + b_T(\mathbf{v}_h, p_h) &= \langle \mathbf{f}_T, \mathbf{v}_h \rangle_0 \,, \\ b_T(\mathbf{u}_h, q_h) - s_n(p_h, q_h) &= 0 \end{aligned} \tag{4.12}$$

holds for all $(\mathbf{v}_h, q_h) \in \mathbf{V}_h \times Q_h$. Since $V_h|_\Gamma \subset H^1(\Gamma)$, we have

$$\begin{aligned} a(\mathbf{u}, \mathbf{v}) = \int_\Gamma \alpha\, \mathbf{u} \cdot \mathbf{v} + 2\nu \left(\mathbf{E}(\mathbf{u}) - u_N \mathbf{H}\right) : \left(\mathbf{E}(\mathbf{v}) - v_N \mathbf{H}\right) \; + \\ \left(\nabla_\Gamma \mathbf{u} - u_N \mathbf{H}\right) \mathbf{w} \cdot \mathbf{v} + \hat{\tau}\, u_N v_N \, \mathrm{d}s, \\ b(\mathbf{v}, q) = \int_\Gamma \mathbf{v} \cdot \nabla_\Gamma q \, \mathrm{d}s \end{aligned} \tag{4.13}$$

for $(\mathbf{u}, \mathbf{v}, q) \in \mathbf{V}_h^2 \times Q_h$, $\hat{\tau} := \alpha + \tau$, due to (2.16) and integration by parts (3.18). Note that (4.13) avoids differentiation

$$\nabla_\Gamma \mathbf{v}_T = \nabla_\Gamma \left(\mathbf{P}\, \mathbf{v}\right)$$

of projected quantities, and hence is more attractive for the implementation of (4.12). We also note that in the context of the trace FEM the off surface extensions of the test and trial functions are readily available, and thus the surface differential operators in (4.13) can be naturally computed employing (4.11) and the results from Section 2.2. For example, for the surface rate-of-strain tensor (2.17) we have

$$\begin{aligned} \mathbf{E}\left(\mathbf{P}\, \mathbf{u}_h\right) = \frac{1}{2}\, \mathbf{P}_\phi \left(\nabla \mathbf{u}_h + \nabla^T \mathbf{u}_h\right) \mathbf{P}_\phi - \left(\mathbf{u}_h \cdot \mathbf{n}_\phi\right) \mathbf{H}_\phi, \quad \text{with} \\ \mathbf{P}_\phi = \mathbf{I} - \mathbf{n}_\phi \otimes \mathbf{n}_\phi, \quad \mathbf{H}_\phi = \mathbf{P}_\phi \frac{\nabla^2 \phi}{\|\nabla \phi\|} \mathbf{P}_\phi, \end{aligned} \tag{4.14}$$

where the bulk gradient $\nabla \mathbf{u}_h$ is well-defined for $\mathbf{u}_h \in \mathbf{V}_h$.

Further we write

$$x \lesssim y \tag{4.15}$$

to state that the inequality $x \leq C y$ holds for quantities x and y with a constant $C = C(\Gamma) > 0$

independent of the mesh parameter h and the position of Γ in the background mesh Ω_h, and similar for $x \gtrsim y$. We write $x \simeq y$ iff both $x \lesssim y$ and $x \gtrsim y$ hold.

We allow the following ranges of parameters:

$$\tau \simeq h^{-2}, \quad \rho_p \simeq h, \quad h \lesssim \rho_u \lesssim h^{-1}. \tag{4.16}$$

Note that $\tau \simeq \tau + \alpha$, so one may equivalently use $\hat{\tau} = \tau$ in the implementation (4.13) of the discretization method. We comment on the choice of the bounds in (4.16):

1. The finite element (discrete) stability analysis in the Section 4.3 together with the error analysis in Section 4.4 require $\rho_u \lesssim h^{-1}$. For the sake of *algebraic* stability, i.e., optimal conditioning of the resulting system of algebraic equations, see (Grande, Lehrenfeld, and Reusken 2018, Section 6), we require $\rho_u \gtrsim h$.

2. The discrete stability analysis requires $\rho_p \gtrsim h$ and the error analysis requires $\rho_p \lesssim h$, which leads to $\rho_p \simeq h$. It is interesting to note that $\rho_p \gtrsim h$ is required not only for algebraic stability but also for the optimal performance of the discretization method.

3. The discrete stability and error analysis yield $1 \lesssim \tau \lesssim h^{-2}$. We choose $\tau \simeq h^{-2}$.

The volumetric term in the definition of A is the so called *volume normal derivative* stabilization first introduced in (Burman, Hansbo, Larson, and Massing 2016; Grande and Reusken 2016) in the context of trace FEM for the scalar Laplace–Beltrami problem on a surface. The term vanishes for the solution of (3.20) since one can always assume an extension $(\mathbf{u}_T^\star)^\phi$ of $\mathbf{u}_T^\star$ that is constant in the (quasi-)normal direction (4.11), i.e.,

$$\left(\nabla(\mathbf{u}_T^\star)^\phi\right)\mathbf{n}_\phi = \mathbf{0} \tag{4.17}$$

in $\mathcal{O}_h$. Similar argument holds for the form s_n and $p^\star$. Thanks to (4.17), $\mathbf{V}_h\big|_\Gamma \subset \mathbf{V}$, and $Q_h\big|_\Gamma \subset$

$L^2(\Gamma)$, the method (4.12) is consistent, i.e.,

$$\begin{aligned} A(\mathbf{u}_T^\star, \mathbf{v}_h) + b_T(\mathbf{v}_h, p^\star) = a(\mathbf{u}_T^\star, \mathbf{v}_h) + b_T(\mathbf{v}_h, p^\star) = \langle \mathbf{f}_T, \mathbf{v}_h \rangle_0 \,, \\ b_T(\mathbf{u}_T^\star, q_h) - s_n(p^\star, q_h) = b_T(\mathbf{u}_T^\star, q_h) = 0 \end{aligned} \tag{4.18}$$

holds for all $(\mathbf{v}_h, q_h) \in \mathbf{V}_h \times Q_h$.

4.3 Stability Analysis

For the discrete surface problem (4.12) the situation is similar to the planar one (i.e., posed in a domain of $\mathbb{R}^d$) in the following sense: While the coercivity of the finite element velocity form follows immediately from the analogous property of the original formulation, the inf-sup stability of the b_T-form for a given pair of finite element spaces is a delicate question. Here we address it for the case of $\mathbf{P}_2$–P_1 trace elements (4.7). Higher-order finite element pairs are analyzed in (Jankuhn, Olshanskii, Reusken, and **Zhiliakov** 2020).

It is natural to study the stability of (4.12) using the following problem-dependent norms on $\mathbf{V}_h$ and Q_h:

$$\|\mathbf{v}\|_A^2 \coloneqq A(\mathbf{v}, \mathbf{v}), \quad \|q\|_h^2 \coloneqq \|q\|_0^2 + s_n(q, q). \tag{4.19}$$

Functionals in (4.19) indeed define norms on $\mathbf{V}_h$ and Q_h thanks to the included volumetric terms, i.e., they define the norms not only on the trace spaces, but also on the spaces of bulk finite element functions in $\mathcal{O}_h$. In particular, for $\tau \gtrsim 1$

$$h^{-\frac{1}{2}} \|\mathbf{v}\|_{L^2(\mathcal{O}_h)} \lesssim \|\mathbf{v}\|_A \quad \text{and} \quad h^{-\frac{1}{2}} \|q\|_{L^2(\mathcal{O}_h)} \lesssim \|q\|_h \tag{4.20}$$

hold for any $\mathbf{v} \in \mathbf{V}_h$ and $q \in Q_h$, see (Grande, Lehrenfeld, and Reusken 2018, Lemma 7.4).

We immediately see that the forms b_T and s_n are continuous and the form A is both coercive and continuous with corresponding constants independent of h and the position of Γ in Ω_h. Thus the finite element formulation (4.12) is well-posed in the product norm

$$\left(\|\cdot\|_A^2 + \|\cdot\|_h^2 \right)^{\frac{1}{2}}$$

if the following discrete inf-sup condition

$$\|q\|_h \lesssim \sup_{\mathbf{v}\in\mathbf{V}_h} \frac{b_T(\mathbf{v},q)}{\|\mathbf{v}\|_A} + s_n^{\frac{1}{2}}(q,q) \tag{LBB$_h$}$$

holds for any $q \in Q_h$. See, e.g., (Ern and Guermond 2013) or (Guzmán and Olshanskii 2018, Section 5) for the case of $s_n \neq 0$. Proving that (LBB$_h$) is satisfied for trace $\mathbf{P}_2$–P_1 elements (4.7) is the main topic of the current section.

Remark 4.3 (Condition (LBB$_h$) is a finite element counterpart of (LBB))**.** Let us take a closer look at condition (LBB$_h$). For the norm on the left-hand side the inequality $\|q\|_h \geq \|q\|_0$ trivially holds. Thanks to (3.23), for the norm in the denominator we have the estimate $\|\mathbf{v}\|_A \gtrsim \|\mathbf{v}\|_{\mathbf{V}}$ for all $\mathbf{v} \in \mathbf{V}_h$. Therefore, (LBB$_h$) yields

$$\|q\|_0 \lesssim \sup_{\mathbf{v}\in\mathbf{V}_h} \frac{b_T(\mathbf{v},q)}{\|\mathbf{v}\|_{\mathbf{V}}} + s_n^{\frac{1}{2}}(q,q),$$

for any $q \in Q_h$. The latter bound resembles (LBB) for finite element spaces up to the term $s_n^{\frac{1}{2}}(q,q)$, which depends on the *normal* derivative of q over the tetrahedra cut by Γ.

Remark 4.4 (s_n vs. common "pressure-stabilization")**.** In the finite elements analysis of the standard planar Stokes problem, it is common to add pressure stabilization in mixed FEMs that do not satisfy the LBB condition, such as equal-order elements, see, e.g., (John 2016). Such a stabilization also results in an additional bilinear (p_h, q_h)-form in the finite element formulation. There is, however, an essential difference between such standard stabilizations of equal-order (or other LBB-unstable) finite element pairs and the volumetric normal pressure stabilization added in (4.12).

For manifolds, such a standard pressure stabilization would mean the penalization of the *tangential* variation of p_h, while s_n defined in (4.10b) imposes a constraint on the *normal* behavior of p_h. For example, for the surface case the classical Brezzi–Pitkäranta stabilization (Brezzi and

Pitkäranta 1984) is given by $\rho_p \int_\Gamma \nabla_\Gamma p \cdot \nabla_\Gamma q \, \mathrm{d}s$ with $\rho_p = O(h^2)$, or in the volumetric form by

$$s_{\text{tang}}(p,q) \coloneqq \rho_p \int_{\mathcal{O}_h} \nabla_\Gamma p \cdot \nabla_\Gamma q \, \mathrm{d}\mathbf{x} \tag{4.21}$$

with ρ_p as in (4.16). Combining (4.21) with the normal volume stabilization one obtains a *full pressure gradient* stabilization

$$s_{\text{full}}(p,q) \coloneqq s_{\text{tang}}(p,q) + s_n(p,q) = \rho_p \int_{\mathcal{O}_h} \nabla p \cdot \nabla q \, \mathrm{d}\mathbf{x}. \tag{4.22}$$

This full pressure gradient stabilization has been used and analyzed in (Olshanskii, Quaini, Reusken, and Yushutin 2018) with $\mathbf{P}_1$–P_1 trace finite elements for the surface Stokes problem. Numerical experiments in Section 6.1.1 show that the stability analysis presented below is sharp in the following sense: From the computed optimal constants c_0 in (LBB_h),

$$c_0\big(\|q\|_0^2 + s_\star(q,q)\big) \leq \sup_{\mathbf{v}\in\mathbf{V}_h} \frac{b_T^2(\mathbf{v},q)}{\|\mathbf{v}\|_A^2} + s_\star(q,q), \quad q \in Q_h, \tag{4.23}$$

we conclude that

1. for $\mathbf{P}_2$–P_1 trace FEM the discretization (4.12) is unstable for $\star = 0$ (no stabilization, $s_0 \coloneqq 0$), but becomes stable with only the normal volume stabilization s_n, while
2. for $\mathbf{P}_1$–P_1 trace FEM the discretization (4.12) is unstable for both s_0 and s_n, and the full-gradient stabilization s_{full} makes it stable.

4.3.1 Equivalent Formulations of Discrete Inf-sup Stability

We outline the structure of our analysis for proving the inf-sup stability condition. We present two equivalent formulations of (LBB_h):

1. First formulation essentially follows from the so-called "Verfürth's trick," which is well-known in the stability analysis of mixed finite element pairs (Verfürth 1984).
2. Based on this, another equivalent formulation is derived that uses the notion of *regular ele-*

ments, which is known in the literature on trace FEM (Burman, Hansbo, and Larson 2015; Demlow and Olshanskii 2012).

The derivation of the latter equivalent formulation is based on a key new result, "neighborhood estimate," which essentially states that for finite element functions the L^2-norm on *any* element $T \in \mathcal{T}_h$ can be controlled by the L^2-norm on a neighboring *regular* element and the L^2-norm of the normal derivative (i.e., normal to the surface) in a small neighborhood. This result may be useful also in other analyses of trace FEMs. The results concerning equivalent formulations of the inf-sup stability condition and the neighborhood estimate are valid for trace finite element pairs (4.7) for all $k \geq 1$. The formulation of the inf-sup stability condition in terms of regular elements is tailor-made for our setting, and in Section 4.3.2 we show that it is satisfied for $k = 1$, i.e., for the $\mathbf{P}_2$–P_1 trace pair (4.7).

Let

$$\Gamma_T \coloneqq \Gamma \cap T \tag{4.24}$$

be the intersection of the surface with a tetrahedron $T \in \mathcal{T}_h$. We make use of the following local trace inequality (Hansbo and Hansbo 2002; Reusken 2015; Guzmán and Olshanskii 2018):

$$h_T \|v\|^2_{L^2(\Gamma_T)} \lesssim \|v\|^2_{L^2(T)} + h_T^2 \|v\|^2_{H^1(T)} \tag{4.25}$$

for all $T \in \mathcal{T}_h$ and $v \in H^1(T)$ and. We further need the following broken seminorm on Q_h:

$$|q|^2_{1,\,h} \coloneqq \sum_{T \in \mathcal{T}_h} h_T \|\nabla q\|^2_{L^2(T)}\,. \tag{4.26}$$

For $\rho_p \simeq h$ we have $|q|_{1,\,h} \simeq s^{\frac{1}{2}}_{\text{full}}(q,q)$ due to (4.4).

Lemma 4.1 (Verfürth's trick for trace FEM)**.** The inf-sup stability condition (LBB_h) is equivalent to

$$|q|_{1,\,h} \lesssim \sup_{\mathbf{v} \in \mathbf{V}_h} \frac{b_T(\mathbf{v}, q)}{\|\mathbf{v}\|_A} + s^{\frac{1}{2}}_n(q,q) \tag{$\text{LBB}_{1,\,h}$}$$

for any $q \in Q_h$.

Proof. From a finite element inverse inequality and (4.20) we get

$$\Big(\sum_{T\in\mathcal{T}_h} h_T \left\|\nabla q\right\|^2_{L^2(T)} \Big)^{\frac{1}{2}} \lesssim h^{-\frac{1}{2}} \left\|q\right\|_{L^2(\mathcal{O}_h)} \lesssim \left\|q\right\|_h$$

for all $q \in Q_h$. Hence, (LBB_h) implies ($\mathrm{LBB}_{1,h}$).

We now show that ($\mathrm{LBB}_{1,h}$) implies (LBB_h). Take $q \in Q_h$. Thanks to the inf-sup property (LBB), there exists $\mathbf{v}_T \in \mathbf{V}_T$ such that

$$b_T(\mathbf{v}_T, q) = \left\|q\right\|_0^2, \qquad \left\|\mathbf{v}_T\right\|_1 \lesssim \left\|q\right\|_0. \tag{4.27}$$

We consider $\mathbf{v}_T^n \in H^1(\mathcal{O}_\epsilon(\Gamma))$, a normal extension of $\mathbf{v}_T$ off the surface to a neighborhood $\mathcal{O}_\epsilon(\Gamma)$ of width $\epsilon = O(h)$ such that $\mathcal{O}_h \subset \mathcal{O}_\epsilon(\Gamma)$. For this normal extension one has

$$\left\|\mathbf{v}_T^n\right\|_{H^1(\mathcal{O}_h)} \simeq h^{\frac{1}{2}} \left\|\mathbf{v}_T\right\|_1, \tag{4.28}$$

see (Olshanskii, Reusken, and Grande 2009b).

A set of neighboring tetrahedra of $T \in \mathcal{T}_h$ is defined as

$$\omega_h(T) \coloneqq \{T' \in \mathcal{T}_h : \overline{T'} \cap \overline{T} \neq \emptyset\}. \tag{4.29}$$

Note that $\omega_h(T) \neq \emptyset$ since $T \in \omega_h(T)$. With a slight abuse of notation, we use $\omega_h(T)$ to also denote a domain formed by neighboring tetrahedra of T, i.e., $\mathrm{int}\left(\cup_{T'\in\omega_h(T)}\overline{T'}\right)$.

We take $\mathbf{v} \coloneqq I_h(\mathbf{v}_T^n) \in \mathbf{V}_h$, where $I_h : H^1(\mathcal{O}_\epsilon(\Gamma)) \to \mathbf{V}_h$ is the Clément interpolation operator. By standard arguments based on stability and approximation properties of $I_h(\mathbf{v}_T^n)$, see (Reusken

2015), one gets

$$
\begin{aligned}
\|\mathbf{v}\|_A^2 &= \|I_h(\mathbf{v}_T^n)\|_A^2 \\
&\lesssim \|I_h(\mathbf{v}_T^n)\|_1^2 + h^{-2}\,\|I_h(\mathbf{v}_T^n)\cdot\mathbf{n}\|_0^2 + h^{-1}\,\|(\nabla I_h(\mathbf{v}_T^n))\,\mathbf{n}\|_{L^2(\mathcal{O}_h)}^2 \\
\mathbf{v}_T\cdot\mathbf{n}=0,\ (4.25)\qquad &\lesssim \sum_{T\in\mathcal{T}_h} h_T^{-1}\,\|I_h(\mathbf{v}_T^n)\|_{H^1(T)}^2 + h^{-2}\,\|(I_h(\mathbf{v}_T^n)-\mathbf{v}_T)\cdot\mathbf{n}\|_0^2 \\
(4.25)\qquad &\lesssim \sum_{T\in\mathcal{T}_h} h_T^{-1}\,\|\mathbf{v}_T^n\|_{H^1(\omega_h(T))}^2 + h^{-2}\sum_{T\in\mathcal{T}_h} h_T^{-1}\,\|I_h(\mathbf{v}_T^n)-\mathbf{v}_T^n\|_{L^2(T)}^2 + \\
&\quad h^{-2}\sum_{T\in\mathcal{T}_h} h_T\,\|I_h(\mathbf{v}_T^n)-\mathbf{v}_T^n\|_{H^1(T)}^2 \\
&\lesssim \sum_{T\in\mathcal{T}_h} h_T^{-1}\,\|\mathbf{v}_T^n\|_{H^1(\omega_h(T))}^2 \lesssim h^{-1}\,\|\mathbf{v}_T^n\|_{H^1(\mathcal{O}_h)}^2 \\
(4.28)\qquad &\lesssim \|\mathbf{v}_T\|_1^2\,.
\end{aligned}
$$

Hence due to (4.27) we obtain

$$
\|\mathbf{v}\|_A \lesssim \|q\|_0\,. \tag{4.30}
$$

Using (4.25) and approximation properties of $I_h(\mathbf{v}_T^n)$ one gets

$$
\|\mathbf{v}_T - I_h(\mathbf{v}_T^n)\|_0 \lesssim h\,\|\mathbf{v}_T\|_1\,, \tag{4.31}
$$

and

$$
\begin{aligned}
b_T(\mathbf{v},q) &= b_T(\mathbf{v}_T,q) - b_T(\mathbf{v}_T - I_h(\mathbf{v}_T^n),q) \\
&\geq \|q\|_0^2 - \|\mathbf{v}_T - I_h(\mathbf{v}_T^n)\|_0\,\|\nabla_\Gamma q\|_0 \\
(4.31)\qquad &\geq \|q\|_0^2 - ch\,\|\mathbf{v}_T\|_1\,\|\nabla_\Gamma q\|_0 \\
&= \|q\|_0^2 - ch\,\|\mathbf{v}_T\|_1\left(\sum_{T\in\mathcal{T}_h}\|\nabla_\Gamma q\|_{L^2(\Gamma_T)}^2\right)^{\frac{1}{2}} \\
(4.25)\qquad &\geq \|q\|_0^2 - ch^{\frac{1}{2}}\,\|\mathbf{v}_T\|_1\left(\sum_{T\in\mathcal{T}_h}\|\nabla q\|_{L^2(T)}^2\right)^{\frac{1}{2}} \\
(4.27)\qquad &\geq \|q\|_0^2 - c\,\|q\|_0\,|q|_{1,h}\,.
\end{aligned}
$$

This and (4.30) yield

$$\|q\|_0 - c\,|q|_{1,\,h} \lesssim \sup_{\mathbf{v}\in\mathbf{V}_h} \frac{b_T(\mathbf{v},q)}{\|\mathbf{v}\|_A}, \tag{4.32}$$

and from (4.32) and ($\mathrm{LBB}_{1,\,h}$) we have

$$\|q\|_0 \lesssim \sup_{\mathbf{v}\in\mathbf{V}_h} \frac{b_T(\mathbf{v},q)}{\|\mathbf{v}\|_A} + s_n^{\frac{1}{2}}(q,q)$$

for $q \in Q_h$, which implies (LBB_h). □

Corollary 4.1 (Full gradient stabilization s_{full})**.** For $\rho_p \gtrsim h$ we have

$$\left(\|q\|_0^2 + s_{\mathrm{full}}(q,q)\right)^{\frac{1}{2}} \lesssim \sup_{\mathbf{v}\in\mathbf{V}_h} \frac{b_T(\mathbf{v},q)}{\|\mathbf{v}\|_A} + s_{\mathrm{full}}^{\frac{1}{2}}(q,q) \tag{4.33}$$

for any $q \in Q_h$. To see this, we square (4.32) add $s_{\mathrm{full}}(q,q)$ to both sides:

$$\begin{aligned}
\|q\|_0^2 + s_{\mathrm{full}}(q,q) &\lesssim \sup_{\mathbf{v}\in\mathbf{V}_h} \frac{b_T^2(\mathbf{v},q)}{\|\mathbf{v}\|_A^2} + |q|_{1,\,h}^2 + s_{\mathrm{full}}(q,q) \\
h_T < h \qquad &\leq \sup_{\mathbf{v}\in\mathbf{V}_h} \frac{b_T^2(\mathbf{v},q)}{\|\mathbf{v}\|_A^2} + \left(h\rho_p^{-1} + 1\right) s_{\mathrm{full}}(q,q) \\
\rho_p \gtrsim h \qquad &\lesssim \sup_{\mathbf{v}\in\mathbf{V}_h} \frac{b_T^2(\mathbf{v},q)}{\|\mathbf{v}\|_A^2} + s_{\mathrm{full}}(q,q),
\end{aligned}$$

which yields (4.33).

Thus the trace FEM (4.12) with s_n replaced with s_{full} is well-posed w.r.t. the norm

$$\left(\|\cdot\|_A^2 + \|\cdot\|_0^2 + s_{\mathrm{full}}(\cdot,\cdot)\right)^{\frac{1}{2}}$$

for any Taylor–Hood pair (4.7), $k \geq 1$, as well as for the $\mathbf{P}_1$–P_1 finite element pair. However, due to the consistency error

$$s_{\mathrm{full}}(p^\star, q) \neq 0, \quad q \in Q_h,$$

cf. (4.18), such a method does not have an optimal order discretization error for Taylor–Hood finite elements.

We now derive another condition that is equivalent to ($\mathrm{LBB}_{1,h}$), in which the norm on the left-hand side of ($\mathrm{LBB}_{1,h}$) is replaced with a weaker one: $\sum_{T\in\mathcal{T}_h}$ is replaced with $\sum_{T\in\mathcal{T}_{\mathrm{reg}\,h}}$,

$$\mathcal{T}_{\mathrm{reg}\,h} \subset \mathcal{T}_h$$

is a subset of "regular elements." The following notion of regular elements appeared earlier in the literature on trace FEM (Demlow and Olshanskii 2012; Burman, Hansbo, and Larson 2015). We define the set of *regular elements* as those $T \in \mathcal{T}_h$ for which the area of the intersection with the surface is not less than $c_{\mathrm{reg}}\, h_T^2$, with some sufficiently small threshold parameter $c_{\mathrm{reg}} > 0$ independent of h and how the surface cuts the bulk mesh Ω_h:

$$\mathcal{T}_{\mathrm{reg}\,h} \coloneqq \{T \in \mathcal{T}_h : \mathrm{area}\,(\Gamma_T) \geq c_{\mathrm{reg}}\, h_T^2\}. \tag{4.34}$$

The value of c_{reg} will be specified in the following Theorem 4.1 which shows that

1. the set $\mathcal{T}_{\mathrm{reg}\,h}$ is "dense" in $\mathcal{T}_h$ the following sense: Every $T \in \mathcal{T}_h$ has a regular element T' in the set of its neighboring tetrahedra (4.29), and
2. for any $q \in Q_h$ the norm $\|q\|_{L^2(T)}$ can essentially be controlled with $\|q\|_{L^2(T')}$ and normal derivatives in a small volume neighborhood.

In addition to (4.26), it is convenient to introduce the following seminorm on Q_h:

$$|q|^2_{1,\,\mathrm{reg}\,h} \coloneqq \sum_{T\in\mathcal{T}_{\mathrm{reg}\,h}} h_T \,\|\nabla q\|^2_{L^2(T)}\,.$$

Theorem 4.1 (Neighborhood estimate)**.** For each $T \in \mathcal{T}_h$

1. there exists $T' \in \omega_h(T) \cap \mathcal{T}_{\mathrm{reg}\,h}$, and
2. a neighborhood estimate

$$\|q\|_{L^2(T)} \lesssim \|q\|_{L^2(T')} + h_T \,\|\mathbf{n}\cdot\nabla q\|_{L^2(\omega_h(T))} + h_T^2 \,\|\nabla q\|_{L^2(\omega_h(T))} \tag{4.35}$$

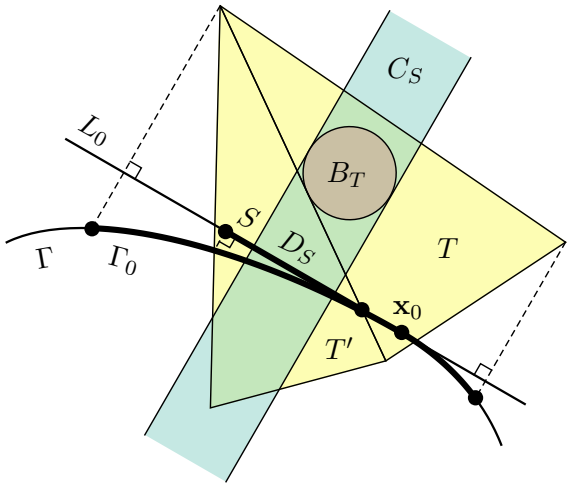

Figure 3: 2-dimensional illustration for the proof of Theorem 4.1: Local graph representation of Γ over the tangent plane $\mathbf{x}_0 + T_{\mathbf{x}_0}\Gamma$

holds for any $q \in Q_h$. A constant (embedded into the notation $\lesssim$, see (4.15)) in the inequality (4.35) depends only on the shape regularity property (4.4) of $\{\mathcal{T}_h\}_{h>0}$ and the (local) smoothness of Γ.

Proof. Consider an arbitrary $T \in \mathcal{T}_h$. First we show that $\omega_h(T) \cap \mathcal{T}_{\mathrm{reg}\, h} \neq \emptyset$. Due to shape regularity (4.4), the number of elements in $\omega_h(T)$ is uniformly bounded w.r.t. h by some constant $N_{\mathcal{T}} = N_{\mathcal{T}}(R_{\mathcal{T}}) \in \mathbb{N}$, i.e.,

$$|\omega_h(T)| \leq N_{\mathcal{T}}.$$

Furthermore, there exists a constant $r_{\mathcal{T}} = r_{\mathcal{T}}(R_{\mathcal{T}}) \in (0, 1]$ such that

$$\mathcal{O}_{r_{\mathcal{T}} h_T}(\mathbf{x}) \cap \mathcal{O}_h \subset \omega_h(T) \tag{4.36}$$

for any $\mathbf{x} \in T$. Here $\mathcal{O}_r(\mathbf{x}) \subset \mathbb{R}^3$ is the ball of radius $r > 0$ centered at $\mathbf{x}$, and $\mathcal{O}_h$ is defined in (4.5).

Fix some $\mathbf{x}_0 \in \Gamma_T$ and let $L_0 \coloneqq \mathbf{x}_0 + T_{\mathbf{x}_0}\Gamma$ be the tangent plane corresponding to the tangent space of Γ at $\mathbf{x}_0$, see (2.4), with the normal vector $\mathbf{n}_0 \perp T_{\mathbf{x}_0}\Gamma$,

$$\mathbf{P}_0 \coloneqq \mathbf{I} - \mathbf{n}_0 \otimes \mathbf{n}_0, \quad \mathbf{P}_0^{\perp} \coloneqq \mathbf{n}_0 \otimes \mathbf{n}_0.$$

Let T_0 be the orthogonal projection of T on the plane L_0, i.e.,

$$T_0 \coloneqq \{\mathbf{x} - \mathbf{P}_0^{\perp}(\mathbf{x} - \mathbf{x}_0) : \mathbf{x} \in T\} \subset L_0.$$

We have

$$\left\| \left(\mathbf{x} - \mathbf{P}_0^{\perp}(\mathbf{x} - \mathbf{x}_0)\right) - \mathbf{x}_0 \right\| = \|\mathbf{P}_0(\mathbf{x} - \mathbf{x}_0)\| \leq \|\mathbf{P}_0\| \, \|\mathbf{x} - \mathbf{x}_0\| = \|\mathbf{x} - \mathbf{x}_0\| \leq h_T$$

for $\mathbf{x} \in T$, i.e., $T_0 \subset \mathcal{O}_{h_T}(\mathbf{x}_0)$. For h_T sufficiently small the surface can be represented as a graph over T_0, i.e., there exists a height function $g : T_0 \to \mathbb{R}$ such that

$$\{\mathbf{x} + g(\mathbf{x})\mathbf{n}_0 : \mathbf{x} \in T_0\}$$

is a subset of Γ. We set $\mathbf{g}(\mathbf{x}) \coloneqq \mathbf{x} + g(\mathbf{x})\mathbf{n}_0$ and write $\Gamma_0 \coloneqq \mathbf{g}(T_0) \subset \Gamma$. We have

$$\begin{aligned} g(\mathbf{x}_0) &= 0, \\ \|g\|_{L^\infty(T_0)} &\leq C_g h_T^2, \end{aligned} \tag{4.37}$$

with a constant C_g that depends only on the local smoothness of Γ. We assume that h_T is sufficiently small such that

$$C_g h_T \leq \frac{1}{2} r_{\mathcal{T}} \tag{4.38}$$

holds with $r_{\mathcal{T}}$ from (4.36). Consider a subset $\hat{T}_0 \subset T_0$ defined as

$$\hat{T}_0 \coloneqq \mathcal{O}_{\frac{1}{2} r_{\mathcal{T}} h_T}(\mathbf{x}_0) \cap T_0. \tag{4.39}$$

Note that the projection T_0 is either a triangle or a convex quadrilateral. From elementary geometry it follows that all interior angles of T_0 are bounded away from zero, and the lower bound depends only on the shape regularity (4.4). This implies that $\operatorname{area}(T_0) \simeq h_T^2$, and there exists a

constant $b_{\mathcal{T}} = b_{\mathcal{T}}(R_{\mathcal{T}}) > 0$ such that

$$\operatorname{area}\left(\mathcal{O}_{r\,h_T}(\mathbf{x}_0) \cap T_0\right) \geq b_{\mathcal{T}}\left(r\,h_T\right)^2$$

holds for any $r \in (0, 1]$. In particular, we have

$$\operatorname{area}\left(\hat{T}_0\right) \geq \frac{1}{4} b_{\mathcal{T}} r_{\mathcal{T}}^2 h_T^2. \tag{4.40}$$

We lift $\hat{T}_0$ to the surface,

$$\hat{\Gamma}_0 \coloneqq \mathbf{g}\left(\hat{T}_0\right) \subset \Gamma_0,$$

and estimate

$$\begin{aligned}
\|\mathbf{g}(\mathbf{x}) - \mathbf{x}_0\| &= \|\mathbf{x} + g(\mathbf{x})\mathbf{n}_0 - \mathbf{x}_0\| \leq \|\mathbf{x} - \mathbf{x}_0\| + |g(\mathbf{x})| \\
&\overset{(4.39)}{\leq} \frac{1}{2} r_{\mathcal{T}} h_T + |g(\mathbf{x})| \\
&\overset{(4.37)}{\leq} \frac{1}{2} r_{\mathcal{T}} h_T + C_g h_T^2 \\
&\overset{(4.38)}{\leq} r_{\mathcal{T}} h_T
\end{aligned}$$

for $\mathbf{x} \in \hat{T}_0$. Thus we have $\hat{\Gamma}_0 \subset \mathcal{O}_{r_{\mathcal{T}} h_T}(\mathbf{x}_0)$. Combining this with $\hat{\Gamma}_0 \subset \mathcal{O}_h$ and (4.36) yields

$$\hat{\Gamma}_0 \subset \omega_h(T) \quad \Rightarrow \quad \hat{\Gamma}_0 = \bigcup_{T' \in \omega_h(T)} \hat{\Gamma}_0 \cap T'.$$

Noting that $\operatorname{area}\left(\hat{\Gamma}_0\right) \geq \operatorname{area}\left(\hat{T}_0\right)$ and using (4.40), we get

$$\frac{1}{4} b_{\mathcal{T}} r_{\mathcal{T}}^2 h_T^2 \leq \operatorname{area}\left(\hat{\Gamma}_0\right) \leq N_{\mathcal{T}} \max_{T' \in \omega_h(T)} \operatorname{area}\left(\hat{\Gamma}_0 \cap T'\right) \leq N_{\mathcal{T}} \max_{T' \in \omega_h(T)} \operatorname{area}\left(\Gamma_0 \cap T'\right).$$

This implies that there exists $T' \in \omega_h(T)$ with $\operatorname{area}\left(\Gamma_0 \cap T'\right) \geq c_\omega h_T^2$,

$$c_\omega \coloneqq \frac{1}{4} N_{\mathcal{T}}^{-1} r_{\mathcal{T}}^2 b_{\mathcal{T}},$$

and the set of *local regular elements*

$$\omega_{\mathrm{reg}\,h}(T) \coloneqq \{T' \in \omega_h(T) : \mathrm{area}\,(T' \cap \Gamma_0) \geq c_\omega h_T^2\}$$

is not empty. Consider $T' \in \omega_{\mathrm{reg}\,h}(T)$. We have

$$\mathrm{area}\,(\Gamma_{T'}) = \mathrm{area}\,(T' \cap \Gamma) \geq \mathrm{area}\,(T' \cap \Gamma_0) \geq c_\omega h_T^2, \tag{4.41}$$

Note that due to (4.4) we have

$$h_T \geq \min_{K \in \mathcal{T}_h} h_K \geq R_{\mathcal{T}}^{-1} \max_{K \in \mathcal{T}_h} h_K \geq R_{\mathcal{T}}^{-1} h_{T'},$$
$$\mathrm{area}\,(\Gamma_{T'}) \geq c_\omega R_{\mathcal{T}}^{-2} h_{T'}^2.$$

With $c_{\mathrm{reg}} \coloneqq c_\omega R_{\mathcal{T}}^{-2}$ in the definition (4.34) of $\mathcal{T}_{\mathrm{reg}\,h}$ we have $T' \in \mathcal{T}_{\mathrm{reg}\,h}$, or

$$\omega_{\mathrm{reg}\,h}(T) \subset \mathcal{T}_{\mathrm{reg}\,h}.$$

This and $\omega_{\mathrm{reg}\,h} \subset \omega_h(T)$ yields

$$\omega_{\mathrm{reg}\,h} \subset \omega_h(T) \cap \mathcal{T}_{\mathrm{reg}\,h} \neq \emptyset.$$

Next we show (4.35). Consider $q \in Q_h$. The surface Γ_0 is the graph of a function g on T_0. Hence, there is a subset $S \subset T_0$ such that

$$T' \cap \Gamma_0 = \mathbf{g}\,(S)\,.$$

Using the surface area formula for the graph and (4.41) we get

$$c_\omega h_T^2 \leq \mathrm{area}\,(T' \cap \Gamma_0) = \int_S \sqrt{1 + \|\nabla_{T_0} g\|^2}\,\mathrm{d}s \leq \sqrt{1 + \max_S \|\nabla_{T_0} g(\cdot)\|^2}\,\mathrm{area}\,(S)\,.$$

Since the surface is tangent to T_0 at $\mathbf{x}_0$, we have $\nabla_{T_0} g(\mathbf{x}_0) = \mathbf{0}$. This and C^2-smoothness of the

surface imply $\|\nabla_{T_0} g\|_{L^\infty(T_0)} \lesssim h$, and hence

$$c_{\mathrm{reg}} h_T^2 \leq (1 + ch^2)\,\mathrm{area}\,(S)\,, \qquad \mathrm{area}\,(S) \gtrsim h_T^2.$$

For the perimeter of S we have

$$\mathrm{length}\,(S) \lesssim \mathrm{length}\,(\partial(T' \cap \Gamma_0)) \lesssim h_T.$$

Since $T' \cap \Gamma$ is simply-connected, so is $T' \cap \Gamma_0$ and S, and there exists a disc $D_S \subset S$ such that

$$\mathrm{radius}(D_S) \gtrsim h_T. \tag{4.42}$$

Let C_S be a corresponding cylinder,

$$C_S \coloneqq \{\mathbf{x} + \alpha \mathbf{n}_0 : \mathbf{x} \in D_S,\ \alpha \in \mathbb{R}\}.$$

Due to $D_S \subset T_0$, (4.42), and the shape regularity (4.4) one can inscribe a ball $B_T \subset C_S \cap T$ such that $\mathrm{radius}(B_T) \gtrsim h_T$, see Figure 3. By a standard scaling and norm equivalence argument it follows that

$$\|q\|_{L^2(T)} \lesssim \|q\|_{L^2(B_T)}$$

holds. Using this we obtain

$$\begin{aligned}
\|q\|^2_{L^2(T)} &\lesssim \|q\|^2_{L^2(B_T)} \lesssim \|q\|^2_{L^2(C_S \cap T)} \lesssim \|q\|^2_{L^2(C_S \cap \omega_h(T))} \\
&\lesssim h_T \|q\|^2_{L^2(T' \cap \Gamma_0)} + h_T^2 \|\mathbf{n}_0 \cdot \nabla q\|^2_{L^2(C_S \cap \omega_h(T))} \\
&\lesssim h_T \|q\|^2_{L^2(\Gamma_{T'})} + h_T^2 \|\mathbf{n}_0 \cdot \nabla q\|^2_{L^2(\omega_h(T))}\,.
\end{aligned}$$

Combining this with $h_T \|q\|_{L^2(\Gamma_{T'})} \lesssim \|q\|_{L^2(T')}$ (which follows from (4.25) and a finite element inverse inequality) and $\|\mathbf{n}_0 - \mathbf{n}(\mathbf{y})\| \lesssim h_T$ for all $\mathbf{y} \in \omega_h(T)$, we have

$$\|q\|^2_{L^2(T)} \lesssim \|q\|^2_{L^2(T')} + h_T^2 \|\mathbf{n} \cdot \nabla q\|^2_{L^2(\omega_h(T))} + h_T^4 \|\nabla q\|^2_{L^2(\omega_h(T))}\,,$$

which completes the proof. □

Remark 4.5 (On the neighboring estimate (4.35))**.** To see the improvement offered by (4.35) over available results, it is instructive to compare (4.35) to a local Sobolev inequality, which is proved by a different argument (Olshanskii, Reusken, and Grande 2009b, Lemma 3.1):

$$\|v\|_{L^2(T)} \leq \|v\|_{L^2(\omega_h(T))} \lesssim \|v\|_{L^2(T')} + h_T \|\nabla v\|_{L^2(\omega_h(T))} \tag{4.43}$$

for any $v \in H^1(\omega_h(T))$. The latter result holds for $v \in H^1(\omega_h(T))$, while in (4.35) we restrict to $q \in Q_h$. In (4.43) the first order term w.r.t. h_T contains the full gradient, whereas in (4.35) only the normal derivative is involved.

The following corollary is needed in the proof of Lemma 4.2 below.

Corollary 4.2. For any $T \in \mathcal{T}_h$ there exists $T' \in \omega_h(T) \cap \mathcal{T}_{\operatorname{reg} h}$ such that

$$\|\nabla q\|_{L^2(T)} \lesssim \|\nabla q\|_{L^2(T')} + \|\mathbf{n} \cdot \nabla q\|_{L^2(\omega_h(T))} + h_T \|\nabla q\|_{L^2(\omega_h(T))} \tag{4.44}$$

for $q \in Q_h$. Furthermore, for $\rho_p \gtrsim h$, and h sufficiently small we have

$$|q|^2_{1,h} \lesssim |q|^2_{1,\operatorname{reg} h} + s_n(q,q). \tag{4.45}$$

for $q \in Q_h$.

Proof. Take $T \in \mathcal{T}_h$ and the corresponding $T' \in \omega_h(T) \cap \mathcal{T}_{\operatorname{reg} h}$ as in Lemma 4.1. Take $q \in Q_h$ and define $c_0 := \int_{T'} q \, \mathrm{d}\mathbf{x} \,/\, \text{volume}\,(T')$. Using a local Poincaré inequality,

$$\|q - c_0\|_{L^2(T')} \lesssim h_T \|\nabla q\|_{L^2(T')},$$

with a finite element inverse inequality and (4.35) we obtain

$$\begin{aligned}\|\nabla q\|_{L^2(T)} &= \|\nabla(q - c_0)\|_{L^2(T)} \\ &\lesssim h_T^{-1} \|q - c_0\|_{L^2(T)} \\ &\lesssim h_T^{-1} \|q - c_0\|_{L^2(T')} + \|\mathbf{n} \cdot \nabla q\|_{L^2(\omega_h(T))} + h_T \|\nabla q\|_{L^2(\omega_h(T))} \\ &\lesssim \|\nabla q\|_{L^2(T')} + \|\mathbf{n} \cdot \nabla q\|_{L^2(\omega_h(T))} + h_T \|\nabla q\|_{L^2(\omega_h(T))} ,\end{aligned}$$

which is the desired estimate (4.44). Squaring and multiplying (4.44) by h_T, summing over $T \in \mathcal{T}_h$, and using a finite overlap property we obtain

$$\begin{aligned}|q|_{1,h}^2 &\leq C \left(|q|_{1,\operatorname{reg} h}^2 + s_n(q,q) + h^2 |q|_{1,h}^2 \right), \text{ or} \\ (1 - Ch^2) |q|_{1,h}^2 &\leq C \left(|q|_{1,\operatorname{reg} h}^2 + s_n(q,q) \right),\end{aligned}$$

with a constant C independent of the mesh size parameter h and position of Γ in the ambient mesh Ω_h. For $h < C^{-\frac{1}{2}}$ we have $1 - Ch^2 > 0$, so

$$|q|_{1,h}^2 \leq \frac{C}{1 - Ch^2} \left(|q|_{1,\operatorname{reg} h}^2 + s_n(q,q) \right)$$

Restricting h further, e.g, $h \leq (2C)^{-\frac{1}{2}} < C^{-\frac{1}{2}}$, yields

$$|q|_{1,h}^2 \leq 2C \left(|q|_{1,\operatorname{reg} h}^2 + s_n(q,q) \right),$$

and thus the result (4.45) holds for h sufficiently small. □

Lemma 4.2. For h sufficiently small, the condition ($\mathrm{LBB}_{1,h}$) is equivalent to

$$|q|_{1,\operatorname{reg} h} \lesssim \sup_{\mathbf{v} \in \mathbf{V}_h} \frac{b_T(\mathbf{v}, q)}{\|\mathbf{v}\|_A} + s_n^{\frac{1}{2}}(q,q) \qquad (\mathrm{LBB}_{1,\operatorname{reg} h})$$

for any $q \in Q_h$.

Proof. Clearly, ($\mathrm{LBB}_{1,h}$) implies ($\mathrm{LBB}_{1,\operatorname{reg} h}$). The reverse follows from (4.45). □

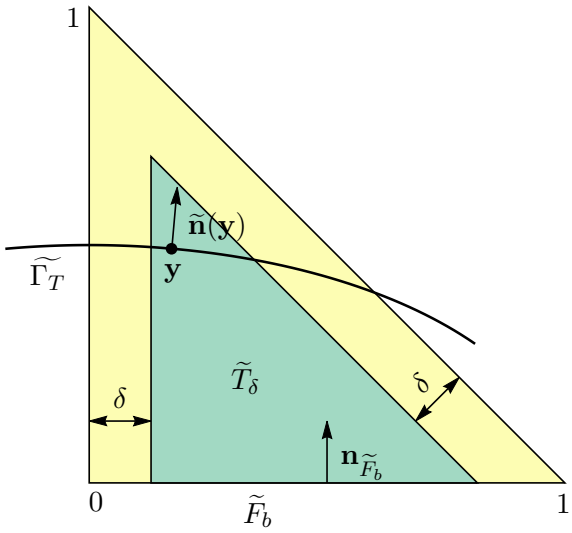

Figure 4: 2-dimensional illustration for the proof of Theorem 4.2: Reference triangle $\widetilde{T}$ (yellow), its base edge $\widetilde{F}_b$, and the corresponding reduced triangle $\widetilde{T}_\delta$ (green).

4.3.2 Well-posedness of Discrete Problem

We are now ready to derive the main result of the stability analysis. We show that the inf-sup stability condition ($\mathrm{LBB}_{1,\,\mathrm{reg}\,h}$) holds for the case of $\mathbf{P}_2$–P_1 trace finite elements (4.7). In the proof we construct a velocity function from $\mathbf{V}_h$, which delivers control over pressure gradients for all *regular* tetrahedra.

Theorem 4.2 (Well-posedness of the discrete problem)**.** Inf-sup stability condition (LBB_h) is satisfied for $\mathbf{P}_2$–P_1 trace finite element pair (4.7) with velocity penalty and stabilization parameters

$$\tau \lesssim h^{-2}, \quad \rho_u \lesssim h^{-1}, \quad \rho_p \gtrsim h,$$

and h sufficiently small.

Proof. Below we prove the statement for ($\mathrm{LBB}_{1,\,\mathrm{reg}\,h}$). Due to Lemmas 4.1 and 4.2 this implies (LBB_h) for h sufficiently small.

Let $\mathcal{E}_h(T)$ be a set of all edges of $T \in \mathcal{T}_h$, $|\mathcal{E}_h(T)| = 6$, and $\mathcal{E}_h \coloneqq \cup_{T\in\mathcal{T}_h}\mathcal{E}_h(T)$ be a set of all edges of $\mathcal{T}_h$. Similarly, we define $\mathcal{E}_{\mathrm{reg}\,h} \coloneqq \cup_{T\in\mathcal{T}_{\mathrm{reg}\,h}}\mathcal{E}_h(T)$ and $\mathcal{E}_{\mathrm{reg}\,h}(T) \coloneqq \mathcal{E}_{\mathrm{reg}\,h} \cap \mathcal{E}_h(T)$. Let $\mathbf{t}_E$ be a (normalized) vector connecting the two endpoints of $E \in \mathcal{E}_h$ and $\phi_E \in V_h^2$ be the quadratic nodal

finite element basis function associated with the middle point of E. For $q \in Q_h$ define $\mathbf{v} \in \mathbf{V}_h$ as follows:

$$\mathbf{v}(\mathbf{x}) \coloneqq \sum_{E \in \mathcal{E}_{\mathrm{reg}\, h}} h_E^2 \phi_E(\mathbf{x}) \left(\mathbf{t}_E \cdot \nabla q(\mathbf{x})\right) \mathbf{t}_E = \sum_{E \in \mathcal{E}_{\mathrm{reg}\, h}} h_E^2 \phi_E(\mathbf{x}) \left(\mathbf{t}_E \otimes \mathbf{t}_E\right) \nabla q(\mathbf{x}). \tag{4.46}$$

For $T \in \mathcal{T}_h$ we obtain

$$\begin{aligned}
\langle \mathbf{v}, \nabla_\Gamma q \rangle_{L^2(\Gamma_T)} &= \langle \mathbf{v}, \mathbf{P}\, \nabla q \rangle_{L^2(\Gamma_T)} \\
&= \sum_{E \in \mathcal{E}_{\mathrm{reg}\, h}(T)} \int_{\Gamma_T} h_E^2 \phi_E \left(|\, \mathbf{P}\, \mathbf{t}_E \cdot \nabla q|^2 + (\mathbf{P}^\perp \mathbf{t}_E \cdot \nabla q)(\mathbf{P}\, \mathbf{t}_E \cdot \nabla q) \right) \mathrm{d}s \\
&\geq \frac{1}{2} \sum_{E \in \mathcal{E}_{\mathrm{reg}\, h}(T)} \int_{\Gamma_T} h_E^2 \phi_E \left(|\, \mathbf{P}\, \mathbf{t}_E \cdot \nabla q|^2 - |\, \mathbf{P}^\perp \mathbf{t}_E \cdot \nabla q|^2 \right) \mathrm{d}s \\
&= \frac{1}{2} \sum_{E \in \mathcal{E}_{\mathrm{reg}\, h}} \int_{\Gamma_T} h_E^2 \phi_E \left(|\, \mathbf{P}\, \mathbf{t}_E \cdot \nabla q|^2 - |(\mathbf{n} \cdot \mathbf{t}_E) \cdot (\mathbf{n} \cdot \nabla q)|^2 \right) \mathrm{d}s \\
\text{Cauchy–Schwarz} \qquad &\geq \frac{1}{2} \sum_{E \in \mathcal{E}_{\mathrm{reg}\, h}(T)} \int_{\Gamma_T} h_E^2 \phi_E \left(|\, \mathbf{P}\, \mathbf{t}_E \cdot \nabla q|^2 - |\mathbf{n} \cdot \nabla q|^2 \right) \mathrm{d}s \\
\phi_E \leq 1,\, h_E \leq h_T,\, |\mathcal{E}_{\mathrm{reg}\, h}(T)| \leq 6 \qquad &\geq \frac{1}{2} \sum_{E \in \mathcal{E}_{\mathrm{reg}\, h}(T)} \int_{\Gamma_T} h_E^2 \phi_E \, |\mathbf{P}\, \mathbf{t}_E \cdot \nabla q|^2 \, \mathrm{d}s - 3 h_T^2 \, \|\mathbf{n} \cdot \nabla q\|_{L^2(\Gamma_T)}^2
\end{aligned}$$

Application of the local trace inequality (4.25) with $v \coloneqq \mathbf{n} \cdot \nabla q$ yields

$$\begin{aligned}
h_T \, \|\mathbf{n} \cdot \nabla q\|_{L^2(\Gamma_T)}^2 &\lesssim \|\mathbf{n} \cdot \nabla q\|_{L^2(T)}^2 + h_T^2 \, \|\mathbf{n} \cdot \nabla q\|_{H^1(T)}^2 \\
&= (1 + h_T^2) \, \|\mathbf{n} \cdot \nabla q\|_{L^2(T)}^2 + h_T^2 \, \|\nabla \left(\mathbf{n} \cdot \nabla q\right)\|_{L^2(T)}^2 \\
\Gamma \in C^2,\, \nabla^2 q\big|_T = \mathbf{0} \qquad &\lesssim \|\mathbf{n} \cdot \nabla q\|_{L^2(T)}^2 + h_T^2 \, \|\nabla q\|_{L^2(T)}^2 ,
\end{aligned}$$

and thus

$$\begin{aligned}
\langle \mathbf{v}, \nabla_\Gamma q \rangle_{L^2(\Gamma_T)} &\geq \frac{1}{2} \int_{\Gamma_T} \sum_{E \in \mathcal{E}_{\mathrm{reg}\, h}(T)} h_E^2 \phi_E \, |\mathbf{P}\, \mathbf{t}_E \cdot \nabla q|^2 \, \mathrm{d}s - \\
&\qquad c_{\mathrm{tr}} \left(h_T \, \|\mathbf{n} \cdot \nabla q\|_{L^2(T)}^2 + h_T^3 \, \|\nabla q\|_{L^2(T)}^2 \right), \text{ or} \\
\langle \mathbf{v}, \nabla_\Gamma q \rangle_{L^2(\Gamma_T)} + h_T \, \|\mathbf{n} \cdot \nabla q\|_{L^2(T)}^2 &\gtrsim \int_{\Gamma_T} \sum_{E \in \mathcal{E}_{\mathrm{reg}\, h}(T)} h_E^2 \phi_E \, |\mathbf{P}\, \mathbf{t}_E \cdot \nabla q|^2 \, \mathrm{d}s - c h_T^3 \, \|\nabla q\|_{L^2(T)}^2 .
\end{aligned} \tag{4.47}$$

We now restrict to $T \in \mathcal{T}_{\mathrm{reg}\, h} \;\Rightarrow\; \mathcal{E}_{\mathrm{reg}\, h}(T) = \mathcal{E}_h(T)$ and estimate the first term in (4.47). Note that $|\Gamma_T| \geq c_{\mathrm{reg}} h_T^2$ holds. Let $\widetilde{T}$ be a reference tetrahedron, see Figure 4, and $\mathbf{G} : \widetilde{T} \to T$ be an affine transformation mapping,

$$\mathbf{G}(\widetilde{\mathbf{x}}) = \mathbf{A}\, \widetilde{\mathbf{x}} + \mathbf{b}, \quad \mathbf{G}\left(\widetilde{T}\right) = T,$$

with some $\mathbf{b} \in \mathbb{R}^3$ and $\mathbf{A} \in \mathbb{R}^{3\times 3}$, $\det \mathbf{A} \neq 0$. Define $\widetilde{\Gamma_T} \coloneqq \mathbf{G}^{-1}(\Gamma_T)$ and $\widetilde{f} \coloneqq f \circ \mathbf{G}$ for a function $f : T \to \mathbb{R}$. Then we have

$$\int_{\Gamma_T} |f| \,\mathrm{d}s \geq c_0 h_T^2 \int_{\widetilde{\Gamma_T}} |\widetilde{f}| \,\mathrm{d}s, \qquad \mathrm{area}\left(\widetilde{\Gamma_T}\right) \geq c_1, \tag{4.48}$$

with constants $c_0 = c_0(R_{\mathcal{T}}) > 0$ and $c_1 = c_1(R_{\mathcal{T}}) > 0$ that depend only on the shape regularity property (4.4). For the normal vector $\widetilde{\mathbf{n}}$ on $\widetilde{\Gamma_T}$ we have

$$\widetilde{\mathbf{n}} = \frac{\mathbf{A}^T\, \mathbf{n} \circ \mathbf{G}}{\left\| \mathbf{A}^T\, \mathbf{n} \circ \mathbf{G} \right\|}.$$

Using $\|\mathbf{A}\| = \|\nabla\, \mathbf{G}\| \lesssim h$ and $\|\nabla \mathbf{n}\|_{L^\infty(\Gamma_T)} \lesssim 1$, we check that

$$\|\nabla \widetilde{\mathbf{n}}\|_{L^\infty\left(\widetilde{\Gamma_T}\right)} \lesssim h.$$

Normals on faces $\widetilde{F}$ of $\widetilde{T}$ are denoted by $\mathbf{n}_{\widetilde{F}}$. For these normals we take orientation the same as that of $\widetilde{\mathbf{n}}$ on $\widetilde{\Gamma_T}$. For $\widetilde{\Gamma_T}$ we choose a corresponding *base face* $\widetilde{F}_b$ as the one that fits best to $\widetilde{\Gamma_T}$ in the following sense:

$$\min_{\widetilde{\Gamma_T}} \left\| \widetilde{\mathbf{n}}(\cdot) - \mathbf{n}_{\widetilde{F}_b} \right\| \leq \min_{\widetilde{\Gamma_T}} \left\| \widetilde{\mathbf{n}}(\cdot) - \mathbf{n}_{\widetilde{F}} \right\|$$

for all faces $\widetilde{F}$ of $\widetilde{T}$, see Figure 4. We take a fixed $\epsilon > 0$ sufficiently small such that $\|\nabla \widetilde{\mathbf{n}}\|_{L^\infty(\widetilde{\Gamma_T})} \leq \epsilon$ holds, i.e., $\widetilde{\Gamma_T}$ is sufficiently close to a plane. This and the minimization property imply that for $\widetilde{F} \neq \widetilde{F}_b$ the angle between $\widetilde{\mathbf{n}}$ and $\mathbf{n}_{\widetilde{F}}$ is uniformly bounded below from zero. To see this, let $\widetilde{\mathbf{y}} \in \widetilde{\Gamma_T}$ be such that

$$\left\| \widetilde{\mathbf{n}}(\widetilde{\mathbf{y}}) - \mathbf{n}_{\widetilde{F}_b} \right\| = \min_{\widetilde{\Gamma_T}} \left\| \widetilde{\mathbf{n}}(\cdot) - \mathbf{n}_{\widetilde{F}_b} \right\|.$$

Then

$$\begin{aligned}\min_{\widetilde{\Gamma_T}} \left\|\widetilde{\mathbf{n}}(\cdot) - \mathbf{n}_{\widetilde{F}}\right\| &\geq \left\|\widetilde{\mathbf{n}}(\widetilde{\mathbf{y}}) - \mathbf{n}_{\widetilde{F}}\right\| - C\epsilon \\ &\geq \left\|\mathbf{n}_{\widetilde{F}_b} - \mathbf{n}_{\widetilde{F}}\right\| - \left\|\widetilde{\mathbf{n}}(\widetilde{\mathbf{y}}) - \mathbf{n}_{\widetilde{F}_b}\right\| - C\epsilon \\ &\gtrsim 1\end{aligned} \tag{4.49}$$

for sufficiently small ϵ.

For $\delta > 0$ sufficiently small we define a reduced tetrahedron

$$\widetilde{T}_\delta \coloneqq \{\mathbf{x} \in \widetilde{T} : \operatorname{dist}(\mathbf{x}, \partial\widetilde{T} \setminus \widetilde{F}_b) \geq \delta\} \subset \widetilde{T},$$

see Figure 4. Note that $\widetilde{T}_\delta$ depends on the base face $\widetilde{F}_b$. Thanks to (4.49) we can estimate

$$\operatorname{area}\left(\widetilde{\Gamma_T} \cap \left(\widetilde{T} \setminus \widetilde{T}_{\delta_0}\right)\right) \lesssim \delta.$$

Therefore, there exists $\delta_0 > 0$, sufficiently small, such that

$$\operatorname{area}\left(\widetilde{\Gamma_T} \cap \widetilde{T}_{\delta_0}\right) \geq \frac{1}{2} c_1$$

holds. Let E be an edge of the base face $F_b \coloneqq \mathbf{G}\left(\widetilde{F}_b\right)$ of T, $E \subset \overline{F_b}$, and ϕ_E the corresponding nodal basis function defined above. We have

$$\widetilde{\phi}_E \geq c_2 \delta_0 \tag{4.50}$$

in $\widetilde{T}_{\delta_0}$, with a suitable generic constant $c_2 > 0$. Thus we obtain

$$\begin{aligned}
\int_{\Gamma_T} \phi_E \,\mathrm{d}s &= \int_{\Gamma_T} |\phi_E| \,\mathrm{d}s \\
(4.48) \qquad &\geq c_0 h_T^2 \int_{\widetilde{\Gamma_T}} \left|\widetilde{\phi}_E\right| \mathrm{d}s \\
&\geq c_0 h_T^2 \int_{\widetilde{\Gamma_T} \cap \widetilde{T}_{\delta_0}} \left|\widetilde{\phi}_E\right| \mathrm{d}s \\
(4.50) \qquad &\geq c_0 c_2 \delta_0 h_T^2 \,\mathrm{area}\left(\widetilde{\Gamma_T} \cap \widetilde{T}_{\delta_0}\right) \\
&\geq \frac{1}{2} c_0 c_1 c_2 \delta_0 h_T^2, \text{ i.e.,} \\
\int_{\Gamma_T} \phi_E \,\mathrm{d}s &\gtrsim h_T^2.
\end{aligned} \tag{4.51}$$

Consider $\mathbf{x}_\star := \arg\min_{\Gamma_T} \|\mathbf{n}(\cdot) - \mathbf{n}_{F_b}\| \in \Gamma_T$ and the corresponding normal vector and projector

$$\mathbf{n}_\star := \mathbf{n}(\mathbf{x}_\star), \quad \mathbf{P}_\star := \mathbf{I} - \mathbf{n}_\star \otimes \mathbf{n}_\star.$$

We have $\|\mathbf{P}(\mathbf{x}) - \mathbf{P}_\star\| \lesssim h$ for $\mathbf{x} \in T$. Using this and (4.51) we can estimate the first term in (4.47) as

$$\begin{aligned}
\int_{\Gamma_T} \sum_{E \in \mathcal{E}_h(T)} h_E^2 \phi_E \left|\mathbf{P}\,\mathbf{t}_E \cdot \nabla q\right|^2 \mathrm{d}s &\gtrsim h_T^2 \sum_{E \subset \overline{F_b}} \int_{\Gamma_T} \phi_E \left|\mathbf{P}\,\mathbf{t}_E \cdot \nabla q\right|^2 \mathrm{d}s \\
&\gtrsim h_T^2 \sum_{E \subset \overline{F_b}} \left|\mathbf{P}_\star\,\mathbf{t}_E \cdot \nabla q|_T\right|^2 \int_{\Gamma_T} \phi_E \,\mathrm{d}s - c h_T^2 \|\nabla q\|_{L^2(T)}^2 \\
&\gtrsim h_T^4 \sum_{E \subset \overline{F_b}} \left|\mathbf{P}_\star\,\mathbf{t}_E \cdot \nabla q|_T\right|^2 - c h_T^2 \|\nabla q\|_{L^2(T)}^2 .
\end{aligned}$$

Due to construction of the base face F_b and the choice of $\mathbf{x}_\star$ we have that $|\mathbf{n}_\star \cdot \mathbf{n}_{F_b}|$ is uniformly bounded away from zero. This implies

$$\sum_{E \subset \overline{F_b}} \left|\mathbf{P}_\star\,\mathbf{t}_E \cdot \nabla q|_T\right|^2 = \sum_{E \subset \overline{F_b}} \left|\mathbf{t}_E \cdot \mathbf{P}_\star \nabla q|_T\right|^2 \gtrsim \left\|\mathbf{P}_\star \nabla q|_T\right\|^2,$$

and thus we get

$$\begin{aligned}
\int_{\Gamma_T} \sum_{E\in\mathcal{E}_h(T)} h_E^2 \phi_E \left|\mathbf{P}\,\mathbf{t}_E\cdot\nabla q\right|^2 \mathrm{d}s &\gtrsim h_T \left\|\mathbf{P}_\star \nabla q\right\|^2_{L^2(T)} - c h_T^2 \left\|\nabla q\right\|^2_{L^2(T)} \\
&\gtrsim h_T \left\|\mathbf{P}\,\nabla q\right\|^2_{L^2(T)} - c h_T^2 \left\|\nabla q\right\|^2_{L^2(T)} \\
&= h_T \left\|\nabla q\right\|^2_{L^2(T)} - h_T \left\|\mathbf{n}\cdot\nabla q\right\|^2_{L^2(T)} - c h_T^2 \left\|\nabla q\right\|^2_{L^2(T)} \\
&= h_T \left(1 - c h_T\right) \left\|\nabla q\right\|^2_{L^2(T)} - h_T \left\|\mathbf{n}\cdot\nabla q\right\|^2_{L^2(T)} \\
h_T < (2c)^{-1} \;\Rightarrow\; 1 - c h_T > \frac{1}{2} \qquad &> \frac{1}{2} h_T \left\|\nabla q\right\|^2_{L^2(T)} - h_T \left\|\mathbf{n}\cdot\nabla q\right\|^2_{L^2(T)}
\end{aligned}$$

Using this in (4.47) we obtain

$$\langle \mathbf{v}, \nabla_\Gamma q\rangle_{L^2(\Gamma_T)} + h_T \left\|\mathbf{n}\cdot\nabla q\right\|^2_{L^2(T)} \gtrsim h_T \left\|\nabla q\right\|^2_{L^2(T)} \tag{4.52}$$

for $T \in \mathcal{T}_{\mathrm{reg}}$ and h_T sufficiently small. Summing (4.52) over $T \in \mathcal{T}_{\mathrm{reg}}$ yields

$$\sum_{T\in\mathcal{T}_{\mathrm{reg}\,h}} \langle \mathbf{v}, \nabla_\Gamma q\rangle_{L^2(\Gamma_T)} + h_T \left\|\mathbf{n}\cdot\nabla q\right\|^2_{L^2(T)} \gtrsim |q|^2_{1,\,\mathrm{reg}\,h}\,.$$

Now, using $\rho_p \gtrsim h$ and noting that replacing $\sum_{T\in\mathcal{T}_{\mathrm{reg}\,h}}$ with $\sum_{T\in\mathcal{T}_h}$ makes the l.h.s. of the above inequality bigger and the r.h.s. smaller conclude that

$$b_T(\mathbf{v}, q) + s_n(q, q) \gtrsim |q|^2_{1,\,\mathrm{reg}\,h} \tag{4.53}$$

holds for h sufficiently small.

We need the following elementary observation: For positive numbers x, y, z the inequality $x + y^2 \geq c z^2$ implies

$$\begin{aligned}
x + y(y+z) &\geq \min\{c, 1\}\, z (y+z), \\
\frac{x}{y+z} + y &\geq \min\{c, 1\}\, z.
\end{aligned}$$

Using this, the estimate (4.53) implies

$$\frac{b_T(\mathbf{v},q)}{|q|_{1,\,\mathrm{reg}\,h}+s_n^{\frac{1}{2}}(q,q)}+s_n^{\frac{1}{2}}(q,q)\gtrsim|q|_{1,\,\mathrm{reg}\,h}\,. \tag{4.54}$$

It remains to estimate $\|\mathbf{v}\|_A$. We consider term-by-term the contributions in $\|\mathbf{v}\|_A^2$. Noting $\|\nabla\phi_E\|_{L^\infty(T)}\lesssim h_T^{-1}$ for $E\subset\overline{T}$ and (4.25) we get

$$\begin{aligned}
2\nu\,\|\mathbf{E}(\mathbf{v}_T)\|_0^2+\alpha\,\|\mathbf{v}\|_0^2&\lesssim\|\mathbf{E}(\mathbf{v})-u_N\,\mathbf{H}\|_0^2+\|\mathbf{v}\|_0^2\\
\Gamma\in C^2\qquad&\lesssim\|\mathbf{E}(\mathbf{v})\|_0^2+\|\mathbf{v}\|_0^2\\
&\lesssim\sum_{T\in\mathcal{T}_h}\|\nabla\mathbf{v}\|_{L^2(\Gamma_T)}^2+\|\mathbf{v}\|_{L^2(\Gamma_T)}^2\\
&\lesssim\sum_{T\in\mathcal{T}_h}h_T^2\,\|\nabla q\|_{L^2(\Gamma_T)}^2\\
&\lesssim\sum_{T\in\mathcal{T}_h}h_T\,\|\nabla q\|_{L^2(T)}^2\\
&=:|q|_{1,\,h}^2\,.
\end{aligned} \tag{4.55}$$

We also have for $\tau\lesssim h^{-2}$ and $\rho_u\lesssim h^{-1}$ the relations

$$\begin{aligned}
\tau\,\|v_N\|_0^2\le\tau\,\|\mathbf{v}\|_0^2&=\tau\sum_{T\in\mathcal{T}_h}\|\mathbf{v}\|_{L^2(\Gamma_T)}^2\\
&\lesssim\tau\sum_{T\in\mathcal{T}_h}h_T^4\,\|\nabla q\|_{L^2(\Gamma_T)}^2\\
&\lesssim\tau\sum_{T\in\mathcal{T}_h}h_T^3\,\|\nabla q\|_{L^2(T)}^2\\
&\lesssim|q|_{1,\,h}^2\,,
\end{aligned} \tag{4.56}$$

and

$$\rho_u\,\|(\nabla\mathbf{v})\,\mathbf{n}\|_{L^2(\mathcal{O}_h)}^2\le\rho_u\sum_{T\in\mathcal{T}_h}\|\nabla\mathbf{v}\|_{L^2(T)}^2\lesssim\rho_u\sum_{T\in\mathcal{T}_h}h_T^2\,\|\nabla q\|_{L^2(T)}^2\lesssim|q|_{1,\,h}^2\,. \tag{4.57}$$

From (4.55)–(4.57) we conclude that $\|\mathbf{v}\|_A\lesssim|q|_{1,\,h}$, and using (4.45) we get

$$\|\mathbf{v}\|_A\lesssim|q|_{1,\,\mathrm{reg}\,h}+s_n^{\frac{1}{2}}(q,q).$$

Combining this with (4.54) completes the proof. □

4.4 A Priori Error Estimates

We consider $\mathbf{P}_2$–P_1 trace finite element pair (4.7). Based on the stability result in Theorem 4.2 an error analysis can be derived with standard arguments combining stability, consistency and interpolation results. See, e.g., (Brezzi and Fortin 2012) for general treatment of saddle-point problems, and (Olshanskii, Quaini, Reusken, and Yushutin 2018) for more specific analysis of the surface Stokes problem. We outline the arguments below and skip most of the details that can be found elsewhere.

First, we introduce the following bilinear form:

$$\mathbf{A}\left((\mathbf{u},p),(\mathbf{v},q)\right) \coloneqq A(\mathbf{u},\mathbf{v}) + b_T(\mathbf{v},p) + b_T(\mathbf{u},q) - s_n(p,q).$$

Then the discrete problem (4.12) has a compact representation: Find $(\mathbf{u}_h, p_h) \in \mathbf{V}_h \times Q_h$ such that

$$\mathbf{A}\left((\mathbf{u}_h,p_p),(\mathbf{v}_h,q_h)\right) = \langle \mathbf{f}_T, \mathbf{v}_h\rangle_0$$

holds for all $(\mathbf{v}_h, q_h) \in \mathbf{V}_h \times Q_h$. This discrete problem has a unique solution, which is denoted by $(\mathbf{u}_h^\star, p_h^\star)$. Due to consistency (4.18), the solution $(\mathbf{u}_T^\star, p^\star)$ of (3.20) satisfies

$$\mathbf{A}\left((\mathbf{u}_T^\star,p^\star),(\mathbf{v}_h,q_h)\right) = \langle \mathbf{f}_T, \mathbf{v}_h\rangle_0 ,$$

and we obtain the Galerkin orthogonality relation:

$$\mathbf{A}\left((\mathbf{u}_T^\star - \mathbf{u}_h^\star, p^\star - p_h^\star),(\mathbf{v}_h,q_h)\right) = 0$$

holds for any $(\mathbf{v}_h, q_h) \in \mathbf{V}_h \times Q_h$.

The inf-sup stability (LBB_h), coercivity of A, and the Galerkin orthogonality results yield the usual bound for the discretization error in terms of an approximation error in the problem-

dependent norms,

$$\|\mathbf{u}_T^\star - \mathbf{u}_h^\star\|_A + \|p^\star - p_h^\star\|_h \lesssim \inf_{(\mathbf{v}_h, q_h)\in \mathbf{V}_h \times Q_h} \left(\|\mathbf{u}_T^\star - \mathbf{v}_h\|_A + \|p^\star - q_h\|_h\right). \tag{4.58}$$

Employing standard interpolation estimates for $\mathbf{P}_2$ and P_1 trace finite elements (Reusken 2015; Olshanskii and Reusken 2017) and assuming the necessary smoothness of $(\mathbf{u}_T^\star, p^\star)$, we get an estimate for the right-hand side of (4.58):

$$\inf_{(\mathbf{v}_h, q_h)\in \mathbf{V}_h \times Q_h} \left(\|\mathbf{u}_T^\star - \mathbf{v}_h\|_A + \|p^\star - q_h\|_h \right) \lesssim h^2 \left(\|\mathbf{u}_T^\star\|_3 + \|p^\star\|_2\right). \tag{4.59}$$

For the $O(h^2)$-bound in (4.59) to hold, it is sufficient to assume the following bounds for the parameters entering definitions of $\|\cdot\|_A$ and $\|\cdot\|_h$ norms:

$$\tau \lesssim h^{-2}, \quad \rho_u \lesssim h^{-1}, \quad \rho_p \lesssim h.$$

Combining these restrictions with those needed for stability and algebraic conditioning, we conclude that, for the parameters satisfying (4.16), equations (4.58) and (4.59) yield the optimal error estimate in the problem-dependent norm

$$\|\mathbf{u}_T^\star - \mathbf{u}_h^\star\|_A + \|p^\star - p_h^\star\|_h \lesssim h^2 \left(\|\mathbf{u}_T^\star\|_3 + \|p^\star\|_2\right). \tag{4.60}$$

The definition of $\|\cdot\|_A$ and $\|\cdot\|_h$ norms and (4.60) together give

$$\|\mathbf{u}_T^\star - \mathbf{P}\,\mathbf{u}_h^\star\|_1 + \|p^\star - p_h^\star\|_0 \lesssim h^2 \left(\|\mathbf{u}_T^\star\|_3 + \|p^\star\|_2\right),$$
$$\|\mathbf{u}_h^\star \cdot \mathbf{n}\|_0 \lesssim h^3 \left(\|\mathbf{u}_T^\star\|_3 + \|p^\star\|_2\right).$$

A duality argument can be applied, see (Olshanskii, Quaini, Reusken, and Yushutin 2018). It results in the optimal error bound in the surface L^2-norm for the velocity:

$$\|\mathbf{u}_T^\star - \mathbf{P}\,\mathbf{u}_h^\star\|_0 \lesssim h^3 \left(\|\mathbf{u}_T^\star\|_3 + \|p^\star\|\right)_2.$$

5 DESIGN OF ITERATIVE SOLVER

Augmented Lagrangian (AL) preconditioning is a potent technique that has been developed to solve some highly non-symmetric algebraic systems having a saddle point structure (Benzi and Olshanskii 2006; Niet and Wubs 2007; Olshanskii and Benzi 2008; ur Rehman, Vuik, and Segal 2008; Benzi, Olshanskii, and Wang 2011; He, Neytcheva, and Capizzano 2011; Börm and Borne 2012; Heister and Rapin 2013; He, Vuik, and Klaij 2018; Moulin, Jolivet, and Marquet 2019; Farrell and Gazca-Orozco 2020). The need to treat such problems numerically emerges from the discretization of systems of PDEs describing the motion of incompressible viscous fluid with dominating inertia effects.

Adopting the terminology of fluid mechanics, the AL-approach augments the velocity subproblem of the system using a suitably weighted incompressibility constraint. This leads to a well conditioned pressure Schur complement matrix, but makes the velocity submatrix more difficult to solve or to precondition. Already in the original work (Benzi and Olshanskii 2006) a special multigrid method has been used to overcome the difficulty associated with preconditioning the velocity block, and recently this technique was extended in (Farrell, Mitchell, and Wechsung 2019; Farrell, Mitchell, Scott, and Wechsung 2021). Nevertheless, the specialized multilevel approach is efficient only if a hierarchy of nested discretizations is available and only for certain finite element velocity–pressure pairs.

In this Chapter we advocate a more general (but still efficient) way to handle the velocity subproblem in the AL-approach. The proposed method consists of computing a (possibly incomplete) LU-factorization of the velocity block (or its subblocks) with further recycling of the factors over several time steps. The factorization can be updated when the velocity field variations significantly change the inertia term in the equations. A simpler strategy adopted here consists of updating preconditioner when the number of outer iterations exceeds a threshold. We shall see that for realistic unsteady 2D flows this results in a very efficient approach, which is robust with respect to the Reynolds number and calls for only a small number of full factorizations over a long-time simulation.

Employing matrix factorizations in algebraic solvers for equations governing the flow of viscous incompressible fluids is not a new theme. It is standard to factorize the discrete pressure Poisson equation. More recently, studies were done regarding different strategies to perform incomplete LU-factorization of the coupled systems for velocity and pressure (Segal, ur Rehman, and Vuik 2010; Dahl and Wille 1992; Konshin, Olshanskii, and Vassilevski 2015; Konshin, Olshanskii, and Vassilevski 2017). We note that the latter cannot be done with the help of position-based incomplete LU, since the pressure block in the matrix may be zero. The augmented Lagrangian approach provides a framework to apply factorization only to the velocity matrix, while retaining the overall excellent preconditioning properties. The velocity matrix results from the discretization of an elliptic part of the system. Therefore, it is typically a positive definite matrix, and LU-factorization is stable without any preprocessing.

Large scale 3D simulations lead to algebraic systems which are still too expensive to factorize exactly and alternative ways of treating the velocity submatrix, e.g., based on geometric/algebraic multigrid, domain decomposition methods, or incomplete factorization can be more feasible and practical. The situation is different for 2D problems, where acceptable resolution is often achieved using the number of degrees of freedom (d.o.f.) affordable by state-of-the-art direct solvers executed on a desktop machine.

5.1 Grad-div Stabilization and Saddle Point System of Linear Algebraic Equations

We proceed by designing an efficient linear solver for a linear system arising from the finite element discretization (4.12) of the surface problem (3.6) from Section 4.2. We start by introducing a stabilized version of the weak problem (4.12). Material in the current chapter extends the work (Olshanskii and **Zhiliakov** 2020).

In order to increase the finite element solution accuracy and improve the performance of the algebraic solver for the case of dominating convection, $\nu \ll 1$, we stabilize (3.20) by including a grad-div type stabilization (Olshanskii and Reusken 2004). Choosing the test function $q \coloneqq \operatorname{div}_\Gamma \mathbf{v}_T = \operatorname{tr} \mathbf{E}(\mathbf{v}_T)$ in the second equation of (3.20), adding it to the first one, and sub-

stituting discrete (4.7) spaces for test and trial spaces, we end up with a stabilized trace FEM: Find $(\mathbf{u}_h, p_h) \in \mathbf{V}_h \times Q_h$ such that

$$\begin{aligned} \underbrace{A(\mathbf{u}_h, \mathbf{v}_h) + \gamma \langle \operatorname{tr} \mathbf{E}(\mathbf{u}_h), \operatorname{tr} \mathbf{E}(\mathbf{v}_h) \rangle_0}_{A_\gamma(\mathbf{u}_h, \mathbf{v}_h) \coloneqq} + b_T(\mathbf{v}_h, q_h) &= \langle \mathbf{f}_T, \mathbf{v}_h \rangle_0 \,, \\ b_T(\mathbf{u}_h, q_h) - s_n(p_h, q_h) &= 0 \end{aligned} \tag{5.1}$$

holds for all $(\mathbf{v}_h, q_h) \in \mathbf{V}_h \times Q_h$. Here we introduced an additional stabilization bilinear form,

$$\gamma \langle \operatorname{tr} \mathbf{E}(\mathbf{u}_h), \operatorname{tr} \mathbf{E}(\mathbf{v}_h) \rangle_0 \,, \tag{5.2}$$

with a parameter $\gamma \geq 0$. Since

$$\langle \operatorname{tr} \mathbf{E}(\mathbf{u}_T^\star), q \rangle_0 = 0$$

holds for the true solution of (3.20) and any $q \in L^2(\Gamma)$, the term (5.2) vanishes if one substitutes $\mathbf{u}_h$ with $\mathbf{u}_T^\star$. Thus the stabilized method (5.1) is consistent.

Since $A_\gamma(\mathbf{v}, \mathbf{v}) \geq A(\mathbf{v}, \mathbf{v})$ for $\mathbf{v} \in \mathbf{V}_h$, A_γ is coercive. Note that

$$\begin{aligned} \|\operatorname{tr} \mathbf{E}(\mathbf{v})\|_0 &= \|\operatorname{tr} \mathbf{E}(\mathbf{v}_T) + v_N \kappa\|_0 \\ \overset{(3.14)}{} \quad &\leq \sqrt{2} \, \|\mathbf{E}(\mathbf{v}_T)\|_0 + \|\kappa\|_\infty \, \|v_N\|_0 \\ \Gamma \in C^2 \quad &\lesssim \|\mathbf{E}(\mathbf{v}_T)\|_0 + \|\mathbf{v}\|_0 \\ &\lesssim \|\mathbf{v}\|_A \end{aligned}$$

for $\mathbf{v} \in \mathbf{V}_h$, and hence A_γ is continuous.

Corollary 5.1. For $\mathbf{P}_2$–P_1 trace finite elements (4.7) the grad-div stabilized problem (5.1) is well-posed in $\left(\|\cdot\|_A^2 + \|\cdot\|_h^2 \right)^{\frac{1}{2}}$, and the error estimates from Section 4.4 hold. We note that the constants in the stability and error estimates depend on parameters ν, γ, and α as studied in (Olshanskii and Reusken 2004).

Let $n_u \coloneqq \dim \mathbf{V}_h$ and $n_p \coloneqq \dim Q_h$. We now turn to the matrix form of the discretized surface

Oseen system and define the velocity, pressure stabilization, and divergence matrices as

$$\begin{aligned} \mathbf{A}_{ij} &\coloneqq A_\gamma(\boldsymbol{\psi}_j, \boldsymbol{\psi}_i), \quad 1 \le i,\ j \le n_u, \\ (\mathbf{C}_\star)_{ij} &\coloneqq s_\star(\psi_j, \psi_i), \quad 1 \le i,\ j \le n_p, \\ \mathbf{B}_{ij} &\coloneqq b_T(\boldsymbol{\psi}_j, \psi_i), \quad 1 \le i \le n_p,\ 1 \le j \le n_u, \end{aligned} \tag{5.3}$$

where $\{\boldsymbol{\psi}_i\}_{i=1,\dots,n_u}$ and $\{\psi_i\}_{i=1,\dots,n_p}$ are the velocity and pressure nodal basis functions spanning $\mathbf{V}_h$ and Q_h, respectively, and $\star \in \{0, n, \text{full}\}$ is a choice of pressure stabilization:

1. absence of stabilization, i.e.,

$$s_0 \coloneqq 0,$$

   implying that $\mathbf{C}_0$ is a zero matrix,

2. the normal derivative stabilization s_n from (4.10b), and

3. the full-gradient stabilization s_{full} from (4.22).

After arranging velocity degrees of freedom (d.o.f.) first and pressure d.o.f. next, we arrive at the system

$$\underbrace{\begin{pmatrix} \mathbf{A} & \mathbf{B}^T \\ \mathbf{B} & -\mathbf{C}_\star \end{pmatrix}}_{\boldsymbol{\mathcal{A}}_\star \coloneqq} \begin{pmatrix} \vec{\mathbf{u}} \\ \vec{\mathbf{p}} \end{pmatrix} = \begin{pmatrix} \vec{\mathbf{f}} \\ \vec{\mathbf{0}} \end{pmatrix}. \tag{5.4}$$

with the (2×2)-block matrix $\boldsymbol{\mathcal{A}}_\star \in \mathbb{R}^{(n_u+n_p)\times(n_u+n_p)}$, two vectors of unknowns $\vec{\mathbf{u}} \in \mathbb{R}^{n_u}$ and $\vec{\mathbf{p}} \in \mathbb{R}^{n_p}$ corresponding to the finite element functions $\mathbf{u}_h$ and p_h in (4.12), respectively, i.e.,

$$\mathbf{u}_h(\mathbf{x}) = \sum_{i=1}^{n_u} \vec{\mathbf{u}}_i \boldsymbol{\psi}_i(\mathbf{x}), \quad p_h(\mathbf{x}) = \sum_{i=1}^{n_p} \vec{\mathbf{p}}_i \psi_i(\mathbf{x}), \tag{5.5}$$

and the right-hand side vectors $\vec{\mathbf{0}} \in \mathbb{R}^{n_p}$ and $\vec{\mathbf{f}} \in \mathbb{R}^{n_u}$,

$$\vec{\mathbf{f}}_i \coloneqq \int_\Gamma \mathbf{f}_T \cdot \boldsymbol{\psi}_i \, \mathrm{d}s, \quad 1 \le i \le n_u.$$

The resulting system (5.4) of linear algebraic equations is non-symmetric and of saddle-point

type with properties resembling those of the $\mathbb{R}^d$-Oseen system, a well-studied problem. See, e.g., (Benzi, Golub, and Liesen 2005; Elman, Silvester, and Wathen 2005). In particular, the problem is increasingly hard to solve for $\nu \ll 1$. One way to avoid this increasing complexity of the linear algebra system is to lag the entire inertia term in time, e.g., to replace the second term in (4.1) with $(\nabla_\Gamma \mathbf{w}^k)\mathbf{w}^k$, ending up with a symmetric Stokes-type problem, same on each time step. However, numerical stability of such implicit-explicit scheme is known to impose a time step restriction of the form

$$\Delta t \leq C(\nu) h^d,$$

where $d = 2$ for two-dimension flows, and $C(\nu)$ decreasing for $\nu \to 0$, see (Temam 2001).

This leads to a serious growth of computational costs for small h and ν despite the ease of linear algebra. In contrast, (4.1) is unconditionally stable with approximation analysis suggesting $\Delta t \simeq h$, see (Girault and Raviart 2012), and our strategy here is to alleviate computational costs by employing a more sophisticated linear algebra solver re-enforced by a recycling algorithm.

5.2 Augmented Lagrangian Preconditioner

An important matrix related to the above system is the pressure Schur complement

$$\mathbf{S} \coloneqq \mathbf{B}\,\mathbf{A}^{-1}\,\mathbf{B}^T + \mathbf{C}_\star, \tag{5.6}$$

which results after elimination of the velocity unknowns from the system. A preconditioner for $\mathbf{S}$ is a necessary ingredient for most iterative solvers that exploit the block structure of $\boldsymbol{\mathcal{A}}_\star$. Following a common practice (Elman, Silvester, and Wathen 2005) we consider the block-triangle right preconditioner for $\boldsymbol{\mathcal{A}}_\star$:

$$\boldsymbol{\mathcal{P}} \coloneqq \begin{pmatrix} \widehat{\mathbf{A}} & \mathbf{B}^T \\ & \widehat{\mathbf{S}} \end{pmatrix}, \tag{5.7}$$

where $\widehat{\mathbf{A}}$ and $\widehat{\mathbf{S}}$ are preconditioners for $\mathbf{A}$ and $\mathbf{S}$, respectively.

5.2.1 Bounds for Eigenvalues of Preconditioned Schur Complement

We continue with the design of the Schur complement preconditioner $\widehat{\mathbf{S}}$. Consider the surface pressure mass matrix $\mathbf{M}_p$ and the pressure Laplace–Beltrami matrix $\mathbf{L}_p$ defined as

$$\begin{aligned} (\mathbf{M}_p)_{ij} &\coloneqq \int_\Gamma \psi_j \psi_i \,\mathrm{d}s, \\ (\mathbf{L}_p)_{ij} &\coloneqq \int_\Gamma \nabla_\Gamma \psi_j \cdot \nabla_\Gamma \psi_i \,\mathrm{d}s, \quad 1 \le i,j \le n_p. \end{aligned} \tag{5.8}$$

For the surface Stokes problem ($\alpha = 0$, $\mathbf{w} = \mathbf{0}$, $\gamma = 0$, $\nu = 1$), the discrete inf-sup condition (LBB_h) implies that the matrix $\mathbf{S}$ is spectrally equivalent to the stabilized pressure mass matrix $\mathbf{M}_p + \mathbf{C}_\star$. However, for $\mathbf{w} \neq \mathbf{0}$, $\gamma = 0$, and $\nu \to 0$ the problem of building a suitable preconditioner for $\mathbf{S}$ is known to be particular difficult. To circumvent it, the authors of (Benzi and Olshanskii 2006) introduced an augmentation to the $(1,1)$-block of the system replacing $\mathbf{A}$ with $\mathbf{A} + \gamma\, \mathbf{B}^T\, \mathbf{M}_p^{-1}\, \mathbf{B}$. Such augmentation is not algebraically consistent in our case due to presence of stabilization, i.e.,

$$\mathbf{C}_\star \neq \mathbf{0} \quad \Rightarrow \quad \mathbf{B}\,\vec{\mathbf{u}} \neq \vec{\mathbf{0}}.$$

We note that $\mathbf{C}_\star \neq \mathbf{0}$ is a typical situation for many unfitted *inf-sup stable* FEM discretizations of the (Navier–)Stokes equations (both in volumes and on surfaces) as well as for stabilized elements (Benzi and Wang 2011). Hence, we suggest to introduce an augmentation on the finite element level, i.e., to add the grad-div term (5.2).

For the planar Oseen problem discretized with standard $\mathbf{P}_2$–P_1 elements one can show that the Schur complement of the algebraically augmented matrix is spectrally equivalent to the pressure mass matrix scaled by $(\gamma + \nu)^{-1}$ for sufficiently large γ, see (Benzi and Olshanskii 2006). We show that similar property holds for the trace finite elements when the algebraic augmentation is replaced by the grad-div stabilization (5.2), i.e., the augmentation term is not of the form $\gamma\, \mathbf{B}^T\, \mathbf{M}_p^{-1}\, \mathbf{B}$.

Since the grad-div stabilization does not deliver the algebraic structure of the augmented Lagrangian as in (Benzi and Olshanskii 2006; Benzi, Olshanskii, and Wang 2011), we cannot make use of the Sherman–Morrison–Woodbury formula or similar representations of the pressure Schur com-

plement of the augmented system. Therefore, we base our proof of the result below on a different argument.

Theorem 5.1 (Bounds for eigenvalues of preconditioned Schur complement)**.** Let

$$\mathbf{S}_M \coloneqq (\nu+\gamma)^{-1}\,\mathbf{M}_p + \mathbf{C}_\star\,. \tag{5.9}$$

Then the eigenvalues $\{\lambda\}$ of the generalized (i.e., preconditioned) Schur complement eigenvalue problem

$$\mathbf{S}\,\vec{\mathbf{p}} = \lambda\,\mathbf{S}_M\,\vec{\mathbf{p}} \tag{5.10}$$

satisfy

$$|\lambda| \le \frac{\nu+\gamma}{\gamma}. \tag{5.11}$$

Moreover, for $\star \neq 0$ (i.e., stable discretization), $\alpha = 1$, and $\nu \le 1$ we have

$$\frac{\nu+\gamma}{\nu^{-1}+\gamma} \lesssim \Re(\lambda), \tag{5.12}$$

with a constant embedded in $\lesssim$, see (4.15), independent of parameters ν and γ.

Proof. Since $\mathbf{S}_M = \mathbf{S}_M^T > 0$, there exists $\mathbf{S}_M^{\frac{1}{2}} = \left(\mathbf{S}_M^{\frac{1}{2}}\right)^T > 0$ so that

$$\begin{aligned}
|\lambda| \le \left\|\mathbf{S}_M^{-1}\,\mathbf{S}\right\| &= \left\|\mathbf{S}_M^{-\frac{1}{2}}\left(\mathbf{S}_M^{-\frac{1}{2}}\,\mathbf{S}\right)\right\| = \left\|\left(\mathbf{S}_M^{-\frac{1}{2}}\,\mathbf{S}\right)\mathbf{S}_M^{-\frac{1}{2}}\right\| \\
&= \sup_{\vec{\mathbf{p}},\vec{\mathbf{q}}\in\mathbb{R}^{m_p}} \frac{\left\langle \mathbf{S}_M^{-\frac{1}{2}}\,\mathbf{S}\,\mathbf{S}_M^{-\frac{1}{2}}\,\vec{\mathbf{p}},\vec{\mathbf{q}}\right\rangle}{\|\vec{\mathbf{p}}\|\,\|\vec{\mathbf{q}}\|} = \sup_{\vec{\mathbf{p}},\vec{\mathbf{q}}\in\mathbb{R}^{m_p}} \frac{\langle \mathbf{S}\,\vec{\mathbf{p}},\vec{\mathbf{q}}\rangle}{\left\|\mathbf{S}_M^{\frac{1}{2}}\,\vec{\mathbf{p}}\right\|\left\|\mathbf{S}_M^{\frac{1}{2}}\,\vec{\mathbf{q}}\right\|} \\
&= \sup_{\vec{\mathbf{p}},\vec{\mathbf{q}}\in\mathbb{R}^{m_p}} \frac{\langle \mathbf{S}\,\vec{\mathbf{p}},\vec{\mathbf{q}}\rangle}{\langle \mathbf{S}_M\,\vec{\mathbf{p}},\vec{\mathbf{p}}\rangle^{\frac{1}{2}}\,\langle \mathbf{S}_M\,\vec{\mathbf{q}},\vec{\mathbf{q}}\rangle^{\frac{1}{2}}}.
\end{aligned} \tag{5.13}$$

Take any $\vec{\mathbf{p}} \in \mathbb{R}^{n_p}$ and set $\vec{\mathbf{u}} \coloneqq \mathbf{A}^{-1}\,\mathbf{B}^T\,\vec{\mathbf{p}}$. Definition (5.6) yields

$$\langle \mathbf{S}\,\vec{\mathbf{p}},\vec{\mathbf{q}}\rangle = \langle \mathbf{B}\,\vec{\mathbf{u}},\vec{\mathbf{q}}\rangle + \langle \mathbf{C}_\star\,\vec{\mathbf{p}},\vec{\mathbf{q}}\rangle$$

for any $\vec{\mathbf{q}} \in \mathbb{R}^{n_p}$. Using (5.3) and (5.5), we rewrite the above in the finite element notation:

$$\begin{aligned} \langle \mathbf{S}\,\vec{\mathbf{p}}, \vec{\mathbf{q}} \rangle &= b_T(\mathbf{u}_h, q_h) + s_\star(p_h, q_h) \\ \text{Cauchy–Schwarz} \qquad &\leq \|\operatorname{tr} \mathbf{E}(\mathbf{u}_h)\|_0 \, \|q_h\|_0 + s_\star(p_h, q_h). \end{aligned} \tag{5.14}$$

From the definition of $\vec{\mathbf{u}}$ we get

$$\mathbf{B}^T \vec{\mathbf{p}} = \mathbf{A}\,\vec{\mathbf{u}} \quad \Rightarrow \quad \left\langle \mathbf{B}^T \vec{\mathbf{p}}, \vec{\mathbf{v}} \right\rangle = \langle \mathbf{A}\,\vec{\mathbf{u}}, \vec{\mathbf{v}} \rangle$$

for any $\vec{\mathbf{v}} \in \mathbb{R}^{n_u}$, or

$$b_T(\mathbf{v}_h, p_h) = A_\gamma(\mathbf{u}_h, \mathbf{v}_h) = A(\mathbf{u}_h, \mathbf{v}_h) + \gamma \, \langle \operatorname{tr} \mathbf{E}(\mathbf{u}_h), \operatorname{tr} \mathbf{E}(\mathbf{v}_h) \rangle_0 \tag{5.15}$$

for any $\mathbf{v}_h \in \mathbf{V}_h$. Application of Cauchy–Schwarz inequality to (5.15) with $\mathbf{v}_h \coloneqq \mathbf{u}_h$ yields

$$\begin{aligned} 0 \leq A(\mathbf{u}_h, \mathbf{u}_h) &= b_T(\mathbf{u}_h, p_h) - \gamma \, \|\operatorname{tr} \mathbf{E}(\mathbf{u}_h)\|_0^2 \\ &\leq \|\operatorname{tr} \mathbf{E}(\mathbf{u}_h)\|_0 \, \|p_h\|_0 - \gamma \, \|\operatorname{tr} \mathbf{E}(\mathbf{u}_h)\|_0^2 \\ &= \|\operatorname{tr} \mathbf{E}(\mathbf{u}_h)\|_0 \left(\|p_h\|_0 - \gamma \, \|\operatorname{tr} \mathbf{E}(\mathbf{u}_h)\|_0 \right), \\ \gamma \, \|\operatorname{tr} \mathbf{E}(\mathbf{u}_h)\|_0 &\leq \|p_h\|_0 \, . \end{aligned}$$

Using this we estimate (5.14) further as

$$\begin{aligned} \langle \mathbf{S}\,\vec{\mathbf{p}}, \vec{\mathbf{q}} \rangle &\leq \gamma^{-1} \, \|p_h\|_0 \, \|q_h\|_0 + s_\star^{\frac{1}{2}}(p_h, p_h) s_\star^{\frac{1}{2}}(q_h, q_h) \\ &= \frac{\nu + \gamma}{\gamma} \, (\nu + \gamma)^{-1} \, \|p_h\|_0 \, \|q_h\|_0 + s_\star^{\frac{1}{2}}(p_h, p_h) s_\star^{\frac{1}{2}}(q_h, q_h) \\ &\leq \frac{\nu + \gamma}{\gamma} \left((\nu + \gamma)^{-1} \, \|p_h\|_0 \, \|q_h\|_0 + s_\star^{\frac{1}{2}}(p_h, p_h) s_\star^{\frac{1}{2}}(q_h, q_h) \right) \\ \text{Cauchy–Schwarz} \qquad &\leq \frac{\nu + \gamma}{\gamma} \left((\nu + \gamma)^{-1} \, \|p_h\|_0^2 + s_\star(p_h, p_h) \right)^{\frac{1}{2}} \left((\nu + \gamma)^{-1} \, \|q_h\|_0^2 + s_\star(q_h, q_h) \right)^{\frac{1}{2}} \\ &= \frac{\nu + \gamma}{\gamma} \, \langle \mathbf{S}_M \, \vec{\mathbf{p}}, \vec{\mathbf{p}} \rangle^{\frac{1}{2}} \, \langle \mathbf{S}_M \, \vec{\mathbf{q}}, \vec{\mathbf{q}} \rangle^{\frac{1}{2}} \, , \end{aligned}$$

and combining it with (5.13) yields (5.11).

Next we show the estimate (5.12) for the real parts of eigenvalues. We need the following result:

$$\inf_{\vec{\mathbf{p}}\in\mathbb{R}^{n_p}} \frac{\langle \mathbf{S}\,\vec{\mathbf{p}},\vec{\mathbf{p}}\rangle}{\langle \mathbf{S}_M\,\vec{\mathbf{p}},\vec{\mathbf{p}}\rangle} \leq \Re(\lambda), \tag{5.16}$$

see (Bendixson 1902). Let $\star \in \{n, \text{full}\}$ and define

$$\|\mathbf{v}_h\|_B^2 \coloneqq \|\mathbf{v}_h\|_0^2 + 2\,\|\mathbf{E}(\mathbf{P}\,\mathbf{v}_h)\|_0^2 + \tau\,\|\mathbf{v}_h\cdot\mathbf{n}\|_0^2 + \rho_u\,\|\partial_n\mathbf{v}_h\|_{L^2(\mathcal{O}_h)}^2\,,$$

i.e., $\|\cdot\|_B = \|\cdot\|_A$ with $\alpha = \nu = 1$ fixed. The inf-sup condition (LBB_h) implies that there exists $\mathbf{l}_h \in \mathbf{V}_h$ with $\|\mathbf{l}_h\|_B = 1$ such that

$$\|p_h\|_0^2 \lesssim b_T^2(\mathbf{l}_h, p_h) + s_\star(p_h, p_h), \tag{5.17}$$

with a constant embedded in $\lesssim$ independent of parameters α, ν and γ. We use (5.15) with $\mathbf{v}_h \coloneqq \mathbf{l}_h$ to estimate the first term in (5.17):

$$\begin{aligned} b_T(\mathbf{l}_h, p_h) &= A_\gamma(\mathbf{u}_h, \mathbf{l}_h) = A(\mathbf{u}_h, \mathbf{l}_h) + \gamma\,\langle \operatorname{tr}\mathbf{E}(\mathbf{u}_h), \operatorname{tr}\mathbf{E}(\mathbf{l}_h)\rangle_0 \\ \text{Cauchy–Schwarz, (3.8)} \qquad &\leq \|\mathbf{u}_h\|_A\,\|\mathbf{l}_h\|_A + \|\nabla_\Gamma\,(\mathbf{P}\,\mathbf{u}_h)\|_0\,\|\mathbf{l}_h\|_0 + \gamma\,\|\operatorname{tr}\mathbf{E}(\mathbf{u}_h)\|_0\,\|\operatorname{tr}\mathbf{E}(\mathbf{l}_h)\|_0\,. \end{aligned}$$

We estimate further

$$
\begin{aligned}
\|\mathbf{l}_h\|_0 &\leq \|\mathbf{l}_h\|_B^2 = 1, \\
\|\operatorname{tr}\mathbf{E}(\mathbf{l}_h)\|_0^2 &= \|\operatorname{tr}\mathbf{E}(\mathbf{P}\,\mathbf{l}_h) + \kappa\,(\mathbf{l}_h\cdot\mathbf{n})\|_0^2 \\
\text{(3.14), } \Gamma\in C^2 \qquad &\lesssim \|\mathbf{E}(\mathbf{P}\,\mathbf{l}_h)\|_0^2 + \|\mathbf{l}_h\cdot\mathbf{n}\|_0^2 \\
&\leq \|\mathbf{E}(\mathbf{P}\,\mathbf{l}_h)\|_0^2 + \|\mathbf{l}_h\|_0^2 \\
&\leq \|\mathbf{l}_h\|_B^2 = 1, \\
\|\nabla_\Gamma\,(\mathbf{P}\,\mathbf{u}_h)\|_0^2 &\leq \|\mathbf{P}\,\mathbf{u}_h\|_1^2 \\
\text{(3.21)} \qquad &\lesssim \|\mathbf{E}\,(\mathbf{P}\,\mathbf{u}_h)\|_0^2 + \|\mathbf{P}\,\mathbf{u}_h\|_0^2 \\
\nu\leq 1,\ \alpha = 1 \qquad &\lesssim \nu^{-1}\,\|\mathbf{u}_h\|_A^2\,, \quad \|\mathbf{l}_h\|_A \leq \|\mathbf{l}_h\|_B = 1.
\end{aligned}
$$

Thus we have

$$
\begin{aligned}
b_T(\mathbf{l}_h, p_h) &\lesssim \left(1+\nu^{-\frac{1}{2}}\right)\|\mathbf{u}_h\|_A + \gamma\,\|\operatorname{tr}\mathbf{E}(\mathbf{u}_h)\|_0 \\
\nu\leq 1 \qquad &\lesssim \nu^{-\frac{1}{2}}\,\|\mathbf{u}_h\|_A + \gamma\,\|\operatorname{tr}\mathbf{E}(\mathbf{u}_h)\|_0 \\
\text{Cauchy–Schwarz} \qquad &\leq \left(\nu^{-1}+\gamma\right)^{\frac{1}{2}}\left(\|\mathbf{u}_h\|_A^2 + \gamma\,\|\operatorname{tr}\mathbf{E}(\mathbf{u}_h)\|_0^2\right)^{\frac{1}{2}} \\
&= \left(\nu^{-1}+\gamma\right)^{\frac{1}{2}}\|\mathbf{u}_h\|_{A_\gamma}\,, \\
b_T^2(\mathbf{l}_h, p_h) &\lesssim \left(\nu^{-1}+\gamma\right)\|\mathbf{u}_h\|_{A_\gamma}^2\,.
\end{aligned}
$$

Substituting the above estimate in (5.17) gives

$$
\begin{aligned}
\langle \mathbf{M}_p\,\vec{\mathbf{p}}, \vec{\mathbf{p}}\rangle = \|p_h\|_0^2 &\lesssim \left(\nu^{-1}+\gamma\right)\|\mathbf{u}_h\|_{A_\gamma}^2 + s_\star(p_h,p_h) \\
\nu^{-1}+\gamma > 1 \qquad &\leq \left(\nu^{-1}+\gamma\right)\left(\|\mathbf{u}_h\|_{A_\gamma}^2 + s_\star(p_h,p_h)\right). \qquad (5.18)
\end{aligned}
$$

Employing (5.14) with $\vec{\mathbf{q}} \coloneqq \vec{\mathbf{p}}$ and (5.15) with skew-symmetry of the inertia term (3.7) we rewrite

the right-hand side of (5.18) in matrix notation:

$$\|\mathbf{u}_h\|^2_{A_\gamma} + s_\star(p_h, p_h) = \langle \mathbf{S}\,\vec{\mathbf{p}}, \vec{\mathbf{p}}\rangle\,.$$

Thus we arrive at $\langle \mathbf{M}_p\,\vec{\mathbf{p}}, \vec{\mathbf{p}}\rangle \lesssim (\nu^{-1}+\gamma)\,\langle \mathbf{S}\,\vec{\mathbf{p}}, \vec{\mathbf{p}}\rangle$, or

$$\frac{\nu+\gamma}{\nu^{-1}+\gamma}\left\langle (\nu+\gamma)^{-1}\,\mathbf{M}_p\,\vec{\mathbf{p}}, \vec{\mathbf{p}}\right\rangle \lesssim \langle \mathbf{S}\,\vec{\mathbf{p}}, \vec{\mathbf{p}}\rangle\,. \tag{5.19}$$

Finally, noting that $\langle \mathbf{C}_\star\,\vec{\mathbf{p}}, \vec{\mathbf{p}}\rangle \le \langle \mathbf{S}\,\vec{\mathbf{p}}, \vec{\mathbf{p}}\rangle$ and $\frac{\nu+\gamma}{\nu^{-1}+\gamma} \le \frac{\nu^{-1}+\gamma}{\nu^{-1}+\gamma} = 1$ we get

$$\frac{\nu+\gamma}{\nu^{-1}+\gamma}\,\langle \mathbf{C}_\star\,\vec{\mathbf{p}}, \vec{\mathbf{p}}\rangle \le \langle \mathbf{S}\,\vec{\mathbf{p}}, \vec{\mathbf{p}}\rangle\,,$$

and adding it to (5.19) yields

$$\frac{\gamma+\nu}{\gamma+\nu^{-1}}\left\langle \underbrace{\left((\gamma+\nu)^{-1}\,\mathbf{M}_p + \mathbf{C}_\star\right)}_{\mathbf{S}_M =}\vec{\mathbf{p}}, \vec{\mathbf{p}}\right\rangle \lesssim \langle \mathbf{S}\,\vec{\mathbf{p}}, \vec{\mathbf{p}}\rangle\,,$$

$$\frac{\gamma+\nu}{\gamma+\nu^{-1}} \lesssim \frac{\langle \mathbf{S}\,\vec{\mathbf{p}}, \vec{\mathbf{p}}\rangle}{\langle \mathbf{S}_M\,\vec{\mathbf{p}}, \vec{\mathbf{p}}\rangle}.$$

Thus the estimate (5.12) on $\Re(\lambda)$ follows from (5.16). □

We see that for large enough γ all eigenvalues are contained in a box in the right half-plane, with the bounds independent of ν. Motivated by estimates (5.11) and (5.12), we define the Schur complement preconditioner through its inverse as follows:

$$\widehat{\mathbf{S}}^{-1} \coloneqq \underbrace{\left((\nu+\gamma)^{-1}\,\mathbf{M}_p + \mathbf{C}_n\right)^{-1}}_{\mathbf{S}_M^{-1} =} + \underbrace{\left(\alpha^{-1}\,\mathbf{L}_p + \mathbf{C}_n\right)^{-1}}_{\mathbf{S}_L^{-1} \coloneqq}. \tag{5.20}$$

The second term is included to deal with the dominating reaction term in the Oseen problem (5.1), i.e., if $\alpha \gg 1$. This part of $\widehat{\mathbf{S}}^{-1}$ resembles the Cahouet–Chabard preconditioner (Cahouet and Chabard 1988). We apply several conjugate gradient iterations to compute the action of $\mathbf{S}_M^{-1}$ and $\mathbf{S}_L^{-1}$ on a vector. Alternatively, these matrices can be also one-time factorized. Since the number

of the pressure d.o.f. is much smaller than the velocity ones, $n_p \ll n_u$, either choice marginally affects the total timings.

Note also that $\mathbf{S}_L$ has a one-dimensional kernel, i.e., the subspace of constant pressures, which we easily handle by iterating in a proper subspace. Strictly speaking, $\mathbf{S}_L^{-1}$ is the pseudo-inverse in our case.

5.2.2 Recycling Strategy

Next we define the preconditioner $\widehat{\mathbf{A}}$ for the velocity block of $\boldsymbol{\mathcal{P}}$. The augmentation has the downside of adding to the $(1,\ 1)$-block of $\boldsymbol{\mathcal{A}}_\star$ the term (5.2) with a large nullspace. For larger γ this makes the matrix $\mathbf{A}$ poor conditioned and hinders the efficiency of standard iterative methods to approximate the action of $\mathbf{A}^{-1}$.

As a more flexible alternative, we explore here direct LU-factorization of $\mathbf{A}$ (or its blocks) at the time $t^k = k\,\Delta t$ and the reuse of these factors for several time steps

$$t^i \to t^{i+1},$$

with $i = k+1, k+2$ etc. In pursuing this line, we consider two strategies of building $\widehat{\mathbf{A}}$:

1. We obtain $\vec{\mathbf{v}} \mapsto \widehat{\mathbf{A}}^{-1}\vec{\mathbf{v}}$ via perform LU-factorization of the full velocity block $\mathbf{A}$. Thus $\widehat{\mathbf{A}}^{-1}\vec{\mathbf{v}} = \mathbf{A}^{-1}\,\vec{\mathbf{v}}$ up to finite precision.

2. We enumerate velocity unknowns componentwise so that the first $n_u\,/\,3$ entries of $\vec{\mathbf{v}}$ correspond to the x-component of the corresponding finite element function $\mathbf{v}_h$, see (5.5), second ones to the y-component, and the last ones to the z-component. Thus $\mathbf{A}$ attains the (3×3)-block form,

$$\mathbf{A} = \begin{pmatrix} \mathbf{A}_{xx} & \mathbf{A}_{xy} & \mathbf{A}_{xz} \\ \mathbf{A}_{yx} & \mathbf{A}_{yy} & \mathbf{A}_{yz} \\ \mathbf{A}_{zx} & \mathbf{A}_{zy} & \mathbf{A}_{zz} \end{pmatrix}.$$

We obtain $\vec{\mathbf{v}} \mapsto \widehat{\mathbf{A}}^{-1}\vec{\mathbf{v}}$ from the block upper-triangle part of $\mathbf{A}$,

$$\mathbf{A}_\Delta \coloneqq \begin{pmatrix} \mathbf{A}_{xx} & \mathbf{A}_{xy} & \mathbf{A}_{xz} \\ & \mathbf{A}_{yy} & \mathbf{A}_{yz} \\ & & \mathbf{A}_{zz} \end{pmatrix},$$

via factorizing each of diagonal blocks $\mathbf{A}_{xx}$, $\mathbf{A}_{yy}$, and $\mathbf{A}_{yy}$ of $\mathbf{A}_\Delta$, and performing block Gaussian elimination. This approach corresponds to the one from (Benzi, Olshanskii, and Wang 2011).

We call the first strategy **full AL-approach** and the second one **modified AL-approach**. The modified AL-approach allows to factorize smaller matrices that structurally resemble stiffness matrices of a conforming FEM applied to an elliptic scalar PDE. This enhanced efficiency comes with a price of slight ν- and h-dependence of the preconditioner performance (Benzi, Olshanskii, and Wang 2011). Numerical experiments in Section 6.2.1 show that in the case of time-dependent 2D flow the price is very tolerable.

Same approaches, of course, apply to reusing incomplete LU-factorizations, but we fix our idea and consider the exact LU. Surface fluid problems are essentially two dimensional, and the number of velocity d.o.f. n_u allows for full LU-factorization. Furthermore, in a curvilinear metric the viscosity term does not simplify to Laplace operators for each velocity component, i.e., for tangential divergence-free $\mathbf{v}_T$ we note that in general

$$\mathbf{P}\,\mathrm{div}_\Gamma\,\mathbf{E}(\mathbf{v}_T) \neq \Delta_\Gamma \mathbf{v}_T$$

with a componentwise Laplace–Beltrami operator Δ_Γ. Therefore, $\mathbf{A}$ does not have a block-diagonal structure for $\gamma = 0$, and adding the γ-term (5.2) does not change the sparsity pattern of the matrix (in contrast to the augmentation in the $\mathbb{R}^d$-case).

To make the algorithm precise, consider the full AL-approach and denote by $\mathbf{L}(k)$ and $\mathbf{U}(k)$ the LU-factors of $\mathbf{A}(k)$ at step k of (4.1). We let $\widehat{\mathbf{A}} = \mathbf{L}(k)\,\mathbf{U}(k)$ to be the preconditioner for

all $\mathbf{A}(k+\Delta k)$, with the index $\Delta k \geq 0$ such that

$$\frac{\#\,\mathrm{iter}(k+\Delta k)}{\#\,\mathrm{iter}(k)} \leq \Delta_{\mathrm{iter}}, \tag{5.21}$$

holds for some fixed parameter $\Delta_{\mathrm{iter}} \geq 1$. Here Δ_{iter} is the maximum allowed increase of the preconditioned outer iterations without updating the preconditioner. The recycling strategy (5.21) for the modified AL-approach is defined in similar manner. Since the system matrix $\boldsymbol{\mathcal{A}}$ is not symmetric and $\widehat{\mathbf{S}}^{-1}$ is nonlinear and iteration-dependent (hence so is $\boldsymbol{\mathcal{P}}$), we use the FGMRES method (Saad 1993) as the outer solver.

6 NUMERICAL EXPERIMENTS

We present results of numerical experiments to support the theoretical results from previous chapters. Software DROPS (Institute of Scientific Computing, RWTH Aachen; Department of Mathematics, University of Houston 2003), packages Belos and Amesos from Trilinos (The Trilinos Project Team 2021), and VTK / Paraview (Schroeder, Martin, and Lorensen 1998; Ahrens, Geveci, and Law 2005) were used for matrix assembling, algebraic solver execution, and solution visualization, respectively. Mathematica computing system (Wolfram Research, Inc. 2021) was used to approximate solutions of (generalized) eigenvalue problems.

6.1 Stokes Problem on Stationary Surfaces

For the first numerical experiment we consider the problem (3.6) with parameters

$$\mathbf{w} = \mathbf{0}, \quad \alpha = \nu = 1, \tag{6.1}$$

i.e., the surface tangential Stokes problem

$$\begin{aligned} \mathbf{u}_T - 2\,\mathbf{P}\,\mathrm{div}_\Gamma\,\mathbf{E}(\mathbf{u}_T) + \nabla_\Gamma p &= \mathbf{f}_T, \\ \mathrm{div}_\Gamma\,\mathbf{u}_T &= 0 \quad \text{on}\Gamma. \end{aligned} \tag{6.2}$$

We choose Γ to be either the unit sphere or a torus, $\Gamma = \Gamma_{\mathrm{sph}}$ or $\Gamma = \Gamma_{\mathrm{tor}}$, with the corresponding level set functions

$$\phi_{\mathrm{sph}}(\mathbf{x}) \coloneqq \|\mathbf{x}\|^2 - 1 \quad \text{and} \quad \phi_{\mathrm{tor}}(\mathbf{x}) \coloneqq (\|\mathbf{x}\|^2 + R^2 - r^2)^2 - 4R^2(x^2 + y^2), \tag{6.3}$$

respectively, $R \coloneqq 1$, $r \coloneqq 1\,/\,5$.

The computational domain is $\Omega \coloneqq (-5/3,\ 5/3)^3$ such that $\Gamma \subset \Omega$ for both examples. To build the initial triangulation $\mathcal{T}_{h_0}$ we divide Ω into 2^3 cubes and further tessellate each cube into 6 tetrahedra. Thus we have $h_0 = 5\,/\,3$. The mesh is gradually refined towards the surface, and $\ell \in \mathbb{N}$

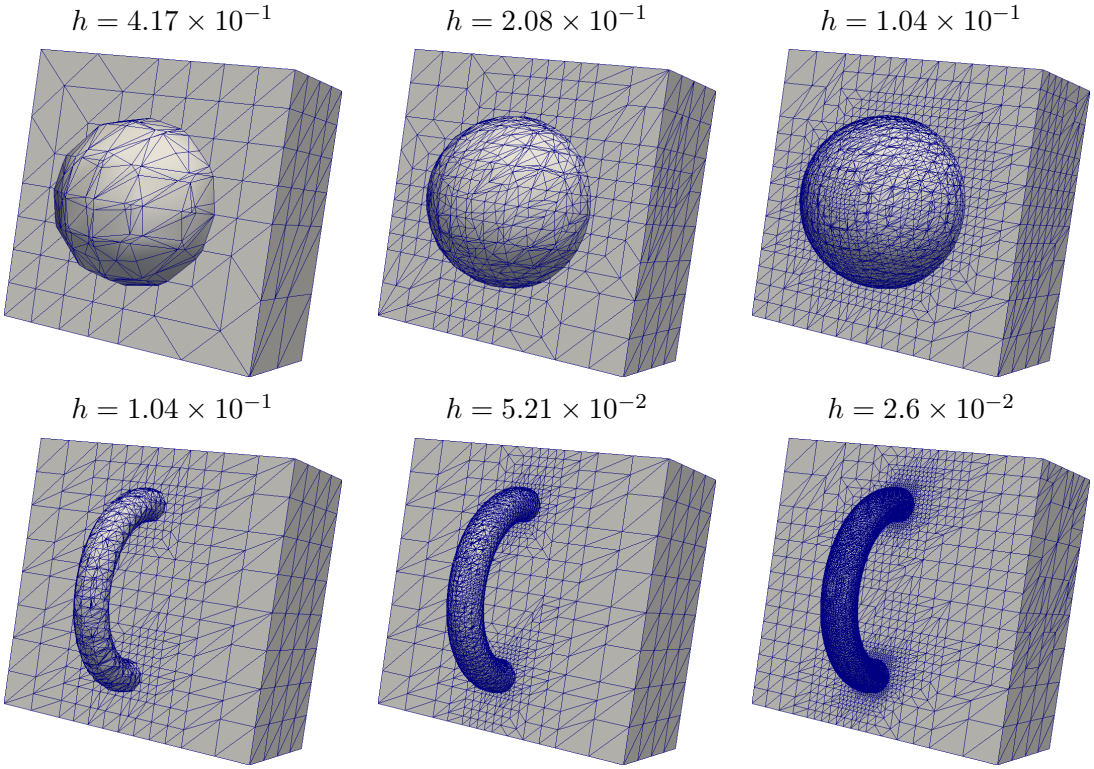

Figure 5: Cuts of the bulk mesh Ω_h and the induced surface mesh for refinement levels ℓ. Top: $\Gamma = \Gamma_{\mathrm{sph}}$, $\ell \in \{1, 2, 3\}$, bottom: $\Gamma = \Gamma_{\mathrm{tor}}$, $\ell \in \{3, 4, 5\}$

denotes the level of refinement, with the mesh size

$$h = h(\ell) = h_0 \times 2^{-\ell} = \frac{5}{3} \times 2^{-\ell},$$

see Figure 5 for an illustration of the bulk meshes and the induced mesh on the embedded surface for three consecutive refinement levels.

We apply the trace FEM from Section 4.2 to discretize (6.2). For the next set of experiments the grad-div stabilization parameter is chosen to be $\gamma = 0$. In the following subsections we

1. numerically compute optimal inf-sup stability constants for the $\mathbf{P}_2$–P_1 and $\mathbf{P}_1$–P_1 trace FEM and

2. show convergence results for the $\mathbf{P}_2$–P_1 trace FEM.

6.1.1 Discrete Inf-sup Stability

The definition (5.8) of the surface pressure mass matrix $\mathbf{M}_p \in \mathbb{R}^{n_p \times n_p}$ yields

$$\langle p_h, q_h \rangle_0 = \langle \vec{\mathbf{q}}, \mathbf{M}_p \, \vec{\mathbf{p}} \rangle \, .$$

We also need auxiliary matrices

$$\mathbf{M}_\star \coloneqq \mathbf{M}_p + \mathbf{C}_\star \quad \Rightarrow \quad \langle p_h, q_h \rangle_0 + s_\star(p_h, q_h) = \langle \vec{\mathbf{q}}, \mathbf{M}_\star \, \vec{\mathbf{p}} \rangle \, . \tag{6.4}$$

which correspond to the natural norms used in the pressure space, e.g., $\mathbf{M}_n$ corresponds to $\|\cdot\|_h$ from (4.19).

We are interested in the generalized eigenvalue problem

$$\mathbf{S}_\star \, \vec{\mathbf{q}} = \lambda \, \mathbf{M}_\star \, \vec{\mathbf{q}}, \tag{6.5}$$

with $\star \in \{0, n, \text{full}\}$. We use the notation

$$0 = \lambda_1 < \lambda_2 \leq \cdots \leq \lambda_{n_p}$$

for the generalized eigenvalues of (6.5). For the stable discretization method we have $\lambda_{n_p} \simeq 1$, and the discrete inf-sup property (4.23) can be rewritten in the matrix-vector notation:

$$c_0 \, \langle \mathbf{M}_\star \, \vec{\mathbf{q}}, \vec{\mathbf{q}} \rangle \leq \langle \mathbf{S}_\star \, \vec{\mathbf{q}}, \vec{\mathbf{q}} \rangle$$

holds for any $\mathbf{q} \in \mathbb{R}^{n_p} \setminus \{\text{const}\}$. See, e.g., (Olshanskii and Tyrtyshnikov 2014, Lemma 5.9). Thus we have

$$c_0 \leq \lambda_2,$$

i.e., for $\star \in \{n, \text{full}\}$ the smallest effective eigenvalue of the generalized Schur complement (6.5) must be bounded away from zero, and the bound must be independent of h and how the surface

cuts the ambient mesh.

Assembling the Schur complement matrix $\mathbf{S}_\star$ becomes prohibitively expensive even for rather small mesh sizes, since one needs to calculate $\mathbf{A}^{-1}$. One possible solution is to write (6.5) in the mixed form, i.e.,

$$\begin{pmatrix} \mathbf{A} & \mathbf{B}^T \\ \mathbf{B} & -\mathbf{C}_\star \end{pmatrix} \begin{pmatrix} \vec{\mathbf{v}} \\ \vec{\mathbf{q}} \end{pmatrix} = -\lambda \begin{pmatrix} & \\ & \mathbf{M}_\star \end{pmatrix} \begin{pmatrix} \vec{\mathbf{v}} \\ \vec{\mathbf{q}} \end{pmatrix}, \quad \text{leading to}$$
$$\begin{pmatrix} \mathbf{A} & \mathbf{B}^T \\ \mathbf{B} & -\mathbf{C}_\star \end{pmatrix} \begin{pmatrix} \vec{\mathbf{v}} \\ \vec{\mathbf{q}} \end{pmatrix} = -\lambda(\epsilon) \underbrace{\begin{pmatrix} \epsilon\,\mathbf{A} & \\ & \mathbf{M}_\star \end{pmatrix}}_{\boldsymbol{\mathcal{M}}_\star^\epsilon \,:=} \begin{pmatrix} \vec{\mathbf{v}} \\ \vec{\mathbf{q}} \end{pmatrix}, \tag{6.6}$$

with $0 < \epsilon \ll 1$. Here we introduced an ϵ-perturbation to the right-hand side matrix to make it Hermitian positive definite. In this form, the problem is suitable for any standard generalized eigenvalue solver that operates with sparse Hermitian matrices. The spectrum of the perturbed problem consists of two sets of eigenvalues,

$$\operatorname{sp}\left((\boldsymbol{\mathcal{M}}_\star^\epsilon)^{-1} \boldsymbol{\mathcal{A}}_\star \right) = \Lambda_\epsilon \cup \Lambda_{\epsilon^{-1}}.$$

The eigenvalues from the first set converge to those of (6.5), i.e.,

$$\lambda(\epsilon) = \lambda + o(1) \text{ as } \epsilon \to 0, \qquad \text{with } \lambda(\epsilon) \in \Lambda_\epsilon \text{ and } \lambda \in \operatorname{sp}\left(\mathbf{M}_\star^{-1} \mathbf{S}_\star \right).$$

For the eigenvalues in the other set we have $-\lambda(\epsilon) = O(\epsilon^{-1})$, $\lambda(\epsilon) \in \Lambda_{\epsilon^{-1}}$. This makes it straightforward for $\epsilon \ll 1$ to identify the eigenvalues we are interested in. To simplify the computation further, we replace the $(1,1)$-block of $\boldsymbol{\mathcal{M}}_\star^\epsilon$ by $\epsilon\,\mathbf{I}$.

To check that our computations are stable with respect to small ϵ and yield consistent results, we solve (6.6) for $\epsilon = 10^{-5}$ and $\epsilon = 10^{-6}$. It turns out that we obtain very close results. Furthermore, for the coarse mesh levels, when solving (6.5) is feasible, we also check that the dense solver for (6.5) and the iterative one for (6.6) with $\epsilon = 10^{-6}$ give eigenvalues that coincide at least up to the first five significant digits.

Tables 1 and 2 report λ_2, i.e., the lower bound for the discrete inf-sup stability constant, and λ_{n_p}, i.e., the maximum eigenvalue so that $\lambda_{n_p} / \lambda_2$ defines the effective condition number, for the following methods:

1. the trace $\mathbf{P}_2$–P_1 finite element method, and
2. the trace $\mathbf{P}_1$–P_1 finite element method from (Olshanskii, Quaini, Reusken, and Yushutin 2018).

For both discretizations we solve the eigenvalue problem (6.6) with different matrices $\mathbf{C}_\star$ which correspond to three choices of pressure stabilization $\star \in \{0, n, \text{full}\}$.

For experiments with the trace $\mathbf{P}_2$–P_1 elements we choose parameters satisfying (4.16),

$$\tau = h^{-2}, \quad \rho_p = h. \tag{6.7}$$

For the velocity volume stabilization choose $\rho_u = h^{-1}$, i.e., the upper extreme for admissible parameters, since for smaller ρ_u the stability constant c_0 from (4.23) can only increase. For the trace $\mathbf{P}_1$–P_1 finite elements we use (6.7) and set $\rho_u = h$, which was the choice in (Olshanskii, Quaini, Reusken, and Yushutin 2018). If the resulting method is inf-sup unstable for $\rho_u \simeq h$, it has the same property also for larger ρ_u.

From Table 1, which shows results for the $\mathbf{P}_2$–P_1 trace elements, we see that for $\mathbf{C}_0$ (no pressure stabilization) λ_2 tends to zero with mesh refinement, which indicates that the discretization is not inf-sup stable. The normal gradient stabilization matrix $\mathbf{C}_n$ is sufficient for the inf-sup stability, λ_2 is uniformly bounded from below, which confirms the main result of the Section 4.2. Of course, including the full pressure gradient term also leads to a stable method, but in this case, the method has consistency errors that are suboptimal, see Corollary 4.1.

For the two cases $\Gamma = \Gamma_{\text{sph}}$ and $\Gamma = \Gamma_{\text{tor}}$ the behavior is essentially the same. From Table 2 we see that only full gradient stabilization matrix $\mathbf{C}_{\text{full}}$ guarantees inf-sup stability of the $\mathbf{P}_1$–P_1 trace elements, which is different to the situation with the $\mathbf{P}_2$–P_1 trace elements.

Next, we illustrate our claim that the optimal inf-sup stability constant c_0 in (LBB) is uniformly bounded with respect to the position of Γ in the background mesh. To this end, we introduce a set

Table 1: Extreme eigenvalues of the preconditioned Schur complement (6.5) for the trace $\mathbf{P}_2$–P_1 finite elements.

$\Gamma = \Gamma_{\text{sph}}$								
h	n_u	n_p	$\mathbf{S}_0$		$\mathbf{S}_n$		$\mathbf{S}_{\text{full}}$	
			λ_2	λ_{n_p}	λ_2	λ_{n_p}	λ_2	λ_{n_p}
8.33×10^{-1}	789	51	2.33×10^{-1}	1.07	6.3×10^{-1}	1.	8.81×10^{-1}	1.
4.17×10^{-1}	3276	190	4.72×10^{-2}	6.97×10^{-1}	5.29×10^{-1}	1.	7.64×10^{-1}	1.
2.08×10^{-1}	11718	664	7.93×10^{-2}	6.7×10^{-1}	5.09×10^{-1}	1.	6.39×10^{-1}	1.
1.04×10^{-1}	48762	2764	3.71×10^{-2}	6.69×10^{-1}	5.03×10^{-1}	1.	5.73×10^{-1}	1.
5.21×10^{-2}	193086	10912	1.81×10^{-3}	6.68×10^{-1}	4.98×10^{-1}	1.	5.36×10^{-1}	1.
2.6×10^{-2}	775998	43864	6.65×10^{-4}	6.65×10^{-1}	4.92×10^{-1}	1.	5.17×10^{-1}	1.

$\Gamma = \Gamma_{\text{tor}}$								
h	n	m	$\mathbf{S}_0$		$\mathbf{S}_n$		$\mathbf{S}_{\text{full}}$	
			λ_2	λ_{n_p}	λ_2	λ_{n_p}	λ_2	λ_{n_p}
2.08×10^{-1}	5580	324	2.15×10^{-1}	9.56×10^{-1}	3.12×10^{-1}	1.	3.4×10^{-1}	1.
1.04×10^{-1}	28116	1580	1.59×10^{-2}	7.6×10^{-1}	3.21×10^{-1}	1.	3.35×10^{-1}	1.
5.21×10^{-2}	116592	6568	1.31×10^{-3}	7.48×10^{-1}	3.21×10^{-1}	1.	3.26×10^{-1}	1.
2.6×10^{-2}	477708	26936	1.9×10^{-4}	7.42×10^{-1}	3.2×10^{-1}	1.	3.22×10^{-1}	1.

of translated surfaces

$$\Gamma \mapsto \Gamma + s\mathbf{s}, \tag{6.8}$$

with some $s \in \mathbb{R}$ and $\mathbf{s} \in \mathbb{R}^3$, $\|\mathbf{s}\| = 1$; see Figure 6.

We repeat eigenvalue computations for the $\mathbf{P}_2$–P_1 trace finite element method, with a fixed mesh size $h = 1.04 \times 10^{-1}$ and a varying translation parameter s in (6.8). Results are reported in Table 3. The results confirm the robustness of the inf-sup stability constant with respect to the position of Γ for the method with the normal derivative stabilization.

6.1.2 Convergence for a Smooth Solution

We set $\Gamma = \Gamma_{\text{sph}}$ and define

$$\mathbf{u}_T^\star(\mathbf{x}) \coloneqq \mathbf{P}_{\mathbf{x}}(-z^2, y, x)^T, \quad p^\star(\mathbf{x}) \coloneqq xy^2 + z \tag{6.9}$$

Table 2: Extreme eigenvalues of the preconditioned Schur complement (6.5) for the trace $\mathbf{P}_1$–P_1 finite elements.

$\Gamma = \Gamma_{\text{sph}}$								
h	n	m	$\mathbf{S}_0$		$\mathbf{S}_n$		$\mathbf{S}_{\text{full}}$	
			λ_2	λ_{n_p}	λ_2	λ_{n_p}	λ_2	λ_{n_p}
8.33×10^{-1}	153	51	1.32×10^{-2}	1.42	7.48×10^{-1}	1.13	9.58×10^{-1}	1.06
4.17×10^{-1}	570	190	5.12×10^{-3}	1.04	5.77×10^{-1}	1.	8.54×10^{-1}	1.
2.08×10^{-1}	1992	664	4.4×10^{-3}	7.93×10^{-1}	3.87×10^{-1}	1.	6.71×10^{-1}	1.
1.04×10^{-1}	8292	2764	2.01×10^{-3}	7.79×10^{-1}	2.19×10^{-1}	1.	5.82×10^{-1}	1.
5.21×10^{-2}	32736	10912	6.04×10^{-5}	9.81×10^{-1}	1.17×10^{-1}	1.	5.37×10^{-1}	1.
2.6×10^{-2}	131592	43864	3.53×10^{-5}	8.67×10^{-1}	5.72×10^{-2}	1.	5.16×10^{-1}	1.
1.3×10^{-2}	525864	175288	2.16×10^{-6}	7.34×10^{-1}	2.84×10^{-2}	1.	5.04×10^{-1}	1.

$\Gamma = \Gamma_{\text{tor}}$								
h	n_p	n_p	$\mathbf{S}_0$		$\mathbf{S}_n$		$\mathbf{S}_{\text{full}}$	
			λ_2	λ_{n_p}	λ_2	λ_{n_p}	λ_2	λ_{n_p}
2.08×10^{-1}	972	324	5.04×10^{-2}	4.93	2.84×10^{-1}	1.35	3.64×10^{-1}	1.19
1.04×10^{-1}	4740	1580	2.99×10^{-3}	3.83	1.58×10^{-1}	1.02	3.35×10^{-1}	1.01
5.21×10^{-2}	19704	6568	1.11×10^{-3}	5.45	7.73×10^{-2}	1.01	3.25×10^{-1}	1.
2.6×10^{-2}	80808	26936	1.2×10^{-4}	5.42	3.07×10^{-2}	1.01	3.21×10^{-1}	1.
1.3×10^{-2}	327036	109012	1.77×10^{-5}	5.23	1.18×10^{-2}	1.01	3.16×10^{-1}	1.

on Γ_{sph}, see Figure 7. We have $\int_\Gamma p^\star \, \mathrm{d}\mathbf{x} = 0$. To define (6.9) in $\mathcal{O}_h$, we use the canonical extension $\mathbf{p}$ from (2.23) and the signed distance function

$$\operatorname{dist}(\mathbf{x}) = \|\mathbf{x}\| - 1$$

defined in $\mathcal{O}_h$.

Note that due to (4.11) and the choice of $\phi = \phi_{\text{sph}}$ in (6.3) we have

$$\mathbf{n}_\phi = \mathbf{n} \circ \mathbf{p},$$

in $\mathcal{O}_h$, i.e., the normal vector $\mathbf{n}_\phi$ induced by $\phi = \phi_{\text{sph}}$ coincides with the canonical extension of $\mathbf{n}$. To approximate the integrands containing $\mathbf{n}_\phi$ and related quantities, e.g., (4.14), we use the nodal P_2-interpolant $I_h^2(\phi)$ defined in $\mathcal{T}_h$. Note that $\phi_{\text{sph}} \in P_2(\mathbb{R}^3)$ implies $I_h^2(\phi_{\text{sph}}) = \phi_{\text{sph}}$, and so the normal vector and related operators can be computed exactly at every quadrature point. To approximate

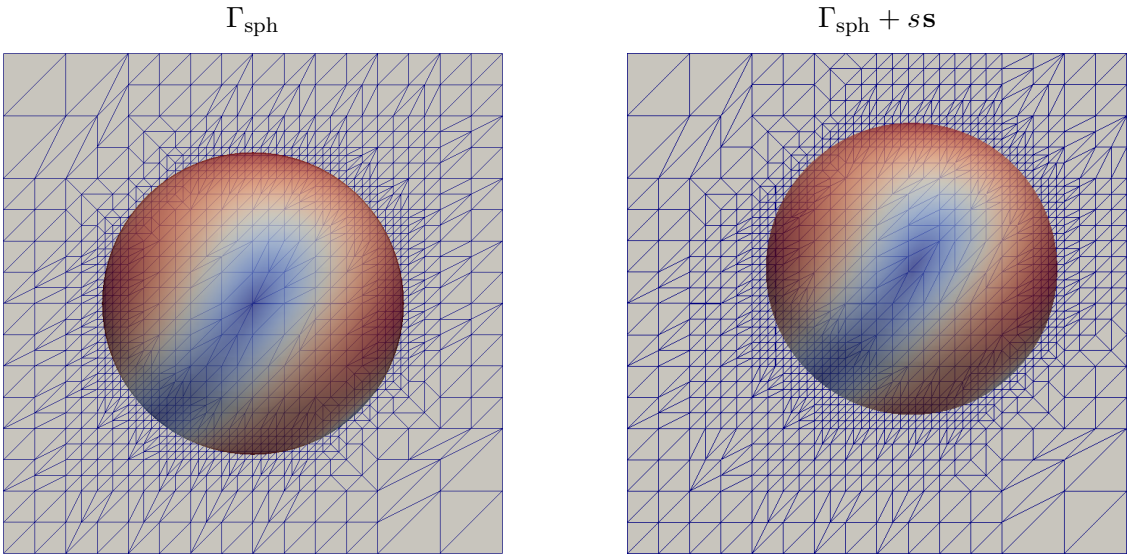

Figure 6: The unit sphere (left) and the shifted unit sphere (right). Here $\mathbf{s} = (1,1,1)^T / \sqrt{3}$, $s = 0.4$, and $h = 5.21 \times 10^{-2}$.

the domain of integration, we use a sufficiently refined piecewise planar approximation $\Gamma_{h\,/\,m}$ of Γ, see Remark 4.2. We take $m \simeq h^{-1}$ so that we have an $O(h^4)$-accurate approximation of the surface.

We use the preconditioned iterative solver as described in Chapter 5 with the final residual tolerance $\|\mathbf{r}_i\| \leq 10^{-8}$. We do not add the grad-div term (5.2) since the problem is stationary, the parameters (6.1) are fixed with the viscosity coefficient $\nu = 1$ being not small, and the linear system is symmetric.

We first consider the convergence rates of the $\mathbf{P}_2$–P_1 trace finite element with the normal derivative volume stabilization matrix $\mathbf{C}_n$. Results are reported in Table 4. From the table we see that the formulation gives optimal convergence rates in all the norms as predicted by the error analysis in Section 4.4.

Table 5 reports results of a further experiment in which the normal derivative volume stabilization for the pressure is replaced by the full gradient stabilization, i.e., the stabilization matrix $\mathbf{C}_{\text{full}}$ is used. This option was discussed in Remark 4.4. It is expected that this results in suboptimal convergence rates due to only $O(h^2)$-consistency of the added term. This is what we see in Table 5, which shows suboptimal rates in L^2-velocity error norm.

Table 3: Extreme eigenvalues of the preconditioned Schur complement (6.5) for the shifted surface $\Gamma + s\mathbf{s}$ for the trace $\mathbf{P}_2$–P_1 finite elements. Here $\mathbf{s} = (1,1,1)^T / \sqrt{3}$ and $h = 1.04 \times 10^{-1}$.

Surface	$\mathbf{S}_0$		$\mathbf{S}_n$	
	λ_2	λ_{n_p}	λ_2	λ_{n_p}
$\Gamma_{\text{sph}} + 0.0\,\mathbf{s}$	3.71×10^{-2}	6.69×10^{-1}	5.03×10^{-1}	1.
$\Gamma_{\text{sph}} + 0.1\,\mathbf{s}$	1.31×10^{-3}	6.87×10^{-1}	5.03×10^{-1}	1.
$\Gamma_{\text{sph}} + 0.2\,\mathbf{s}$	1.25×10^{-3}	6.70×10^{-1}	5.03×10^{-1}	1.
$\Gamma_{\text{sph}} + 0.3\,\mathbf{s}$	1.04×10^{-2}	6.72×10^{-1}	5.03×10^{-1}	1.
$\Gamma_{\text{sph}} + 0.4\,\mathbf{s}$	5.32×10^{-4}	6.72×10^{-1}	5.03×10^{-1}	1.

Surface	$\mathbf{S}_0$		$\mathbf{S}_n$	
	λ_2	λ_{n_p}	λ_2	λ_{n_p}
$\Gamma_{\text{tor}} + 0.00\,\mathbf{s}$	1.59×10^{-2}	7.6×10^{-1}	3.21×10^{-1}	1.
$\Gamma_{\text{tor}} + 0.05\,\mathbf{s}$	9.20×10^{-3}	1.14	3.21×10^{-1}	1.
$\Gamma_{\text{tor}} + 0.10\,\mathbf{s}$	3.00×10^{-3}	1.91	3.19×10^{-1}	1.
$\Gamma_{\text{tor}} + 0.15\,\mathbf{s}$	8.67×10^{-3}	1.02	3.21×10^{-1}	1.
$\Gamma_{\text{tor}} + 0.20\,\mathbf{s}$	6.68×10^{-3}	3.04	3.21×10^{-1}	1.

6.2 Kelvin–Helmholtz Instability

Next we consider the surface tangential Navier–Stokes problem (3.5) with $\rho = 1$ and $\mathbf{f}_T = \mathbf{0}$, i.e.,

$$\begin{aligned} \partial_t \mathbf{u}_T + (\nabla_\Gamma \mathbf{u}_T)\,\mathbf{u}_T - 2\nu\,\mathbf{P}\,\operatorname{div}_\Gamma \mathbf{E}(\mathbf{u}_T) + \nabla_\Gamma p = 0, \\ \operatorname{div}_\Gamma \mathbf{u}_T = 0 \quad \text{on } \Gamma, \end{aligned} \tag{6.10}$$

to simulate the mixing layer of isothermal incompressible viscous surface fluid at several Reynolds numbers. The setup resembles the classical problem of the Kelvin–Helmholtz instability (KH). For a detailed discussion of the planar analogue we refer to (Schroeder, John, Lederer, Lehrenfeld, Lube, and Schöberl 2019) and references therein. At higher Reynolds numbers the flow exhibits sharp internal layers and intensive vortical dynamics, offering a good test problem for both discretizations methods and flow solvers.

As in the previous example, we choose Γ to be either the unit sphere or a torus, $\Gamma = \Gamma_{\text{sph}}$ or $\Gamma = \Gamma_{\text{tor}}$, with the corresponding level set functions (6.3). For the torus, we set $R \coloneqq 1$ and $r \coloneqq 1/2$.

The design of numerical experiment for the sphere follows (Lederer, Lehrenfeld, and Schöberl

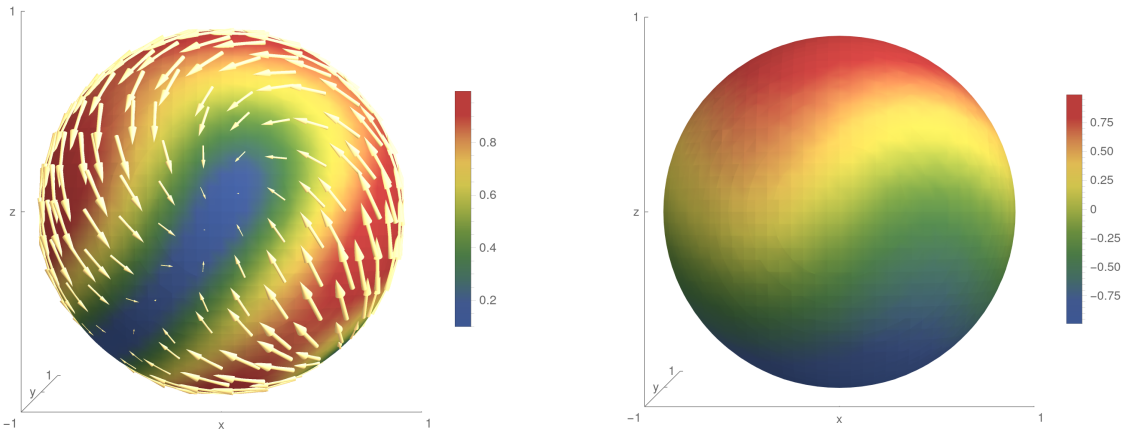

Figure 7: Exact velocity solution $\mathbf{u}_T^\star$ (left) and pressure solution $p^\star$ (right) on Γ_{sph} as in (6.9)

Table 4: Convergence results for the trace $\mathbf{P}_2$–P_1 finite elements with the normal derivative stabilization $\star = n$

h	$\|\mathbf{u}_T^\star - \mathbf{u}_h\|_1$	Order	$\|\mathbf{u}_T^\star - \mathbf{u}_h\|_0$	Order	$\|p^\star - p_h\|_0$	Order	$\|\mathbf{u}_h \cdot \mathbf{n}\|_0$	Order
8.3×10^{-1}	2.2		6.4×10^{-1}		7.4×10^{-1}		4.5×10^{-1}	
4.2×10^{-1}	3.8×10^{-1}	2.5	6.1×10^{-2}	3.4	1.2×10^{-1}	2.6	5.3×10^{-2}	3.1
2.1×10^{-1}	9.2×10^{-2}	2.1	5.8×10^{-3}	3.4	2.5×10^{-2}	2.2	4.9×10^{-3}	3.4
$1. \times 10^{-1}$	2.2×10^{-2}	2.1	5.6×10^{-4}	3.4	6.1×10^{-3}	2.1	$5. \times 10^{-4}$	3.3
5.2×10^{-2}	5.3×10^{-3}	2.	5.2×10^{-5}	3.4	1.6×10^{-3}	1.9	4.9×10^{-5}	3.4
2.6×10^{-2}	1.3×10^{-3}	2.	5.2×10^{-6}	3.3	4.1×10^{-4}	2.	$5. \times 10^{-6}$	3.3
1.3×10^{-2}	3.4×10^{-4}	2.	$6. \times 10^{-7}$	3.1	$1. \times 10^{-4}$	2.	5.8×10^{-7}	3.1

2020; Jankuhn, Olshanskii, Reusken, and **Zhiliakov** 2020). Consider a parametrization

$$\boldsymbol{\chi}(\xi_1, \xi_2) := \begin{pmatrix} \cos(2\pi\xi_1)\cos(\pi\xi_2) \\ \sin(2\pi\xi_1)\cos(\pi\xi_2) \\ -\sin(\pi\xi_2) \end{pmatrix}, \quad \boldsymbol{\xi} \in \Xi := \left(\frac{1}{2}, \frac{1}{2}\right)^2$$

of the unit sphere $\Gamma_{\text{sph}} = \boldsymbol{\chi}\left(\overline{\Xi}\right)$ around $\boldsymbol{\chi}(\mathbf{0}) = \mathbf{e}_1 \in \Gamma_{\text{sph}}$, see (2.2). The coordinates ξ_1 and ξ_2 are (renormalized) azimuthal and polar angles, respectively. Let $\hat{\boldsymbol{\tau}}_\alpha$ be the normalized basis vectors spanning $T\Gamma_{\text{sph}}$, $\hat{\boldsymbol{\tau}}_\alpha := \nabla_\Gamma \xi_\alpha \,/\, \|\nabla_\Gamma \xi_\alpha\|$. The initial velocity field is given by the counter-rotating upper and lower hemispheres with velocity speed approximately equal to one closer to the equator and vanishing at poles. The velocity field has a sharp transition layer along equator, where we add

Table 5: Convergence results for the trace $\mathbf{P}_2$–P_1 finite elements with the full gradient stabilization $\star = \text{full}$

h	$\|\mathbf{u}_T^\star - \mathbf{u}_h\|_1$	Order	$\|\mathbf{u}_T^\star - \mathbf{u}_h\|_0$	Order	$\|p^\star - p_h\|_0$	Order	$\|\mathbf{u}_h \cdot \mathbf{n}\|_0$	Order
8.3×10^{-1}	1.6		7.8×10^{-1}		1.3		3.5×10^{-1}	
4.2×10^{-1}	6.9×10^{-1}	1.2	3.9×10^{-1}	1.	8.1×10^{-1}	6.3×10^{-1}	5.4×10^{-2}	2.7
2.1×10^{-1}	2.4×10^{-1}	1.5	1.3×10^{-1}	1.6	3.1×10^{-1}	1.4	4.9×10^{-3}	3.4
$1. \times 10^{-1}$	8.1×10^{-2}	1.6	3.6×10^{-2}	1.8	1.1×10^{-1}	1.5	$5. \times 10^{-4}$	3.3
5.2×10^{-2}	2.4×10^{-2}	1.8	9.5×10^{-3}	1.9	3.2×10^{-2}	1.7	4.9×10^{-5}	3.4
2.6×10^{-2}	6.5×10^{-3}	1.9	2.4×10^{-3}	2.	8.8×10^{-3}	1.9	$5. \times 10^{-6}$	3.3
1.3×10^{-2}	1.8×10^{-3}	1.8	6.1×10^{-4}	2.	2.5×10^{-3}	1.8	5.9×10^{-7}	3.1

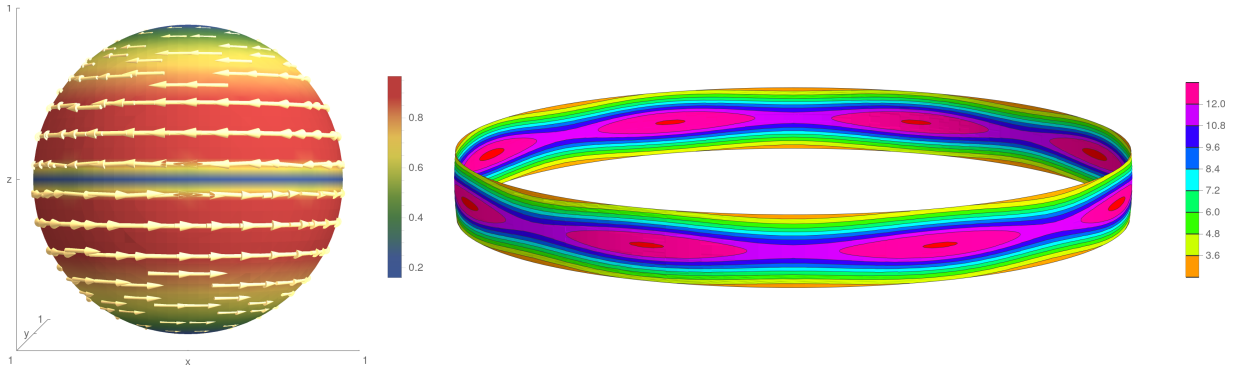

Figure 8: Left: Initial velocity field $\mathbf{u}_T(\cdot, 0)$ from (6.11). Right: The initial vorticity, $\operatorname{curl}_\Gamma \mathbf{u}_T(\cdot, 0)$, in the strip $|z| \leq 2\delta_0$. We see that the initial perturbation consists of 8 vortices squeezed around equator.

perturbation to trigger the development of the vortical strip:

$$\begin{aligned} \mathbf{u}_T\left(\boldsymbol{\chi}\left(\boldsymbol{\xi}\right), 0\right) &\coloneqq d_{\boldsymbol{\chi}}(\xi_2)\left(\tanh\left(\frac{2\xi_2}{\delta_0}\right)\hat{\boldsymbol{\tau}}_1(\boldsymbol{\xi}) + c_n\,\mathbf{curl}_\Gamma\,\psi_{\boldsymbol{\chi}}(\boldsymbol{\xi})\right), \\ \psi_{\boldsymbol{\chi}}(\boldsymbol{\xi}) &\coloneqq \exp\left\{-\frac{\xi_2^2}{\delta_0^2}\right\}\left(a_a\cos(m_a\pi\xi_1) + a_b\cos(m_b\pi\xi_2)\right), \end{aligned} \tag{6.11}$$

where d is the distance from Γ_{sph} to the z-axis. We take $\delta_0 \coloneqq 0.05$ (for $|z| \gtrsim \delta_0$ the velocity field is close to a rigid body rotation around the z-axis), $c_n \coloneqq 10^{-2}$ (perturbation parameter), and $a_a = 1$, $m_a = 16$, $a_b = 0.1$, $m_b = 20$ (perturbation magnitudes and frequencies). The initial velocity field is illustrated in Figure 8. Note that the velocity field (6.11) is tangential by construction.

Note that $\hat{\boldsymbol{\tau}}_1 \in T\Gamma_{\text{tor}}$. For the torus initial condition we use the same formula (6.11) with one

modification: The scaling factor d is chosen as

$$d(\mathbf{x}) \coloneqq \sqrt{x^2+y^2} - (R-r) = \sqrt{x^2+y^2} - \frac{1}{2},$$

and thus the initial velocity field vanishes on the inner ring of the torus.

The Reynolds number $\mathrm{Re} \simeq \nu^{-1}\delta_0$ is based on $\|\mathbf{u}_T(\cdot,0)\|_\infty \simeq 1$ and the initial layer width. We perform numerical simulations with $\nu = \nu(k) = 10^{-k}\,/\,2$ which corresponds to $\mathrm{Re} = \mathrm{Re}(k) = 10^{k-1}$ for $k \in \{3,4,5\}$, i.e.,

$$\mathrm{Re} \in \{10^2, 10^3, 10^4\}.$$

The final time T is chosen to be 20 and 60 for the sphere and torus, respectively. For the time discretization and linearization of (6.10) we apply the second order semi-implicit scheme (4.2) from Section 4.1, and for the space discretization we employ the grad-div stabilized trace FEM (5.1) from Chapter 5 with $\mathbf{P}_2$–P_1 Taylor–Hood finite elements. The mesh construction and the choice of stabilization and penalty parameters is the same as in Section 6.1. We consider three mesh refinement levels $\ell \in \{4,5,6\}$ with the corresponding number of time steps $n_t \in \{320, 640, 1280\}$ and $n_t \in \{960, 1920, 3840\}$ for the sphere and torus, respectively, i.e., we have

$$\Delta t = \Delta t(\ell) = 2^{-\ell} \simeq h(\ell), \quad \alpha = \alpha(\ell) = \frac{3}{2} \times 2^{\ell} \simeq h^{-1}(\ell). \tag{6.12}$$

In Figure 9 we show several snapshots of the surface vorticity distributions starting from the initial condition. The solution reproduces the well known flow pattern of the planar KH instability development, which includes the initial vortices formation in the layer followed by pairing and self-organization into larger vortices. Conservation of the initial zero angular momentum prevents further pairing. The two remaining vortices should decay for $t \to \infty$ due to energy dissipation.

Figure 10 visualizes the vorticity field of the KH flow on the torus for $\mathrm{Re} = 10^4$ ($\nu = 10^{-5}\,/\,2$). The initial stage of the vortical layer formation and small vortices pairing is similar to the case of the sphere and the plane. The different geometry (and topology) of the torus apparently affects the interaction of larger vortices. From the time of about 20 units there are 4 large vortices formed, which further travel in the both toroidal and poloidal directions without pairing up to time $t = 45$.

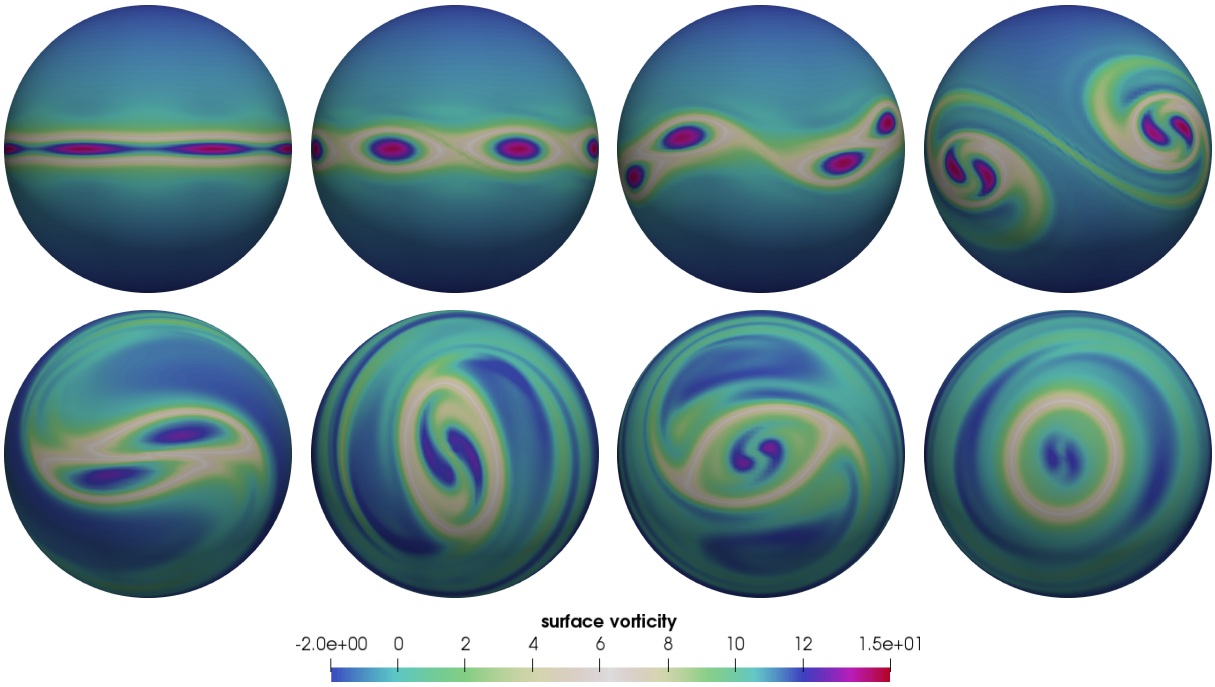

Figure 9: KH flow at $\mathrm{Re} = 10^4$ on the unit sphere Γ_{sph}: Snapshots of the surface vorticity $w_h = \mathrm{curl}_{\Gamma_h} \mathbf{u}_h$ for $t \in \{0, 2.5, 5, 6.25, 10, 12.5, 15, 20\}$. Click here for the full animation.

After $t = 45$ the motions loses any apparent axial symmetry and becomes rather complex (see the animation).

In the following subsections we

1. test the robustness of the algebraic solver from Chapter 5 w.r.t. varying parameters h, $\alpha \simeq h^{-1}$, and ν. We do not study the dependence of optimal γ on these parameters. It is known (Olshanskii, Lube, Heister, and Löwe 2009) that there is a wide range of quasi-optimal values of the grad-div stabilization parameter γ such that the solution quality is almost insensitive to the parameter variation, and hence γ can be taken smaller or larger depending on other considerations. For simplicity we adopt $\gamma = 1$ for the full AL-approach, and mesh-dependent γ for the modified AL-approach. Next we

2. explore the energy dissipation of the computed solutions and compare the results of the surface KH flow with a planar (i.e., posed in a domain in $\mathbb{R}^2$) benchmark.

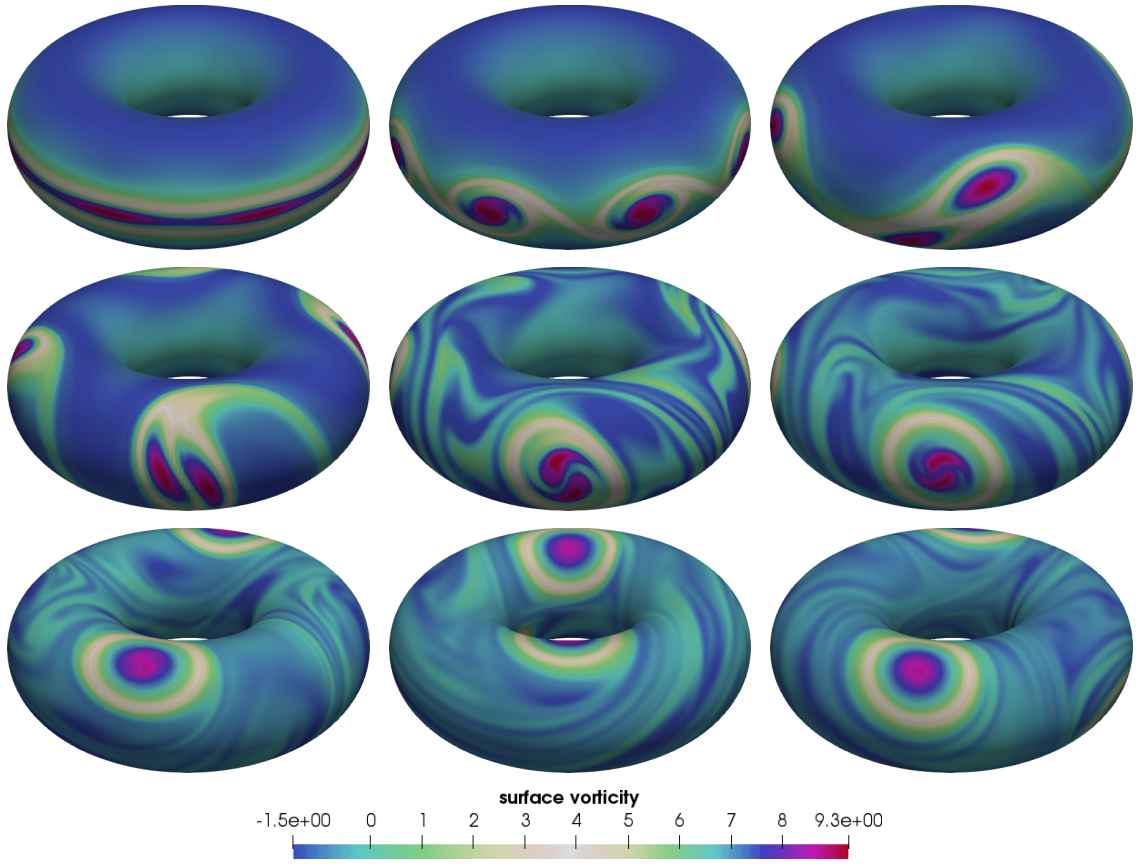

Figure 10: KH flow at $\mathrm{Re} = 10^4$ on the torus Γ_{tor}, $R = 1$, $r = 1/2$: snapshots of the surface vorticity $w_h = \mathrm{curl}_{\Gamma_h} \mathbf{u}_h$ for $t \in \{0, 2.3, 8.4, 9.3, 14, 18.7, 25.7, 30.4, 35\}$. Click here for the full animation.

6.2.1 Algebraic Solver Robustness

First we fix the viscosity parameter $\nu = 10^{-4}/2$ and vary the mesh size h. The number of unknowns grows by a factor of four from one level to the next one, and the parameter α in (5.1) increases two times for each refinement level, see (6.12). The FGMRES outer iterative solver with the full AL-preconditioner is applied to solve the system of algebraic equations on each time step. We use zero vector as the initial guess and the drop of residual by a factor of 10^8 as the stopping criterium.

Table 6 summarizes the solver averaged statistics over the time of simulation $t \in [0, 20]$. We see that the percentage of re-initializations of the preconditioner (this is when we compute new LU-factors) is small and decreases for finer mesh levels. The later can be due to the growth of α and more significant role of the diffusion term for smaller h. The choice of $\Delta_{\mathrm{iter}} = 5$ in (5.21) keeps the average number of FGMRES iterations about 30 with a very slight variation among

Table 6: Full AL-preconditioned FGMRES solver statistics for $\Gamma = \Gamma_{\text{sph}}$, fixed $\nu = 10^{-4}/2$, and varying h ($\alpha \simeq h^{-1}$). The total number of time steps n_t for three mesh levels reported are 320, 640, and 1280, respectively, leading to $\alpha \in \{24, 48, 96\}$.

# d.o.f.	T_{assemble}	% factor steps	"fresh" LU-steps			all steps		
			N_{iter}	T_{factor}	T_{linsol}	N_{iter}	T_{factor}	T_{linsol}
51526	3.55	3.44	9.00	1.72×10^1	0.53	33.53	0.59	2.15
203998	18.6	1.88	8.33	1.76×10^2	2.55	32.77	3.30	10.3
819862	180	0.86	7.55	1.73×10^3	12.1	29.86	14.9	49.9

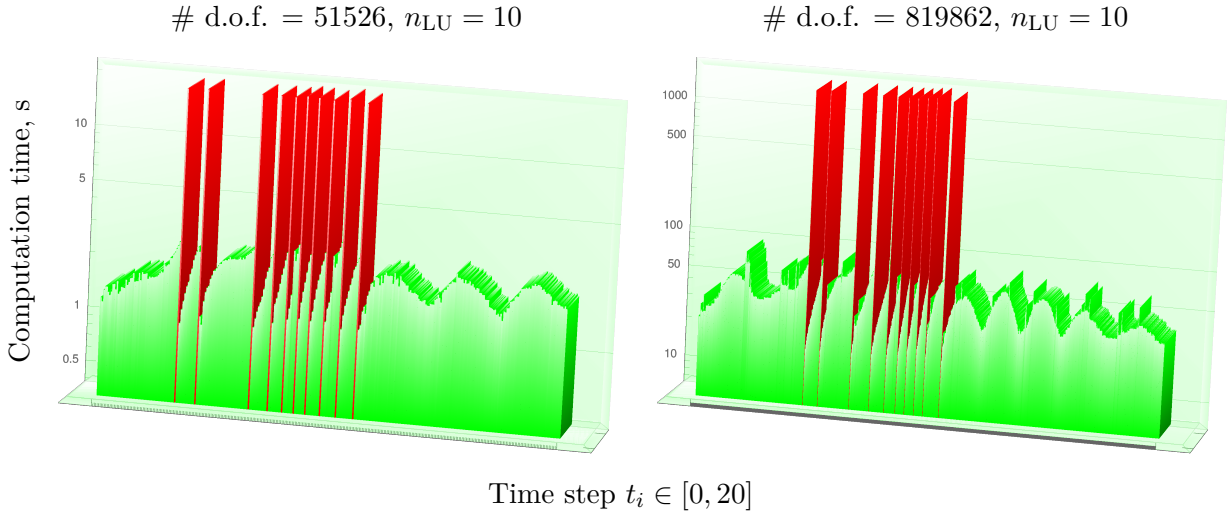

Figure 11: Computation time ($T_{\text{factor}} + T_{\text{linsol}}$) in log-scale vs. time step. Red bars correspond to time steps for which new factors are computed, n_{LU} is a number of such steps.

refinement levels. To compare, the number of FGMRES iterations with "fresh" LU-factorization in $\widehat{\mathbf{A}}$ is about 8. As expected, factorizing the matrix $\widehat{\mathbf{A}}$ is by far the most computationally expensive procedure (see T_{factor} in "fresh LU-steps" table section). However, due to the heavy and efficient recycling, overall the expense of the factorization is minor compared to the iterations cost (cf. T_{factor} and T_{linsol} in "all steps" table section). This allows to keep the *averaged* computation cost of the linear solver comparable and even less than the cost of matrix assembling.

This balance is further visualized in Figure 11 for two mesh levels, where we see that the time steps with updated LU-factors are more expensive but rare. It is interesting to note that most updates are needed for $t \in [4, 10]$, when vortixes are paring.

Because of the additional refinement used to define numerical quadratures, see Remark 4.2,

the matrix assembling time grows superlinear in our examples. The optimal complexity here can be obtained by using isoparametric trace finite elements (Lehrenfeld 2016; Jankuhn, Olshanskii, Reusken, and **Zhiliakov** 2020) which are not implemented in the software we use.

Next we repeat the simulation of the KH problem on the sphere but now for several values the viscosity parameter and the finest discretization level. All parameters of the algebraic solver are the same as above. The averaged statistics of the solver for this set of experiments are summarized in Table 7. It appears that the solver is remarkably w.r.t. the variation of the viscosity parameter. For higher Reynolds numbers we see only a slight increase of the percentage of time steps, where the preconditioner is updated by the new LU-factors. Figure 12 illustrates the balance between computationally expensive but rare steps with updated preconditioner and the majority of calculations with the recycled AL-preconditioner.

We now consider the surface KH flow on the torus. For the given values of outer and inner radius the surface area of Γ_{tor} is approximately 1.57 times the surface of the unit sphere. This explains why we get larger systems in terms of the number of d.o.f. for the same levels of mesh refinement in this example. This makes the problem naturally suitable for testing the recycling strategy with the modified AL-preconditioner. In general, the modified AL-preconditioner is less robust with respect to ν and h, so its efficient use needs some tuning.

Following recommendations in (Benzi, Olshanskii, and Wang 2011) we find optimal value for γ on a coarse level, and then apply $1\,/\,\sqrt{2}$-rule to scale it for finer mesh levels. This leads us to $\gamma_3 = 0.04$ for the third refinement level, and

$$\gamma = \gamma(\ell) = 2^{\frac{3-\ell}{2}} \times \gamma_3$$

for the refinement levels from 4 to 6, $\ell \in \{4, 5, 6\}$. These are the levels we use to report the solver statistics in Table 8. In this experiment, we take the velocity field and pressure from the previous time step as the initial guess in FGMRES and relax the stopping criterium to the relative drop of residual by 10^6, $\|\mathbf{r}_i\| < 10^{-6}\,\|\mathbf{b}\|$. The number of iterations increased compared to the full AL-preconditioner, since only the block upper-triangle part of the matrix $\mathbf{A}$ is used to define $\widehat{\mathbf{A}}$. We also see a slight increase of the iteration number for h getting smaller, which is also the observation

Table 7: Full AL-preconditioned FGMRES solver statistics for $\Gamma = \Gamma_{\text{sph}}$, fixed $h = 2.6 \times 10^{-2}$ (# d.o.f. = 819862, $\alpha = 96$), and varying ν.

ν	T_{assemble}	% factor steps	"fresh" LU-steps			all steps		
			N_{iter}	T_{factor}	T_{linsol}	N_{iter}	T_{factor}	T_{linsol}
$\frac{1}{2} \times 10^{-3}$	177	0.391	7.00	1.59×10^3	9.87	32.87	6.23	50.7
$\frac{1}{2} \times 10^{-4}$	180	0.859	7.55	1.73×10^3	12.1	29.86	14.9	49.9
$\frac{1}{2} \times 10^{-5}$	198	0.938	7.75	1.81×10^3	12.4	31.95	17	50.2

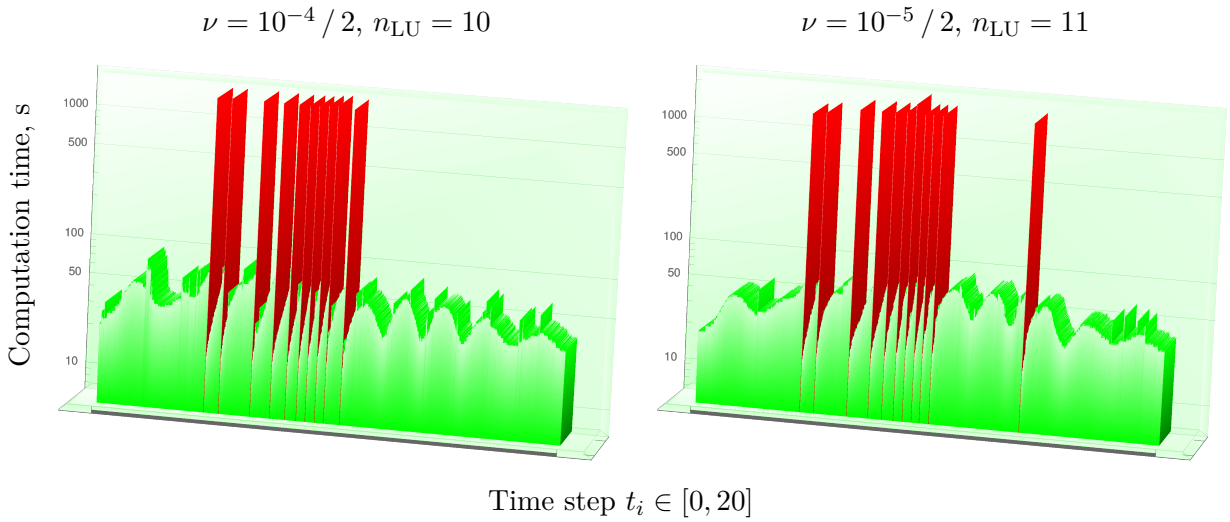

Figure 12: Computation time ($T_{\text{factor}} + T_{\text{linsol}}$) in log-scale vs. time step. Red bars correspond to time steps for which new factors are computed, n_{LU} is a number of such steps.

in (Benzi, Olshanskii, and Wang 2011). The overall computation time is dominated by the matrix assembly because of the non-optimal numerical quadrature, as discussed above. If we take the time of assembly off the table, then the recycling strategy turns out to be very effective also with the modified AL-preconditioner. The average time of factorization per one solve is negligible and each factorization is more efficient in terms of time and memory requirements since it is done for each individual velocity block.

It is out of scope for this dissertation to carry out a systematic comparison of the full and modified AL-preconditioners. Results in this direction can be found in (Benzi, Olshanskii, and Wang 2011). For the factorize–recycle framework introduced here, our general recommendation is the following: If the storage of factors is affordable, then use the full AL-preconditioner as the

Table 8: Modified AL-preconditioned FGMRES solver statistics for $\Gamma = \Gamma_{\text{tor}}$, fixed $\nu = 10^{-5}/2$, and varying h ($\alpha \in \{24, 48, 96\}$). The total number of time steps n_t for three mesh levels reported are 960, 1920, and 3840, respectively.

# d.o.f.	γ	T_{assemble}	% factor steps	"fresh" LU-steps			all steps		
				N_{iter}	T_{factor}	T_{linsol}	N_{iter}	T_{factor}	T_{linsol}
78244	0.028	7.65	6.25×10^{-1}	37.33	1.63	2.94	68.31	1.02×10^{-2}	5.02
315792	0.020	38.3	4.17×10^{-1}	42.75	18.1	16.3	75.32	7.55×10^{-2}	24.6
1279180	0.014	324	3.65×10^{-1}	64.71	181	97.6	75.51	6.61×10^{-1}	112

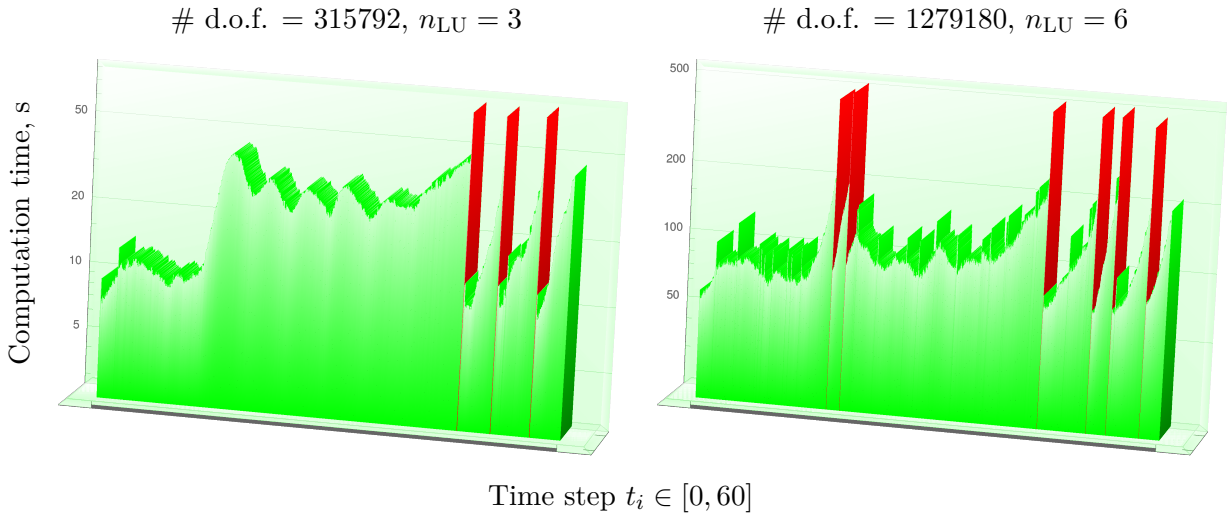

Figure 13: Computation time ($T_{\text{factor}} + T_{\text{linsol}}$) in log-scale vs. time step. Red bars correspond to time steps for which new factors are computed, n_{LU} is a number of such steps.

most robust and free of parameter tuning; Otherwise, switch to the modified AL-preconditioner and tune γ so that the number of outer iterations is somewhat higher but comparable to the full AL-approach case.

6.2.2 Energy Dissipation and Comparison with $\mathbb{R}^2$-Benchmark

We next assess the method by monitoring the energy dissipation of the computed solutions on three subsequent levels. To have a better insight into the expected behavior, we note that the initial velocity $\mathbf{u}_T(\cdot, 0)$ is L^2-orthogonal to all rigid tangential motions of Γ (also known as Killing

velocity fields), i.e., functions from

$$\mathbf{V}_{\text{kill}} \coloneqq \{\mathbf{v}_T \in \mathbf{V}_T : \mathbf{E}(\mathbf{v}_T) = \mathbf{0}\}.$$

It is straightforward to check that a velocity field $\mathbf{u}_T$ satisfying (6.10) preserves this orthogonality condition for all $t > 0$, and hence it satisfies the following Korn inequality:

$$\|\mathbf{u}_T\|_0 \leq C_K(\Gamma)\, \|\mathbf{E}(\mathbf{u}_T)\|_0 \,. \tag{6.13}$$

For the total kinetic energy

$$\mathcal{E}(t) \coloneqq \frac{1}{2}\, \|\mathbf{u}_T(\cdot, t)\|_0^2 \,,$$

testing (6.10) with $\mathbf{v}_T = \mathbf{u}_T$ and applying (6.13) leads to the following identity and a corresponding energy bound:

$$\mathrm{d}_t \mathcal{E}(t) = -2\nu\, \|\mathbf{E}(\mathbf{u}_T(\cdot, t))\|_0^2 \leq -\frac{4\nu}{C_K^2(\Gamma)}\, \mathcal{E}(t) \quad \Rightarrow \quad \mathcal{E}(t) \leq \mathcal{E}(0) \exp\left\{-\frac{4\nu t}{C_K^2(\Gamma)}\right\}. \tag{6.14}$$

We outline an approach for estimating the Korn constant $C_K(\Gamma)$. The best value of this constant is obtained if $C_K^{-2}(\Gamma)$ is the smallest strictly positive eigenvalue of the diffusion operator $-\mathbf{P}\,\mathrm{div}_\Gamma\,\mathbf{E}$ restricted to the space of tangential divergence free vector fields, see (6.13). We have the following relation between this surface diffusion operator and the Hodge-de Rham operator Δ_Γ^H (Jankuhn, Olshanskii, and Reusken 2018, equation (3.18)):

$$-2\,\mathbf{P}\,\mathrm{div}_\Gamma\,\mathbf{E}(\mathbf{v}_T) = \Delta_\Gamma^H \mathbf{v}_T - 2K\,\mathbf{v}_T$$

for any $\mathbf{v}_T \in \mathbf{V}_T$ such that $\mathrm{div}_\Gamma\,\mathbf{v}_T = 0$. The Gauss curvature of the unit sphere Γ_{sph} is equal to unity, $K = 1$. The eigenvalues of Δ_Γ^H are given by

$$\lambda_k(\Delta_\Gamma^H) = k(k+1), \quad k \in \mathbb{N}$$

for $\Gamma = \Gamma_{\text{sph}}$, see (Chow, Chu, Glickenstein, Guenther, Isenberg, Ivey, Knopf, Lu, Luo, and Ni 2007,

Table 9: Five smallest eigenvalues of (6.16). The first eigenvalue μ_1 corresponds to a constant pressure mode, eigenvalues μ_2, μ_3, and μ_4 correspond to 3 Killing vector fields on the unit sphere, and μ_5 is an estimate for the Korn constant $C_K^{-2}(\Gamma)$. The results are reported for $\epsilon = 10^{-7}$ (we verified that 8 significant digits of μ_5 stay the same for $\epsilon = 10^{-6}$).

h	$n_u + n_p$	μ_1	μ_2	μ_3	μ_4	μ_5
1.04×10^{-1}	51526	1.03×10^{-12}	3.6×10^{-4}	3.86×10^{-4}	3.86×10^{-4}	2.0029
5.21×10^{-2}	203998	1.28×10^{-13}	1.45×10^{-5}	1.84×10^{-5}	1.84×10^{-5}	2.00018
2.6×10^{-2}	819862	2.97×10^{-14}	7.87×10^{-7}	1.06×10^{-6}	1.06×10^{-6}	2.00001

p. 349). The tangential rigid motions are eigenfunctions corresponding to λ_1. Hence, we estimate

$$\begin{aligned} C_K^{-2}(\Gamma) &= \inf_{\substack{\mathbf{v}_T \in \mathbf{V}_T \setminus \mathbf{V}_{\text{kill}} \\ \operatorname{div}_\Gamma \mathbf{v}_T = 0}} \frac{\|\mathbf{E}(\mathbf{v}_T)\|_0^2}{\|\mathbf{v}_T\|_0^2} = \inf_{\substack{\mathbf{v}_T \in \mathbf{V}_T \setminus \mathbf{V}_{\text{kill}} \\ \operatorname{div}_\Gamma \mathbf{v}_T = 0}} \frac{\frac{1}{2}\left\langle \Delta_\Gamma^H \mathbf{v}_T - 2K\mathbf{v}_T, \mathbf{v}_T \right\rangle_0}{\|\mathbf{v}_T\|_0^2} \\ &\geq \inf_{\mathbf{v}_T \in \mathbf{V}_T \setminus \mathbf{V}_{\text{kill}}} \frac{\frac{1}{2}\left\langle \Delta_\Gamma^H \mathbf{v}_T - 2K\mathbf{v}_T, \mathbf{v}_T \right\rangle_0}{\|\mathbf{v}_T\|_0^2} = \frac{1}{2}\left(\lambda_2(\Delta_\Gamma^H) - 2\right) = 2, \end{aligned} \tag{6.15}$$

resulting in $C_K^2(\Gamma) \leq \frac{1}{2}$.

We confirm the estimate (6.15) numerically. To this end, consider a generalized eigenvalue problem

$$\begin{pmatrix} \mathbf{A}_K & \mathbf{B}^T \\ \mathbf{B} & -\mathbf{C}_n \end{pmatrix} \begin{pmatrix} \vec{\mathbf{v}} \\ \vec{\mathbf{q}} \end{pmatrix} = \mu(\epsilon) \begin{pmatrix} \mathbf{M} & \\ & \epsilon\,\mathbf{I} \end{pmatrix} \begin{pmatrix} \vec{\mathbf{v}} \\ \vec{\mathbf{q}} \end{pmatrix} \tag{6.16}$$

with the velocity mass matrix

$$\mathbf{M}_{ij} \coloneqq \int_\Gamma \boldsymbol{\psi}_j \cdot \boldsymbol{\psi}_i \,\mathrm{d}s, \quad 1 \leq i, j < n_u,$$

and the sum $\mathbf{A}_K$ of the velocity diffusion, normal penalty, and volume stabilization matrices, i.e.,

$$\langle \vec{\mathbf{u}}, \mathbf{A}_K\, \vec{\mathbf{v}} \rangle = \int_\Gamma \mathbf{E}(\mathbf{u}_h) : \mathbf{E}(\mathbf{v}_h) + \tau\,(\mathbf{u}_h \cdot \mathbf{n})\,(\mathbf{v}_h \cdot \mathbf{n})\,\mathrm{d}s + \rho_u \int_{\mathcal{O}_h} \partial_n \mathbf{u}_h \cdot \partial_n \mathbf{v}_h \,\mathrm{d}\mathbf{x}$$

for any $\vec{\mathbf{u}}$, $\vec{\mathbf{v}} \in \mathbb{R}^{n_u}$. Akin to (6.6), we introduced an ϵ-perturbation in the right-hand side matrix of (6.16) to make it Hermitian positive definite, so that the problem is solvable by any standard generalized eigenvalue solver that operates with sparse Hermitian matrices.

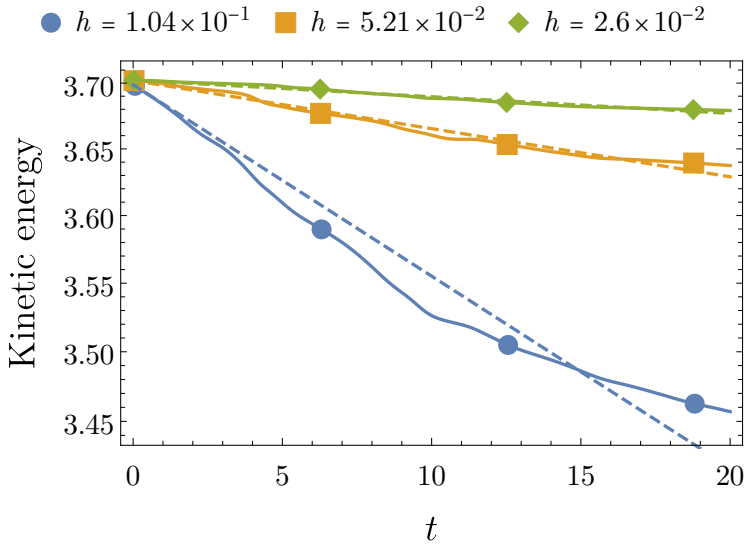

h	β
1.04×10^{-1}	3.96×10^{-3}
5.21×10^{-2}	9.96×10^{-4}
2.6×10^{-2}	3.44×10^{-4}

Figure 14: Left: Numerical kinetic energies $\mathcal{E}_h(t) \coloneqq 1/2\,\|\mathbf{u}_h(\cdot,t)\|_0^2$ as functions of time for the mesh refinement levels $\ell \in \{4,5,6\}$ (straight lines) and corresponding exponential fitting (dashed lines). Right: Values of the exponent β in the fitting function $B\exp\{-\beta t\}$.

Results of the numerical solution of (6.16) are shown in Table 9, which confirm the estimate (6.15). Moreover, the results strongly suggest $C_K(\Gamma)^2 = 1/2$ for $\Gamma = \Gamma_{\text{sph}}$. Substituting this in the estimate (6.14) for the kinetic energy, we arrive at the bound

$$\mathcal{E}(t) \leq \mathcal{E}(0)\exp\{-8\nu t\} = \mathcal{E}(0)\exp\left\{-4\times 10^{-5} t\right\}. \tag{6.17}$$

In Figure 14 we show the kinetic energy plots for the computed solutions together with exponential fitting. There are two obvious reasons for the computed energy to decay faster than the upper estimate (6.17) suggests: the presence of numerical diffusion and the persistence of higher harmonics in the true solution. On the finest mesh the numerical solution looses about 0.5% of kinetic energy up to the point when the solution is dominated by two counter-rotating vortices. This compares well to results computed with a higher order method in (Schroeder, John, Lederer, Lehrenfeld, Lube, and Schöberl 2019) for the planar case with $\text{Re} = 10^4$.

6.3 Navier–Stokes Problem on Evolving Surface with Prescribed Motion

For the last set of numerical experiments we consider the evolving surface tangential Navier–Stokes problem (3.3) with $\rho = 1$, i.e.,

$$\begin{aligned} (\mathbf{P}\,\dot{\mathbf{u}}_T + u_N\,\mathbf{H}\,\mathbf{u}_T) - 2\nu\,\mathbf{P}\,\mathrm{div}_\Gamma\,\mathbf{E}(\mathbf{u}_T) + \nabla_\Gamma p &= \mathbf{b}_T, \\ \mathrm{div}_\Gamma\,\mathbf{u}_T &= g \quad \text{on } \Gamma_{t>0}, \end{aligned} \tag{6.18}$$

with the right-hand sides

$$g \coloneqq -u_N\kappa, \qquad \mathbf{b}_T \coloneqq \mathbf{f}_T + 2\nu\,\mathbf{P}\,\mathrm{div}_\Gamma(u_N\,\mathbf{H}) + \frac{1}{2}\nabla_\Gamma u_N^2. \tag{6.19}$$

The initial triangulation is built as explained in Section 6.1. Further, the mesh is refined in a sufficiently large neighborhood of a surface so that tetrahedra cut by Γ_t belong to the same refinement level for all $t \in I$. We apply the BDF2 time stepping scheme to discretize (6.18) in time. To approximate the inertia term

$$\mathbf{P}\,\dot{\mathbf{u}}_T + u_N\,\mathbf{H}\,\mathbf{u}_T = \mathbf{P}\,(\partial_t \mathbf{u}_T^e + (\nabla \mathbf{u}_T^e)\,\mathbf{u}) + u_N\,\mathbf{H}\,\mathbf{u}_T$$

at the time $t = t^k$, we use the fact that u_N is given and apply (4.2). Thus at every time step $t = t^k$ we solve

$$\begin{aligned} \mathbf{P}\,[\mathbf{u}]_t^k + \mathbf{P}\left(\nabla \mathbf{u}^k\right)\left(\mathbf{w}^k + u_N^k \mathbf{n}\right) + u_N^k\,\mathbf{H}\,\mathbf{u}^k - 2\nu\,\mathbf{P}\,\mathrm{div}_\Gamma\,\mathbf{E}(\mathbf{u}^k) + \nabla_\Gamma p^k &= \mathbf{b}^k, \\ \mathrm{div}_\Gamma\,\mathbf{u}^k &= 0 \end{aligned} \tag{6.20}$$

on $\Gamma = \Gamma_{t^k}$, where the surface operators $\mathbf{P}$, $\mathbf{H}$, ∇_Γ etc. are constructed for Γ_{t^k}. The trace $\mathbf{P}_2$–P_1 Taylor–Hood finite element method is applied for the space discretization of (6.20) with the choice (6.7) of the stabilization and penalty parameters. To ensure that the previous step velocities required for the construction of $[\mathbf{u}]_t^k$ and $\mathbf{w}^k$ are defined on Γ_{t^k}, we discretize the problem in a

(sufficiently wide) narrowband $\mathcal{O}_h(t)$ of the surface for $t < t^k$. The width of $\mathcal{O}_h(t)$ is dependent on u_N and Δt. Note that the velocity volume stabilization term naturally enforces the velocity solution to be constant in the (quasi-)normal directions of the surface. For the rigorous analysis of the trace FEM method for the evolving surface case we refer to (Olshanskii, Reusken, and **Zhiliakov** 2022).

6.3.1 Convergence for a Smooth Solution

To verify the implementation and check the convergence order of the discrete solution, we set up an experiment with a known tangential flow along an expanding / contracting sphere. In this example the total area of Γ is not preserved, but it allows to prescribe a flow $\mathbf{u}_T$ analytically and calculate the right-hand sides in (6.18).

We choose $\nu = 5 \times 10^{-3}$ and consider $t \in [0, 1]$. The surface Γ is given by its distance function

$$\operatorname{dist}(\mathbf{x}, t) \coloneqq \|\mathbf{x}\| - r(t), \quad r(t) \coloneqq 1 + \frac{1}{4}\sin(2\pi t), \tag{6.21}$$

The surface normal velocity is then $\mathbf{u}_N = u_N \mathbf{n}$, with

$$u_N(t) = \mathrm{d}_t r(t) = \frac{\pi \cos(2\pi t)}{2}, \quad \mathbf{n}(\mathbf{x}) = \frac{\mathbf{x}}{\|\mathbf{x}\|}. \tag{6.22}$$

The exact solution is given by

$$\mathbf{u}_T^\star(\mathbf{x}, t) \coloneqq \mathbf{P}(\mathbf{x}, t)(1 - 2t, 0, 0)^T, \quad p^\star(\mathbf{x}) \coloneqq xy^2 + z, \tag{6.23}$$

and the right-hand sides $\mathbf{b}_T$ and $g = \operatorname{div}_\Gamma \mathbf{u}_T + u_N \kappa$ are computed accordingly from (6.18) and (6.21)–(6.23). For numerical integration, the exact solutions and right-hand sides are extended along normal directions of Γ.

The numerical solution was computed on four consecutive meshes with refinement levels $\ell \in \{2, \dots, 5\}$ and the time step $\Delta t = 0.05$ on level 2. The time is halved for each consecutive spatial refinement. The narrowband mesh together with the embedded surface Γ_t and computed velocity solution $\mathbf{u}_h$

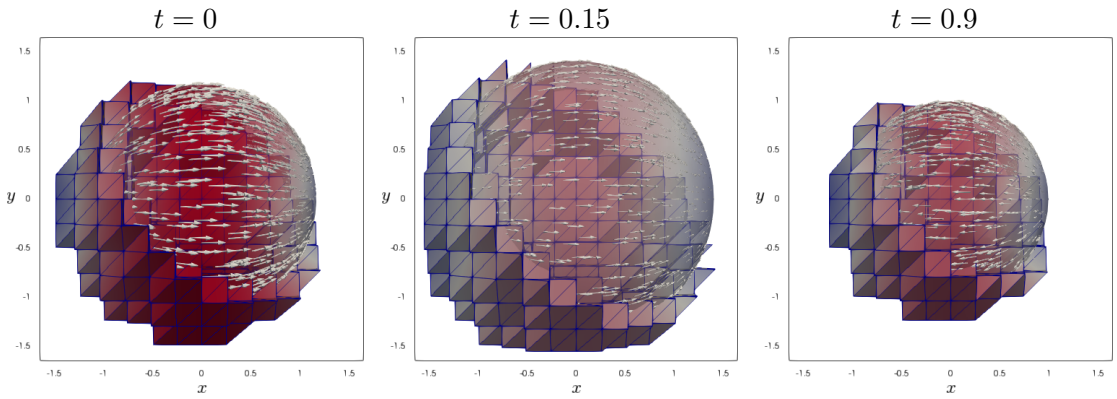

Figure 15: Illustration of the narrowband mesh and velocity solution at the mesh refinement level $\ell = 3$ for the tangential flow along an expanding / contracting sphere.

Mesh level ℓ	2	3	4	5
h	4.17×10^{-1}	2.08×10^{-1}	1.04×10^{-1}	5.21×10^{-2}
Averaged # d.o.f.	4.41×10^{3}	1.73×10^{4}	6.82×10^{4}	2.73×10^{5}

$\|\mathbf{u}_T^\star - \mathbf{u}_h\|_{\mathbf{1}}$	Order	$\|\mathbf{u}_T^\star - \mathbf{u}_h\|_{\mathbf{0}}$	Order	$\|p^\star - p_h\|_{\mathbf{0}}$	Order
9.3×10^{-1}		1.3×10^{-1}		3.2×10^{-1}	
1.9×10^{-1}	2.3	9.9×10^{-3}	3.72	3.5×10^{-2}	3.2
4.3×10^{-2}	2.13	9.2×10^{-4}	3.42	7.3×10^{-3}	2.27
1.2×10^{-2}	1.92	1.2×10^{-4}	2.98	1.8×10^{-3}	2.02

Table 10: Convergence results for the tangential flow along an expanding / contracting sphere.

are illustrated in Figure 15.

In Table 10 we show the mesh parameter h and the resulting (averaged over all time steps) number of active d.o.f. We see that one refinement leads to approximately four times more d.o.f. Table 10 further reports the velocity and pressure errors measured in (approximate) $\mathbf{\Gamma}_I$-norms

$$\|\mathbf{v}\|_{\mathbf{1}}^2 \coloneqq \int_0^1 \|\mathbf{v}(\cdot,t)\|_{H^1(\Gamma_t)}^2 \,\mathrm{d}t, \quad \|\mathbf{v}\|_{\mathbf{0}}^2 \coloneqq \int_0^1 \|\mathbf{v}(\cdot,t)\|_{L^2(\Gamma_t)}^2 \,\mathrm{d}t, \quad \|f\|_{\mathbf{0}}^2 \coloneqq \int_0^1 \|f(\cdot,t)\|_{L^2(\Gamma_t)}^2 \,\mathrm{d}t.$$

These norms were computed using a quadrature rule for the time integration. Results demonstrate the expected second order convergence in the "natural" norms and a higher order for the velocity error in the $L^2(\mathbf{\Gamma}_I)$-norm ($\mathbf{0}$-norm). These orders are optimal for the $\mathbf{P}_2$–P_1 elements used.

6.3.2 Tangential Flow on a Deforming Sphere

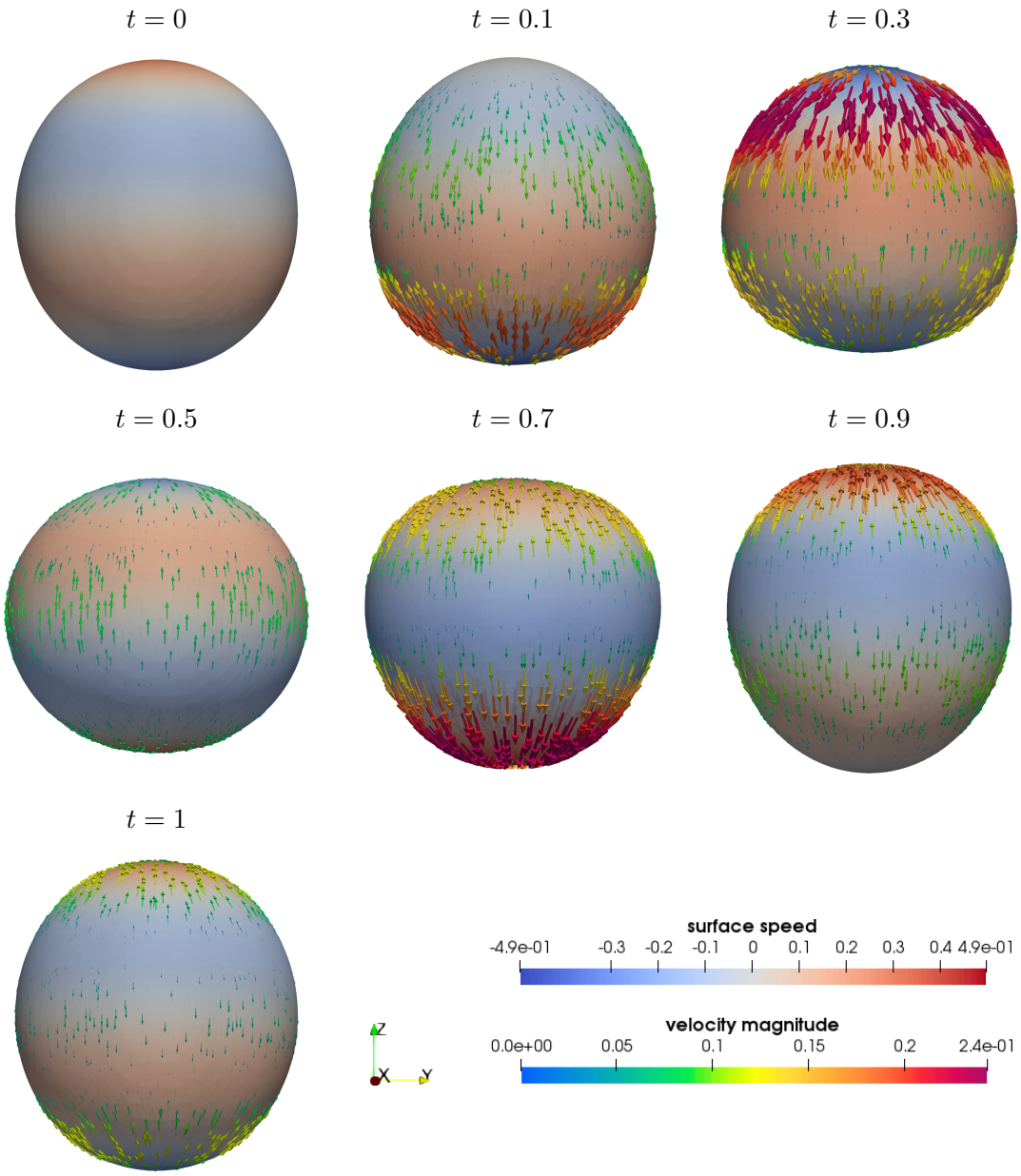

Figure 16: Visualization of the velocity field for axisymmetric deformations of the unit sphere. Mesh level $\ell = 4$, $\Delta t = 0.01$. Click here to see the full animation.

In this numerical example we consider a deforming unit sphere and compute the induced tangential flow, i.e., the numerical solution of (6.18) with $\mathbf{f}_T = \mathbf{0}$ and $u_N \simeq U_N$ such that the inextensibility condition is (approximately) preserved, see below. Denote by $\Gamma_0 = \Gamma_{\text{sph}}$ the reference sphere of

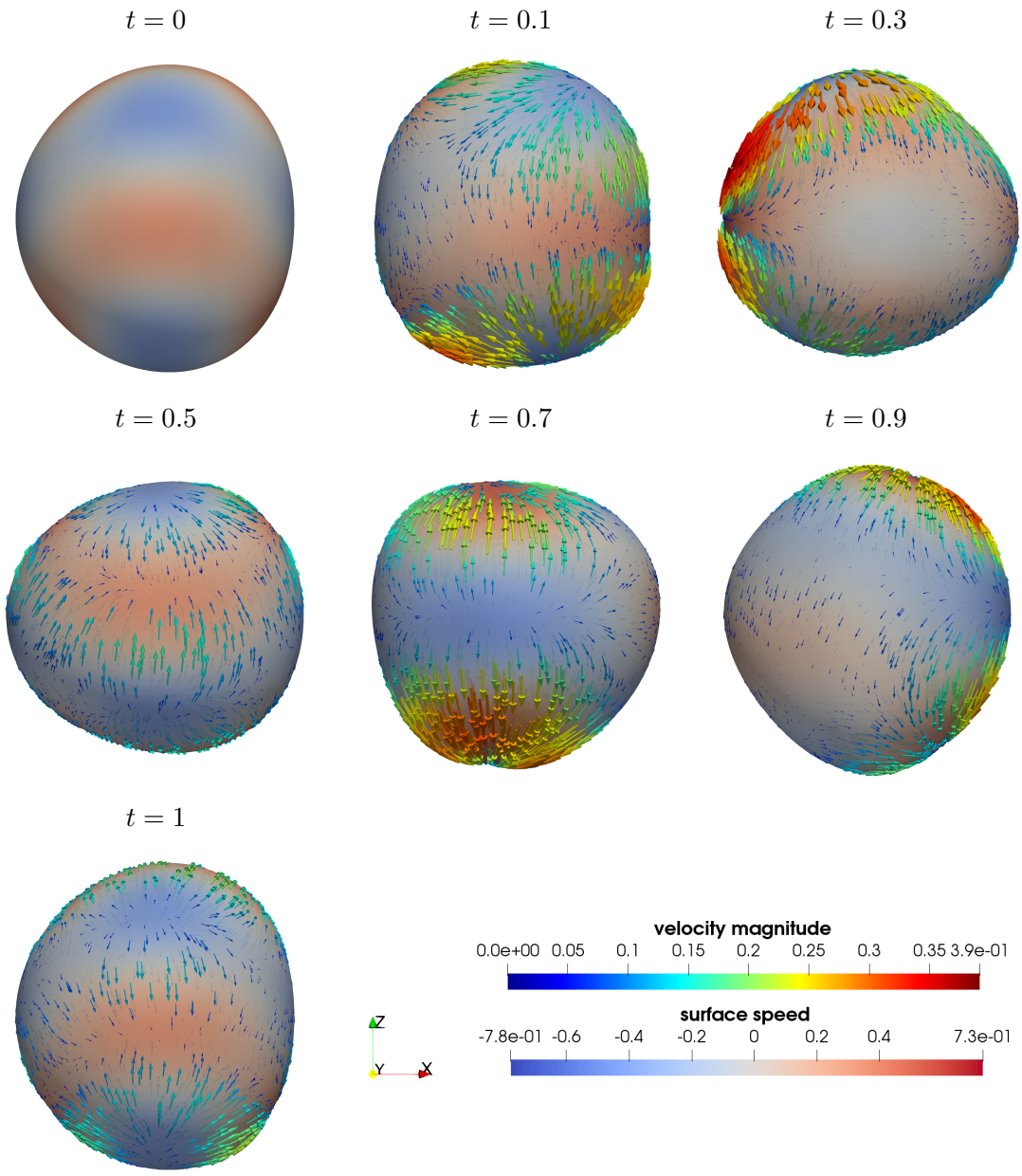

Figure 17: Visualization of the velocity field for asymmetric deformations of the unit sphere. Mesh level $\ell = 4$, $\Delta t = 0.01$. Click here to see the full animation.

radius 1. Consider a parametrization $\boldsymbol{\chi} : \Xi \to \Gamma_0$ of the unit sphere with ξ_1 and ξ_2 being the polar and azimuthal angles, respectively, $\Xi = [0, \pi] \times [0, 2\pi)$, and denote by $\boldsymbol{\xi} \mapsto \mathcal{H}_n^m(\boldsymbol{\xi})$ the normalized spherical harmonic of degree n and order m, $\|\mathcal{H}_n^m\|_{L^2(\Gamma_0)} = 1$. For the evolving surface we consider

as ansatz

$$\Gamma_t = \{r(\boldsymbol{\xi},t)\boldsymbol{\chi}(\boldsymbol{\xi}) : r(\boldsymbol{\xi},t) \coloneqq 1 + \sum_{n=1}^{N} \sum_{|m|\le n} A_{nm}(t)\mathcal{H}_n^m(\boldsymbol{\xi}),\ \boldsymbol{\xi}\in\Xi\}, \tag{6.24}$$

with suitably chosen time-dependent coefficients $A_{nm} = A_{nm}(t)$. The function

$$\delta r(\boldsymbol{\xi},t) \coloneqq \sum_{n=1}^{N} \sum_{|m|\le n} A_{nm}(t)\mathcal{H}_n^m(\boldsymbol{\xi})$$

describes the radial deformation.

We assume small oscillations, $|\delta r| \ll 1$. Under this assumption, an accurate approximation $U_N \simeq u_N$ of the surface normal speed u_N is given by

$$U_N \coloneqq \mathrm{d}_t \delta r = \sum_{n=1}^{N} \sum_{|m|\le n} \mathcal{H}_n^m \,\mathrm{d}_t A_{nm}. \tag{6.25}$$

We want the surface to be inextensible, i.e., $\mathrm{d}_t \operatorname{area}_\Gamma(t) \equiv 0$. Appropriate coefficients A_{nm} such that we have inextensibility can be determined as follows. Application of the surface Reynolds transport formula (2.34) and integration by parts gives for the variation of surface area:

$$\mathrm{d}_t \operatorname{area}_\Gamma(t) = \mathrm{d}_t \int_{\Gamma_t} 1 \,\mathrm{d}s = \int_{\Gamma_t} \operatorname{div}_{\Gamma_t} \mathbf{u}_N(\cdot,t)\,\mathrm{d}s = \int_{\Gamma_t} \kappa(\cdot,t)\,u_N(\cdot,t)\,\mathrm{d}s. \tag{6.26}$$

For the (doubled) mean curvature we have

$$\begin{aligned}\kappa &= 2 - 2\delta r - \Delta_\Gamma \delta r = 2 - \sum_{n=1}^{N} \sum_{|m|\le n} \left(2A_{nm}\mathcal{H}_n^m - n(n+1)A_{nm}\mathcal{H}_n^m\right) \\ &= 2 + \sum_{n=1}^{N} (n(n+1)-2) \sum_{|m|\le n} A_{nm}\mathcal{H}_n^m.\end{aligned}$$

see (Lamb 1924). Using $\int_{\Gamma_0} \mathcal{H}_n^m = 0$ for $n \in \mathbb{N}$ and orthonormality property

$$\int_{\Gamma_0} \mathcal{H}_n^m \mathcal{H}_{n'}^{m'} \,\mathrm{d}s = \delta_n^{n'} \delta_m^{m'}$$

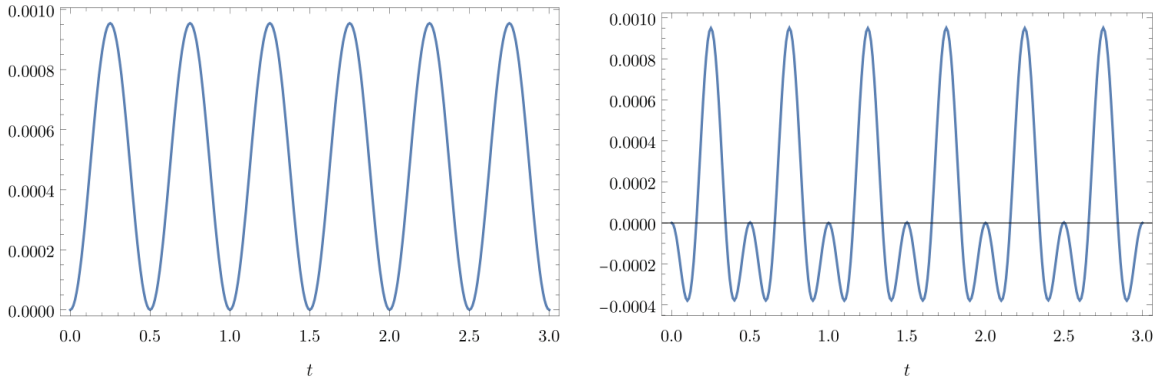

Figure 18: Relative surface area variation $(\operatorname{area}\Gamma_0 - \operatorname{area}\Gamma_t) \,/\, \operatorname{area}\Gamma_0$ as a function of time for axisymmetric (left plot) and asymmetric (right plot) deformations of the sphere.

we compute the area variation

$$\mathrm{d}_t \operatorname{area}_\Gamma(t) \simeq \int_{\Gamma_t} \kappa(\cdot,t) U_N(\cdot,t)\,\mathrm{d}s = \sum_{n=1}^{N} (n-1)(n+2) \sum_{|m|\le n} A_{nm}\,\mathrm{d}_t A_{nm}. \tag{6.27}$$

Based on this formula we set

$$A_{20} \coloneqq \frac{\epsilon}{2}\cos(\omega t), \quad A_{30} \coloneqq \frac{\epsilon}{\sqrt{10}}\sin(\omega t),$$

and $A_{nm} \coloneqq 0$ for other coefficients. For this choice of coefficients one easily verifies that (6.27) gives zero. The evolving surface tangential Navier–Stokes equations (6.18) are then discretizad and solved with the right-hand side given by (6.19) with u_N replaced with U_N from (6.25). The initial velocity is zero.

In the first numerical example we let $\epsilon \coloneqq 0.2$, $\omega = 2\pi$, $\nu = 10^{-4}/2$, and include $\mathcal{H}^0_2$ and $\mathcal{H}^0_3$: two zonal spherical harmonics of degree 2 and 3. The relative variation of the surface area in the left plot of Figure 18 shows less than 0.1% of surface variation, which is due to approximation errors and finite (rather than infinitesimal) deformations. The latter causes an approximation error in (6.25).

The velocity field induced by these axisymmetric deformations of the sphere is visualized in Figure 16. We see that the velocity pattern is dominated by a sink-and-source flow driven by the term $-\kappa u_N$ on the right-hand side of the divergence condition in (6.18).

We repeat the experiment, but decrease the viscosity to $\nu = 10^{-5}\,/\,2$ and add two more spherical harmonics: $\mathcal{H}_3^1$ and $\mathcal{H}_4^3$, the sectorial harmonic and the tesseral one, respectively. This addition makes the surface deformation asymmetric. The radial displacement in this experiment is then given by

$$\begin{aligned}\delta r(\boldsymbol{\xi}, t) = 0.2 \left(\frac{1}{2} \cos(2\pi t) \mathcal{H}_2^0(\boldsymbol{\xi}) + \frac{1}{\sqrt{10}} \sin(2\pi t) \mathcal{H}_3^0(\boldsymbol{\xi}) \right) \; + \\ 0.1 \left(\frac{1}{2} \cos(4\pi t) \mathcal{H}_3^1(\boldsymbol{\xi}) + \frac{5}{18} \sin(4\pi t) \mathcal{H}_4^2(\boldsymbol{\xi}) \right).\end{aligned}$$

Again, the coefficients are such that the surface area stays constant according to (6.27). The resulting velocity field is visualized in Figure 17. The velocity pattern is still dominated by the sink-and-source flow as in the previous experiment. Note that in both cases there are no outer forces, and the flow is driven completely by geometrical deformation.

BIBLIOGRAPHY

Author's Contributions

Institute of Scientific Computing, RWTH Aachen; Department of Mathematics, University of Houston (2003)
DROPS: CFD tool for simulating two-phase flows.
NOTE: The UH branch is available at https://github.com/56th/drops.
URL: http://www.igpm.rwth-aachen.de/DROPS.

Jankuhn T., Olshanskii M., Reusken A., and **Zhiliakov** A. (2020)
"Error analysis of higher order trace finite element methods for the surface Stokes equations."
IN: Journal of Numerical Mathematics.
DOI: 10.1515/jnma-2020-0017.

Olshanskii M., Reusken A., and **Zhiliakov** A. (2021)
"Inf-sup stability of the trace $\mathbf{P}_2$–P_1 Taylor–Hood elements for surface PDEs."
IN: Mathematics of Computation.
DOI: 10.1090/mcom/3551.

— (2022)
"Tangential Navier–Stokes equations on evolving surfaces: Analysis and simulations."
IN: arXiv (preprint).
DOI: 10.48550/arxiv.2203.01521.

Olshanskii M. and **Zhiliakov** A. (2020)
"Recycling augmented Lagrangian preconditioner in an incompressible fluid solver."
IN: Numerical Linear Algebra with Applications.
DOI: 10.1002/nla.2415.

Palzhanov Y., **Zhiliakov** A., Quaini A., and Olshanskii M. (2021)
"A decoupled, stable, and linear FEM for a phase-field model of variable density two-phase incompressible surface flow."
IN: Computer Methods in Applied Mechanics and Engineering 387. ISSN: 0045-7825.
DOI: 10.1016/j.cma.2021.114167.

Zhiliakov A., Svyatskiy D., Olshanskii M., Kikinzon E., and Shashkov M. (2019)
"A higher order approximate static condensation method for multi-material diffusion problems."
IN: Journal of Computational Physics.

Zhiliakov A., Wang Y., Quaini A., Olshanskii M., and Majd S. (2021)
"Experimental validation of a phase-field model to predict coarsening dynamics of lipid domains in multicomponent membranes."
IN: Biochimica et Biophysica Acta – Biomembranes 1863.
DOI: 10.1016/j.bbamem.2020.183446.

References

Ahrens J., Geveci B., and Law C. (2005)
"Paraview: An end-user tool for large data visualization."
IN: The visualization handbook 717.8.

Arroyo M. and DeSimone A. (2009)
"Relaxation dynamics of fluid membranes."
IN: Phys. Rev. E 79.3, p. 031915.

Aubin T. (1982)
Nonlinear analysis on manifolds. Monge-Ampere equations. Berlin: Springer.

Barrett J. W., Garcke H., and Nürnberg R. (2020)
"Chapter 4 – Parametric finite element approximations of curvature-driven interface evolutions."
Geometric Partial Differential Equations – Part I. Ed. by A. Bonito and R. H. Nochetto. Vol. 21. Handbook of Numerical Analysis. Elsevier, pp. 275–423.
DOI: 10.1016/bs.hna.2019.05.002.

Bendixson I. (1902)
"Sur les racines d'une équation fondamentale."
IN: Acta Mathematica 25, pp. 359–365.
DOI: 10.1007/bf02419030.

Benzi M., Golub G., and Liesen J. (2005)
"Numerical solution of saddle point problems."
IN: Acta numerica 14, p. 1.

Benzi M. and Olshanskii M. (2006)
"An augmented Lagrangian-based approach to the Oseen problem."
IN: SIAM Journal on Scientific Computing 28.6, pp. 2095–2113.

Benzi M., Olshanskii M., and Wang Z. (2011)
"Modified augmented Lagrangian preconditioners for the incompressible Navier–Stokes equations."
IN: International Journal for Numerical Methods in Fluids 66.4, pp. 486–508.

Benzi M. and Wang Z. (2011)
"Analysis of augmented Lagrangian-based preconditioners for the steady incompressible Navier–Stokes equations."
IN: SIAM Journal on Scientific Computing 33.5, pp. 2761–2784.

Bonito A., Demlow A., and Licht M. (2020)
"A Divergence-Conforming Finite Element Method for the Surface Stokes Equation."
IN: SIAM Journal on Numerical Analysis 58.5, pp. 2764–2798.
DOI: 10.1137/19m1284592.

Börm S. and Borne S. L. (2012)
"$\mathcal{H}$-LU factorization in preconditioners for augmented Lagrangian and grad-div stabilized saddle point systems."
IN: International Journal for Numerical Methods in Fluids 68, pp. 83–98.

Brandner P. and Reusken A. (2020)
"Finite element error analysis of surface Stokes equations in stream function formulation."

IN: ESAIM: M2AN 54.6, pp. 2069–2097.
DOI: 10.1051/m2an/2020044.

Brandner P., Reusken A., and Schwering P. (2021)
"On derivations of evolving surface Navier–Stokes equations."
IN: arXiv preprint arXiv:2110.14262.

Brenner H. (2013)
Interfacial transport processes and rheology. Elsevier.

Brezzi F. and Fortin M. (2012)
Mixed and hybrid finite element methods. Vol. 15. Springer Science & Business Media.

Brezzi F. and Pitkäranta J. (1984)
"On the stabilization of finite element approximations of the Stokes equations." *Efficient solutions of elliptic systems*. Springer, pp. 11–19.

Burman E., Hansbo P., and Larson M. G. (2015)
"A stabilized cut finite element method for partial differential equations on surfaces: The Laplace–Beltrami operator."
IN: Computer Methods in Applied Mechanics and Engineering 285, pp. 188–207.

Burman E., Hansbo P., Larson M. G., and Massing A. (2016)
"A cut discontinuous Galerkin method for the Laplace–Beltrami operator."
IN: IMA Journal of Numerical Analysis, drv068.

Cahouet J. and Chabard J.-P. (1988)
"Some fast 3D finite element solvers for the generalized Stokes problem."
IN: International Journal for Numerical Methods in Fluids 8.8, pp. 869–895.

Cermelli P., Fried E., and Gurtin M. E. (2005)
"Transport relations for surface integrals arising in the formulation of balance laws for evolving fluid interfaces."
IN: Journal of Fluid Mechanics 544, pp. 339–351.
DOI: 10.1017/s0022112005006695.

Chow B., Chu S.-C., Glickenstein D., Guenther C., Isenberg J., Ivey T., Knopf D., Lu P., Luo F., and Ni L. (2007)
The Ricci flow: techniques and applications. American Mathematical Society Providence.

Ciarlet P. G. (2013)
Linear and nonlinear functional analysis with applications. Vol. 130. Siam.

Dahl O. and Wille S. Ø. (1992)
"An ILU preconditioner with coupled node fill-in for iterative solution of the mixed finite element formulation of the 2D and 3D Navier–Stokes equations."
IN: International Journal for Numerical Methods in Fluids 15.5, pp. 525–544.
DOI: 10.1002/fld.1650150503.

Delfour M. C. and Zolésio J.-P. (2011)
Shapes and geometries: metrics, analysis, differential calculus, and optimization. SIAM.

Demlow A. and Olshanskii M. (2012)
"An adaptive surface finite element method based on volume meshes."
IN: SIAM Journal on Numerical Analysis 50, pp. 1624–1647.

Elman H., Silvester D., and Wathen A. (2005)
Finite Elements and Fast Iterative Solvers. Oxford: Oxford University Press.

Ern A. and Guermond J.-L. (2013)
Theory and practice of finite elements. Vol. 159. New York: Springer.

Farrell P. E. and Gazca-Orozco P. A. (2020)
"An augmented Lagrangian preconditioner for implicitly constituted non-Newtonian incompressible flow."
IN: SIAM Journal on Scientific Computing 42.6, B1329–B1349.

Farrell P. E., Mitchell L., and Wechsung F. (2019)
"An augmented Lagrangian preconditioner for the 3D stationary incompressible Navier–Stokes equations at high Reynolds number."
IN: SIAM Journal on Scientific Computing 41.5, A3073–A3096.

Farrell P. E., Mitchell L., Scott L. R., and Wechsung F. (2021)
"A Reynolds-robust preconditioner for the Scott–Vogelius discretization of the stationary incompressible Navier–Stokes equations."
IN: The SMAI journal of computational mathematics 7, pp. 75–96. ISSN: 2426-8399.
DOI: 10.5802/smai-jcm.72.

Fries T.-P. (2018)
"Higher-order surface FEM for incompressible Navier-Stokes flows on manifolds."
IN: International Journal for Numerical Methods in Fluids 88.2, pp. 55–78.

Fuller G. G. and Vermant J. (2012)
"Complex fluid-fluid interfaces: Rheology and structure."
IN: Annual review of chemical and biomolecular engineering 3, pp. 519–543.

Girault V. and Raviart P.-A. (2012)
Finite element methods for Navier–Stokes equations: theory and algorithms. Vol. 5. Springer Science & Business Media.

Grande J., Lehrenfeld C., and Reusken A. (2018)
"Analysis of a high-order trace finite element method for PDEs on level set surfaces."
IN: SIAM Journal on Numerical Analysis 56.1, pp. 228–255.

Grande J. and Reusken A. (2016)
"A higher order finite element method for partial differential equations on surfaces."
IN: SIAM Journal on Numerical Analysis 54.1, pp. 388–414.

Gross B., Trask N., Kuberry P., and Atzberger P. (2020)
"Meshfree methods on manifolds for hydrodynamic flows on curved surfaces: A Generalized Moving Least-Squares (GMLS) approach."
IN: Journal of Computational Physics 409.
DOI: 10.1016/j.jcp.2020.109340.

Gurtin M. E. and Murdoch A. I. (1975)
"A continuum theory of elastic material surfaces."
IN: Archive for Rational Mechanics and Analysis 57.4, pp. 291–323.

Gurtin M. E., Fried E., and Anand L. (2010)
The Mechanics and Thermodynamics of Continua. Cambridge University Press.
DOI: 10.1017/cbo9780511762956.

Guzmán J. and Olshanskii M. (2018)
"Inf-sup stability of geometrically unfitted Stokes finite elements."
IN: Mathematics of Computation 87.313, pp. 2091–2112.

Hansbo A. and Hansbo P. (2002)
"An unfitted finite element method, based on Nitsche's method, for elliptic interface problems."
IN: Comput. Methods Appl. Mech. Engrg. 191, pp. 5537–5552.

Hansbo P. and Larson M. (2016)
"A stabilized finite element method for the Darcy problem on surfaces."
IN: IMA Journal of Numerical Analysis, drw041.
DOI: 10.1093/imanum/drw041.

Hansbo P., Larson M., and Larsson K. (2019)
"Analysis of finite element methods for vector Laplacians on surfaces."
IN: IMA Journal of Numerical Analysis.

He X., Neytcheva M., and Capizzano S. S. (2011)
"On an augmented Lagrangian-based preconditioning of Oseen type problems."
IN: BIT Numerical Mathematics 51.4, pp. 865–888.

He X., Vuik C., and Klaij C. M. (2018)
"Combining the augmented Lagrangian preconditioner with the simple Schur complement approximation."
IN: SIAM Journal on Scientific Computing 40.3, A1362–A1385.

Heister T. and Rapin G. (2013)
"Efficient augmented Lagrangian-type preconditioning for the Oseen problem using Grad-Div stabilization."
IN: International Journal for Numerical Methods in Fluids 71.1, pp. 118–134.

Jankuhn T., Olshanskii M., and Reusken A. (2018)
"Incompressible fluid problems on embedded surfaces: Modeling and variational formulations."
IN: Interfaces and Free Boundaries 20.3, pp. 353–377.

John V. (2016)
Finite element methods for incompressible flow problems. Springer.

Konshin I., Olshanskii M., and Vassilevski Y. (2015)
"ILU preconditioners for nonsymmetric saddle-point matrices with application to the incompressible Navier–Stokes equations."
IN: SIAM Journal on Scientific Computing 37.5.
DOI: 10.1137/15m1012311.

— (2017)
"LU factorizations and ILU preconditioning for stabilized discretizations of incompressible

Navier–Stokes equations."
IN: Numerical Linear Algebra with Applications 24.3.
DOI: 10.1002/nla.2085.

Lamb H. (1924)
Hydrodynamics. University Press.

Lederer P. L., Lehrenfeld C., and Schöberl J. (2020)
"Divergence-free tangential finite element methods for incompressible flows on surfaces."
IN: International Journal for Numerical Methods in Engineering 121.11, pp. 2503–2533.
DOI: 10.1002/nme.6317.

Lehrenfeld C. (2016)
"High order unfitted finite element methods on level set domains using isoparametric mappings."
IN: Computer Methods in Applied Mechanics and Engineering 300, pp. 716–733.

Lehrenfeld C., Olshanskii M., and Xu X. (2018)
"A stabilized trace finite element method for partial differential equations on evolving surfaces."
IN: SIAM Journal on Numerical Analysis 56.3, pp. 1643–1672.

Mikula K., Remesíková M., Sarkoci P., and Sevcovic D. (2014)
"Manifold Evolution with Tangential Redistribution of Points."
IN: SIAM J. Sci. Comput. 36.

Morigi S. (2010)
"Geometric surface evolution with tangential contribution."
IN: Journal of Computational and Applied Mathematics 233.5.
NOTE: Special Issue Dedicated to William B. Gragg on the Occasion of His 70th Birthday, pp. 1277–1287. ISSN: 0377-0427.
DOI: 10.1016/j.cam.2007.04.052.

Moulin J., Jolivet P., and Marquet O. (2019)
"Augmented Lagrangian preconditioner for large-scale hydrodynamic stability analysis."
IN: Computer Methods in Applied Mechanics and Engineering 351, pp. 718–743.

Niet A. C. de and Wubs F. W. (2007)
"Two preconditioners for saddle point problems in fluid flows."
IN: International Journal for Numerical Methods in Fluids 54.4, pp. 355–377.

Nitschke I., Voigt A., and Wensch J. (2012)
"A finite element approach to incompressible two-phase flow on manifolds."
IN: Journal of Fluid Mechanics 708, pp. 418–438.

Nitschke I., Reuther S., and Voigt A. (2019)
"Hydrodynamic interactions in polar liquid crystals on evolving surfaces."
IN: Phys. Rev. Fluids 4.
DOI: 10.1103/physrevfluids.4.044002.

Olshanskii M., Quaini A., Reusken A., and Yushutin V. (2018)
"A Finite Element Method for the Surface Stokes Problem."
IN: SIAM Journal on Scientific Computing 40.4, A2492–a2518.

Olshanskii M. and Benzi M. (2008)
"An augmented Lagrangian approach to linearized problems in hydrodynamic stability."
IN: SIAM Journal on Scientific Computing 30.3, pp. 1459–1473.

Olshanskii M., Lube G., Heister T., and Löwe J. (2009)
"Grad-div stabilization and subgrid pressure models for the incompressible Navier–Stokes equations."
IN: Computer Methods in Applied Mechanics and Engineering 198.49.
DOI: 10.1016/j.cma.2009.09.005.

Olshanskii M., Palzhanov Y., and Quaini A. (2021)
"A comparison of Cahn-Hilliard and Navier-Stokes-Cahn-Hilliard models on manifolds."
DOI: 10.48550/arxiv.2110.15873.

Olshanskii M., Quaini A., and Sun Q. (2021)
"An unfitted finite element method for two-phase Stokes problems with slip between phases."
IN: Journal of Scientific Computing 89.2, pp. 1–23.

— (2022)
"A finite element method for two-phase flow with material viscous interface."
IN: Computational Methods in Applied Mathematics 22.2, pp. 443–464.
DOI: 10.1515/cmam-2021-0185.

Olshanskii M., Reusken A., and Grande J. (2009a)
"A Finite Element method for elliptic equations on surfaces."
IN: SIAM Journal on Numerical Analysis 47, pp. 3339–3358.

Olshanskii M. and Reusken A. (2004)
"Grad-div stablilization for Stokes equations."
IN: Mathematics of Computation 73.248, pp. 1699–1718.

— (2017)
"Trace finite element methods for PDEs on surfaces." *Geometrically Unfitted Finite Element Methods and Applications*. Springer, pp. 211–258.

Olshanskii M., Reusken A., and Grande J. (2009b)
"A finite element method for elliptic equations on surfaces."
IN: SIAM journal on numerical analysis 47.5, pp. 3339–3358.

Olshanskii M. and Tyrtyshnikov E. (2014)
Iterative methods for linear systems: theory and applications. SIAM.

Olshanskii M. and Yushutin V. (2019)
"A Penalty Finite Element Method for a Fluid System Posed on Embedded Surface."
IN: Journal of Mathematical Fluid Mechanics 21.1, p. 14.

Osher S. and Sethian J. A. (1988)
"Fronts propagating with curvature-dependent speed: Algorithms based on Hamilton-Jacobi formulations."
IN: Journal of Computational Physics 79.1, pp. 12–49. ISSN: 0021-9991.
DOI: 10.1016/0021-9991(88)90002-2.

Prüss J. and Simonett G. (2016)
Moving interfaces and quasilinear parabolic evolution equations. Vol. 105. Springer.

Rahimi M., DeSimone A., and Arroyo M. (2013)
"Curved fluid membranes behave laterally as effective viscoelastic media."
IN: Soft Matter 9.46, pp. 11033–11045.

Rangamani P., Agrawal A., Mandadapu K. K., Oster G., and Steigmann D. J. (2013)
"Interaction between surface shape and intra-surface viscous flow on lipid membranes."
IN: Biomechanics and modeling in mechanobiology 12.4, pp. 833–845.

Reusken A. (2015)
"Analysis of trace finite element methods for surface partial differential equations."
IN: IMA Journal of Numerical Analysis 35.4, pp. 1568–1590.

Reuther S. and Voigt A. (2018)
"Solving the incompressible surface Navier–Stokes equation by surface finite elements."
IN: Physics of Fluids 30.1, p. 012107.

Saad Y. (1993)
"A Flexible Inner-Outer Preconditioned GMRES Algorithm."
IN: SIAM Journal on Scientific Computing 14.2, pp. 461–469.
DOI: 10.1137/0914028.

Schroeder P. W., John V., Lederer P. L., Lehrenfeld C., Lube G., and Schöberl J. (2019)
"On reference solutions and the sensitivity of the 2D Kelvin-Helmholtz instability problem."
IN: Comput. Math. Appl. 77, pp. 1010–1028.

Schroeder W., Martin K. M., and Lorensen W. E. (1998)
The visualization toolkit an object-oriented approach to 3D graphics.

Scriven L. (1960)
"Dynamics of a fluid interface equation of motion for Newtonian surface fluids."
IN: Chemical Engineering Science 12.2, pp. 98–108.

Segal A., ur Rehman M., and Vuik C. (2010)
"Preconditioners for incompressible Navier–Stokes solvers."
IN: Numerical Mathematics: Theory, Methods and Applications 3.3, pp. 245–275.
DOI: 10.4208/nmtma.2010.33.1.

Slattery J. C., Sagis L., and Oh E.-S. (2007)
Interfacial transport phenomena. Springer Science & Business Media.

Temam R. (2001)
Navier–Stokes equations: theory and numerical analysis. Vol. 343. American Mathematical Soc.

The Trilinos Project Team (2021)
The Trilinos project website.
URL: https://trilinos.github.io.

Torres-Sánchez A., Millán D., and Arroyo M. (2019)
"Modelling fluid deformable surfaces with an emphasis on biological interfaces."
IN: Journal of fluid mechanics 872, pp. 218–271.

ur Rehman M., Vuik C., and Segal G. (2008)
"A comparison of preconditioners for incompressible Navier–Stokes solvers."
IN: International Journal for Numerical methods in fluids 57.12, pp. 1731–1751.

Verfürth R. (1984)
"Error estimates for a mixed finite element approximation of the Stokes equations."
IN: RAIRO-Analyse numérique 18.2, pp. 175–182.

Wang Y., Palzhanov Y., Quaini A., Olshanskii M., and Majd S. (2022)
"Lipid domain coarsening and fluidity in multicomponent lipid vesicles: A continuum based model and its experimental validation."
IN: Biochimica et Biophysica Acta (BBA)-Biomembranes, p. 183898.

Wolfram Research, Inc. (2021)
Mathematica, Version 13.0.0.
URL: https://www.wolfram.com/mathematica.